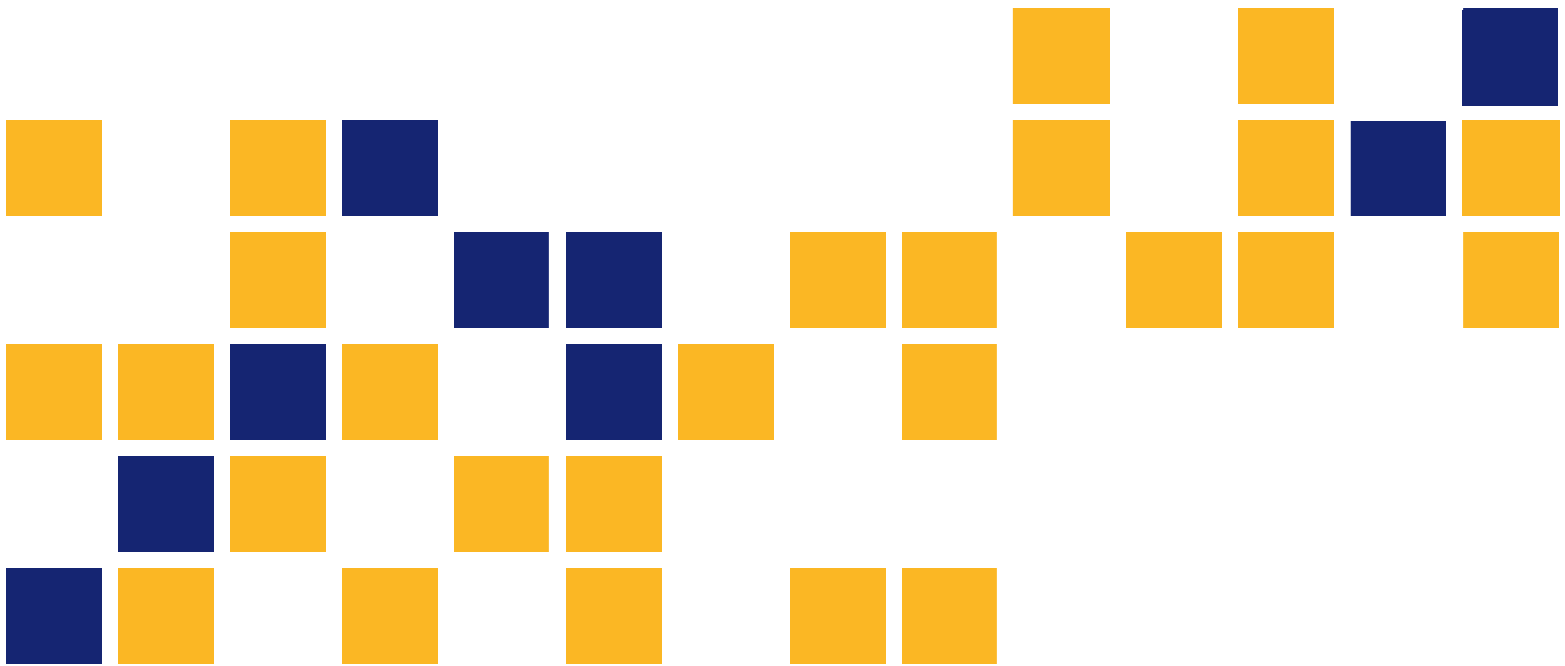# Capacity of Scour-Damaged Bridges, Part 2: Integrated Analysis Program (IAP)—A Program for the Analysis of Lateral Performance of Pile-Supported Structures under Scour Conditions

Cheng Lin
Caroline Bennett, Ph.D., P.E.
Jie Han, Ph.D., P.E.
Robert Parsons, Ph.D., P.E.
A. David Parr, Ph.D.
The University of Kansas

AD ASTRA PER ASPERA

Kansas
Department of Transportation

This page intentionally left blank.

1	Report No. K-TRAN: KU-10-2	2	Government Accession No.	3	Recipient Catalog No.

4	Title and Subtitle		5	Report Date
	Capacity of Scour-Damaged Bridges, Part 2: Integrated Analysis Program (IAP)—A Program for the Analysis of Lateral Performance of Pile-Supported Structures under Scour Conditions			November 2013
			6	Performing Organization Code

7	Author(s)	8	Performing Organization Report No.
	Cheng Lin; Caroline Bennett, Ph.D., P.E.; Jie Han, Ph.D., P.E.; Robert Parsons, Ph.D., P.E.; A. David Parr, Ph.D.		

9	Performing Organization Name and Address	10	Work Unit No. (TRAIS)
	The University of Kansas Civil, Environmental & Architectural Engineering Department 1530 West 15th Street Lawrence, Kansas 66045-7609	11	Contract or Grant No. C1862

12	Sponsoring Agency Name and Address	13	Type of Report and Period Covered
	Kansas Department of Transportation Bureau of Research 2300 SW Van Buren Street Topeka, Kansas 66611-1195		Final Report March 2010–May 2013
		14	Sponsoring Agency Code RE-0531-01

15 Supplementary Notes

For more information, write to address in block 9.

16 Abstract

Scour is the removal of soils in the vicinity of bridge foundations, resulting in a reduced capacity of the foundations, which can increase the risk of bridge failure. To minimize bridge failure, the Federal Highway Administration (FHWA) has established a requirement that all state highway agencies should evaluate whether bridges in their inventory are scour-susceptible. Accordingly, it is critical that state Departments of Transportation (DOTs) are able to determine quickly and effectively which bridges in their inventories are scour-critical, enabling responsible management of those bridges during and after scour events. It is of importance to identify and explore analytical methods for determining bridge system susceptibility to scour events.

To analyze bridge behavior under scour conditions, the bridge should be considered as a whole system including interactions between soil, foundation, and bridge superstructure behavior. To this end, the *Integrated Analysis Program (IAP)* has been developed; the IAP software is specifically aimed at analyzing lateral behavior of pile-supported bridges under scour conditions. However, the IAP is also able to deal with a variety of other structures (e.g. water/oil tanks, offshore platforms, and buildings) in addition to bridge structures. The IAP consists of two components: the *Soil Spring Module (SSM)* and the structural analysis software, *STAAD.Pro 2007*. The purpose of the SSM is to capture the effects of soils that support pile foundations as a series of nonlinear soil springs based on the soil load-displacement curves (i.e. *p-y* curves). With the seamless link between the SSM and STAAD.Pro 2007 using OpenSTAAD 2.6 functionality, the soil model (expressed as nonlinear soil springs) is successfully integrated with a traditional structural analysis model. In this report, operation of the IAP, technical development, and four examples are presented.

The first section of this report has been devoted to the operation of the IAP (Chapters 2 and 3). Most of the content of this section is focused on the operation of the SSM, since operation of STAAD.Pro is well-documented in its proprietary user's manual. The description of the operation of the SSM includes topics such as how to retrieve pile parameters from STAAD.Pro, input soil parameters, and how to perform a scour analysis.

The second section of this report presents the technical development of the SSM (Chapters 4 and 5), including descriptions of the *p-y* curves for different soil types (e.g. sand, soft/stiff clays, and rocks), generation of multilinear soil springs from the *p-y* curves, and the approximate approach chosen to account for second-order structural stability effects. Methodology for code development is also presented in this section.

Finally, four examples demonstrating use of the IAP are presented in Chapter 6. These examples cover the topics of a laterally loaded single pile, a laterally loaded pile group, an entire bridge, and determining the buckling capacity of a bridge and bridge piles. The step-by-step instruction for each example is shown during the analysis. Results obtained from using the IAP approach for analyzing the laterally loaded single pile and pile group were compared to results obtained from analyses performed using both LPILE and FB-Multiper, and the calculated results were shown to agree very well. Finally, behavior of an entire bridge was investigated using IAP and a discussion regarding scour effects on the lateral behavior of the bridge and buckling capacity of the bridge and bridge piles has been presented.

17	Key Words	18	Distribution Statement
	Scour, Bridge		No restrictions. This document is available to the public through the National Technical Information Service, Springfield, Virginia 22161

19	Security Classification (of this report)	20	Security Classification (of this page)	21	No. of pages	22	Price
	Unclassified		Unclassified		108		

Form DOT F 1700.7 (8-72)

Capacity of Scour-Damaged Bridges Part 2: Integrated Analysis Program (IAP)—A Program for the Analysis of Lateral Performance of Pile-Supported Structures under Scour Conditions

Final Report

Prepared by

Cheng Lin
Caroline Bennett, Ph.D., P.E.
Jie Han, Ph.D., P.E.
Robert Parsons, Ph.D., P.E.
A. David Parr, Ph.D.
The University of Kansas

PREFACE

The Kansas Department of Transportation's (KDOT) Kansas Transportation Research and New-Developments (K-TRAN) Research Program funded this research project. It is an ongoing, cooperative and comprehensive research program addressing transportation needs of the state of Kansas utilizing academic and research resources from KDOT, Kansas State University and the University of Kansas. Transportation professionals in KDOT and the universities jointly develop the projects included in the research program.

NOTICE

The authors and the state of Kansas do not endorse products or manufacturers. Trade and manufacturers names appear herein solely because they are considered essential to the object of this report.

This information is available in alternative accessible formats. To obtain an alternative format, contact the Office of Transportation Information, Kansas Department of Transportation, 700 SW Harrison, Topeka, Kansas 66603-3754 or phone (785) 296-3585 (Voice) (TDD).

DISCLAIMER

The contents of this report reflect the views of the authors who are responsible for the facts and accuracy of the data presented herein. The contents do not necessarily reflect the views or the policies of the state of Kansas. This report does not constitute a standard, specification or regulation.

Executive Summary

Scour is the removal of soils in the vicinity of bridge foundations, resulting in a reduced capacity of the foundations, which can increase the risk of bridge failure. To minimize bridge failure, the Federal Highway Administration (FHWA) has established a requirement that all state highway agencies should evaluate whether bridges in their inventory are scour-susceptible. Accordingly, it is critical that state Departments of Transportation (DOTs) are able to determine quickly and effectively which bridges in their inventories are scour-critical, enabling responsible management of those bridges during and after scour events. It is of importance to identify and explore analytical methods for determining bridge system susceptibility to scour events.

To analyze bridge behavior under scour conditions, the bridge should be considered as a whole system including interactions between soil, foundation, and bridge superstructure behavior. To this end, the ***Integrated Analysis Program (IAP)*** has been developed; the IAP software is specifically aimed at analyzing lateral behavior of pile-supported bridges under scour conditions. However, the IAP is also able to deal with a variety of other structures (e.g. water/oil tanks, offshore platforms, and buildings) in addition to bridge structures. The IAP consists of two components: the ***Soil Spring Module (SSM)*** and the structural analysis software, ***STAAD.Pro 2007***. The purpose of the SSM is to capture the effects of soils that support pile foundations as a series of nonlinear soil springs based on the soil load-displacement curves (i.e. *p-y* curves). With the seamless link between the SSM and STAAD.Pro 2007 using OpenSTAAD 2.6 functionality, the soil model (expressed as nonlinear soil springs) is successfully integrated with a traditional structural analysis model. In this report, operation of the IAP, technical development, and four examples are presented.

The first section of this report has been devoted to the operation of the IAP (Chapters 2 and 3). Most of the content of this section is focused on the operation of the SSM, since operation of STAAD.Pro is well-documented in its proprietary user's manual. The description of the operation of the SSM includes topics such as how to retrieve pile parameters from STAAD.Pro, input soil parameters, and how to perform a scour analysis.

The second section of this report presents the technical development of the SSM (Chapters 4 and 5), including descriptions of the *p-y* curves for different soil types (e.g. sand,

soft/stiff clays, and rocks), generation of multilinear soil springs from the *p-y* curves, and the approximate approach chosen to account for second-order structural stability effects. Methodology for code development is also presented in this section.

Finally, four examples demonstrating use of the IAP are presented in Chapter 6. These examples cover the topics of a laterally loaded single pile, a laterally loaded pile group, an entire bridge, and determining the buckling capacity of a bridge and bridge piles. The step-by-step instruction for each example is shown during the analysis. Results obtained from using the IAP approach for analyzing the laterally loaded single pile and pile group were compared to results obtained from analyses performed using both LPILE and FB-Multipier, and the calculated results were shown to agree very well. Finally, behavior of an entire bridge was investigated using IAP and a discussion regarding scour effects on the lateral behavior of the bridge and buckling capacity of the bridge and bridge piles has been presented.

Acknowledgements

Table of Contents

ix

List of Tables

List of Figures

Chapter 1: Introduction

The Integrated Analysis Program (IAP) serves to analyze the pile-supported structures (e.g. bridges, offshore platforms, etc.) under scour conditions, which involves the interactions of soil, foundation, and superstructure elements. Present practice usually involves performing separate analyses for the superstructure and substructure because widely-used software packages are typically designed specifically either for structural modeling or for foundation modeling, but do not consider the superstructure and substructure as an integrated system. For example, the prevalent structural analysis software packages (e.g. STAAD.Pro, RISA, etc.) lack sufficient soil analysis functions, especially for nonlinear soil behavior, while foundation analysis software packages (e.g. LPILE, GROUP, etc.) are fairly effective in analyzing laterally loaded piles in a variety of soils but do not have any functions for modeling superstructures. One exception is the software FB-Multipier, which was originally developed for analyzing behavior of pile group A and has been improved to account for superstructure modeling; however, the structural analysis functionalities of FB-Multipier are still limited when compared to structural analysis packages such as STAAD.Pro and RISA. For instance, FB-Multipier was only developed for bridge structures and is unable to account for bridge superstructure elements above the girders (i.e. bridge deck, suspension bridges, etc.).

Hence, it was necessary to develop a software package that is able to consider a bridge as a system, and to capture the effects of scour on the bridge system. To achieve the integrated analysis, the IAP was developed to integrate a Soil Spring Module (SSM) developed at the University of Kansas to the structural analysis software, STAAD.Pro 2007. Integration between the SSM and STAAD.Pro 2007 was accomplished using the functionality of OpenSTAAD v.2.6. The SSM captures the effect of soils that support pile foundations by simulating them as a series of nonlinear soil springs based on soil load-displacement curves (i.e. p-y, t-z, or t-θ curves). Note in this version of the IAP, only lateral soil behavior (i.e. p-y curves) is considered in the SSM, and thus the current version of IAP deals with lateral behavior of pile-supported structures. With the seamless link between the SSM and STAAD.Pro, the soil model (expressed as nonlinear soil springs) is successfully integrated to the structure model such that an integrated analysis of the whole structure can be accomplished. Hence, the IAP consists of

two components: the SSM and STAAD.Pro 2007. In this manual, operation of the IAP is presented; however most of the contents of this report are focused on the operation and technical development of the SSM as the functionality of STAAD.Pro is well-documented (Bentley System Inc. 2007). Finally, four examples are provided for the users' reference.

Chapter 2: Operation of IAP

The IAP captures the behavior of an entire bridge by integrating the two analysis components: the structure model and the soil model. The structure model is built by the user in STAAD.Pro, and must include both pile and superstructure elements. The soil model is generated in the SSM through a series of user-inputted values via a graphical user interface (GUI). The IAP achieves the analysis by combining the STAAD.Pro and SSM components. Figures 2.1 and 2.2 outline the operational procedure for IAP, which can be summarized as follows:

1. First, the user must build the structure model in STAAD.Pro 2007, including the bridge superstructure and foundation elements. The base units in STAAD.Pro must be metric; however, the units used in the specific STAAD file may be either metric or US.

2. Next, the user should select a single pile or pile group in structure model in STAAD.Pro, and then switch to the SSM interface while the STAAD.Pro model is open,

3. In the SSM, the user should input soil parameters and scour depths, and assign soil supports to the selected piles;

4. The user should return to the structure model in STAAD.Pro, where the structure model will now include the soil model (i.e. nonlinear soil springs);

5. The user can now perform any desired analyses in STAAD.Pro. to determine bridge performance characteristics that include soil-structure interaction effects.

STAAD.Pro	SSM	STAAD.Pro

Build a geometrical structure model	Input soil parameters for soil layers	Apply loads to the model
↓	↓	↓
Assign properties	Generate linear or nonlinear soil springs	Select analysis function
↓	↓	↓
Select piles to be applied with soil supports	Execute "Scour"	Perform analysis
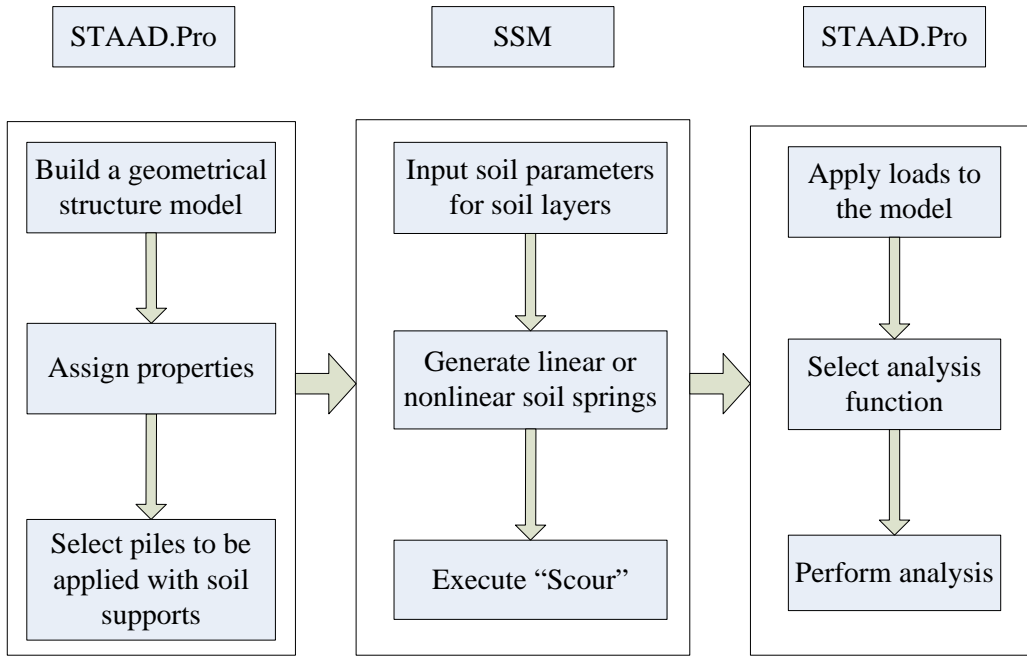
FIGURE 2.1
Operation Procedure for IAP

| Structure model | Input of soil parameters |

| Structure model plus soil model | Profile of soil model |

| In STAAD.Pro | In the SSM |
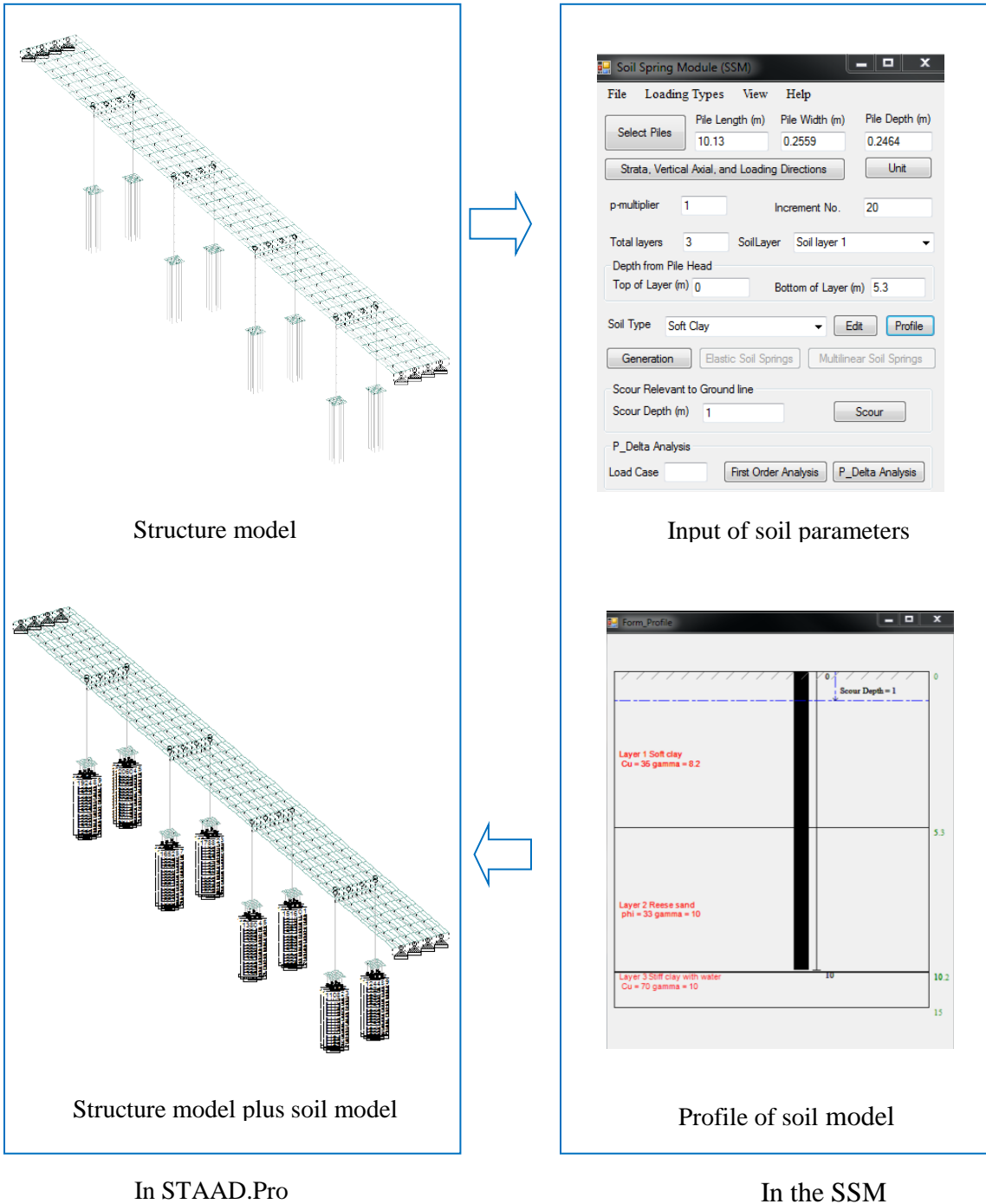
FIGURE 2.2
Illustration of Running the IAP

The seamless link between the SSM and STAAD.Pro is achieved through use of the OpenSTAAD functionality in STAAD.Pro that allows external programs (e.g., the SSM) to access the internal functions, routines, and graphical commands embedded in STAAD.Pro. The

SSM was programmed using Visual Basic 2010 Express to generate the soil models that are described as series of nonlinear Winkler springs derived from *p-y* curves. The following sections will present how the SSM operates and was developed.

Chapter 3: Operation of Soil Spring Module (SSM)

In order to run the SSM, STAAD.Pro should be opened in advance. After opening the SSM program, the GUI interface of the SSM appears as shown in Figure 3.1. The SSM can automatically search for the location of an opened STAAD file (.std file). If the SSM input file has been previously built, the user can use "**Open**" under the "**File**" menu to open the input file that is saved with the name of **SSM_input.txt**. Once the SSM input file is opened, all the pile and soil parameters are inputted in the SSM. Note that the SSM can directly find the SSM_Input.txt without giving the path when the SSM input file and STAAD file are at the same address file. Because the SSM only recognizes the address file where the STAAD file is saved, any attempt to open **SSM_Input.txt** at a different address than that where the STAAD file is saved will produce an error. If no SSM input file has been previously saved, the user should retrieve the pile dimensions from the structure model and input the soil parameters in order to generate the *p-y* curves within the SSM.
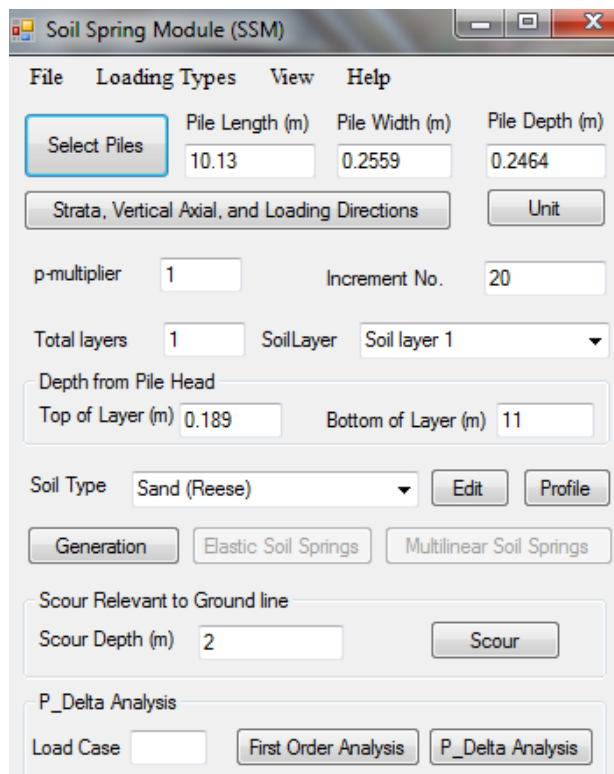
FIGURE 3.1
The SSM Interface

The general procedure for operating the SSM is as follows:

1. *Select* piles to be assigned with soil supports by clicking "**Select Piles**" in the SSM.

2. *Specify* the load type, such as static or cyclic loading, under the menu of "**Load Types**" in the SSM.

3. *Select* the axis corresponding to vertical soil strata, global vertical axis in STAAD.Pro, and lateral load direction in global axis, by opening the button "**Strata, Vertical Axial, and Loading Directions**" in the SSM.

4. *Select* the desired units for input by clicking the button "**Unit**" in the SSM.

5. *Input* soil parameters in terms of numbers of soil layers, as well as the elevations, soil type and the corresponding parameters for each layer in the SSM. The "**Edit**" button is for inputting soil parameters, and the "**Profile**" button is for viewing the soil profile.

6. *Generate* the soil springs after inputting all required soil and pile parameters by clicking the button "**Generation**" in the SSM.

7. *Assign* elastic soil springs to structure model in STAAD.Pro by clicking "**Elastic Soil Springs**" in the SSM.

8. *Assign* nonlinear soil springs to structure model in STAAD.Pro by clicking "**Multilinear Soil Springs**" in the SSM.

9. *Input* a scour depth and click "**Scour**" in the SSM to capture scour effects in the STAAD.Pro model. The **"Scour"** command removes previously-assigned nonlinear springs to the specified depth in the STAAD.Pro model and revises spring stiffness for remaining springs in the model.

Depending on the needs of the specific analysis, the user can select various commands provided in the SSM. Therefore, each command provided in the SSM is described in detail in the following discussion.

3.1 Select Piles

If all of the piles in a pile group have the same dimensions, such as pile length and cross section, then they can be selected together to receive soil spring supports. However, piles with different dimensions should be selected separately to be applied with soil springs. If a pile group is selected, the p-multiplier that accounts for group effect is involved. When an entire pile group is selected, the p-multiplier value for each pile in the pile group is computed internally in the SSM, and does not allow for changes by the user. The p-multiplier is only permitted to be user-specified when the piles within the pile group are selected individually. Once piles are selected, pile dimensions including length and cross section dimensions are displayed in the textboxes of the SSM.

3.2 Pile Length

Pile length is the length of all selected piles in a pile group, or of a selected single pile.

3.3 Pile Width

Pile width is the cross-sectional width of the pile, as illustrated in Figure 3.2. If the pile cross section is circular or hollow, then the pile width should be taken as equal to the pile outside diameter.

3.4 Pile Depth

Pile depth is the depth of the cross section as illustrated in Figure 3.2. For circular or pipe piles, pile depth refers to outside diameter of the pile.
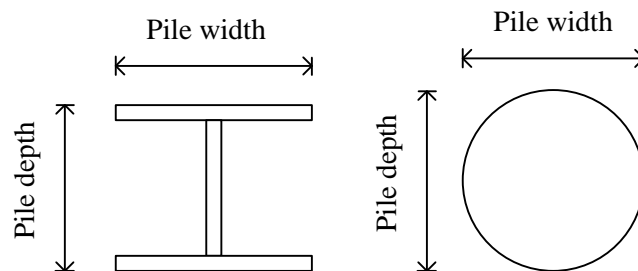
FIGURE 3.2
Illustration of Pile Cross-Sectional Dimensions
in the SSM

3.5 Strata, Vertical Axial and Loading Directions

By clicking the button "Strata, Vertical Axial and Loading Directions", a new window is opened. In the new window, three selections are required that include "Axis corresponding to vertical strata", "Global Vertical Axis in STAAD", and "Lateral Load Direction in Global Axis".

3.6 Axis Corresponding to Vertical Strata

This input field refers to the global standard axis in STAAD.Pro along which the soil strata are deposited. The axis corresponding to vertical strata is taken as the Y-axis by default. The user can change it as necessary.

3.7 Global Vertical Axis in STAAD

This input field refers to the global axis in the vertical direction, and by default is the Y-axis in STAAD.Pro. However, it may sometimes be the Z-axis since models imported from AutoCAD often set the Z-axis as the default global vertical axis.

3.8 Lateral Load Direction in Global Axis

This input field refers to the direction of lateral loading applied to the pile(s) in terms of the global axes in STAAD.Pro. The SSM program assumes the positive X axis as the default lateral load direction, that is "+X". The sign of "+" in front of each axis indicates the positive direction along that axis; the "-"sign represents the direction of lateral load applied to the pile is negative along the corresponding axis.

3.9 Unit

The commonly-used English and Metric units for length and force are provided as options within the SSM. The user should note that mixed use of English and Metric units will produce an error within the SSM.

3.10 *p*-Multiplier

The *p*-multiplier is used to account for pile group effects by reducing the lateral soil resistance to an individual pile that exists within a pile group. Because small spacing between piles within a pile group results in overlapped soil zones behind the piles, the soil resistance to a pile in a group is smaller than that to an identical single pile that is not in a pile group. The *p*-multiplier is defined as the ratio of soil resistance for a pile within a pile group to that for an identical single pile that is not in a pile group. The *p*-multiplier value depends on the spacing between piles in a pile group. Figure 3.3 shows how the *p*-multiplier may be determined based on the ratio of center-to-center spacing of piles to the diameter or width of the pile (S/D). Such a calculation for *p*-multiplier as shown in Figure 3.3 was adopted in the SSM.
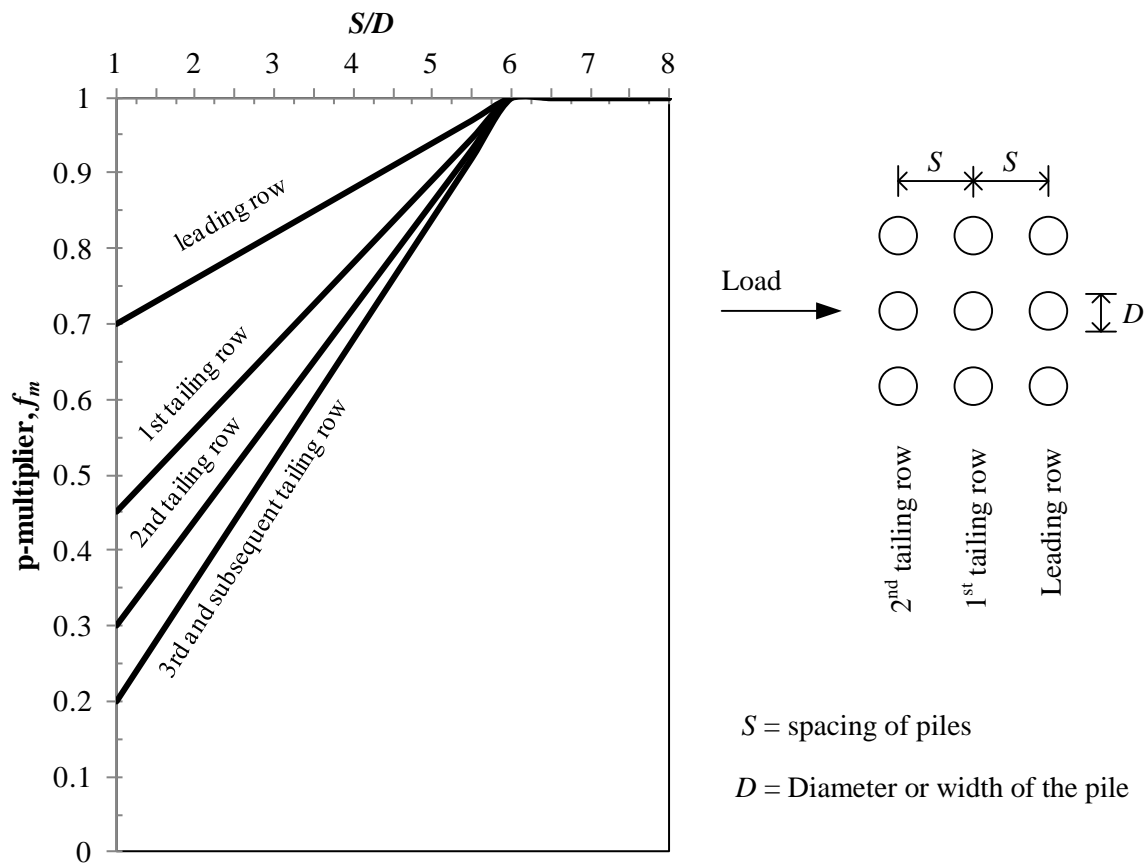
(Mokwa et al. 2000)

FIGURE 3.3
Determination of *p*-Mulitplier, *f*$_m$, in a Pile Group

11

3.11 Increment No.

Increment No. refers to the number by which a pile is divided into small segments with equal length. The user can set the increment number to any level desired; increasing the increment number will increase the accuracy of the solution.

3.12 Total Layers

The **"Total layers"** input field refers to the total numbers of soil layers encountered by the selected pile(s).

3.13 "Soil Layer"

SoilLayer corresponds to one specific soil layer. Once the total numbers of soil layers are assigned, each soil layer in the drop box is available for selection.

3.14 Depth from Pile Head

This input field allows the user to specify the location of soil layers with respect to the location of the pile head. "**Top of Layer**" corresponds to the distance to the top of the selected soil layer measured from the pile head; while "**Bottom of Layer**" corresponds to the distance to the bottom of the selected soil layer measured from pile head. Both values inputted should be positive numbers.

3.15 "Soil Type"

This input field allows the user to specify the type of soil that exists in each soil layer, using a pull-down list of options in the SSM. Soil type herein is associated with the *p-y* curve for laterally loaded piles; accordingly, each soil type corresponds to a particular *p-y* curve. Eight default *p-y* curves and one user-defined *p-y* curve are available for any selected soil layer. Once a *p-y* curve is selected, click the **"Edit"** button to input the corresponding soil properties for the *p-y* curve. Soil properties required for different *p-y* curves are illustrated in the following discussion for these soil types: (a) **soft clay**; (b) **stiff clay in the presence of free water**; (c) **stiff clay without free water**; (d) **Reese sand**; (e) **API sand**; (f) **silt**; (g) **strong rock**; (h) **weak rock**; and (i) **user-inputted soil properties**.

3.15.1 Soft Clay

Soft clay requires the input of <u>effective unit weight</u>, <u>undrained shear strength</u>, <u>and principle strain corresponding to half the maximum stress (ε_{50})</u> as shown in Figure 3.4. The ε_{50} value can be determined as the strain value corresponding to half the maximum stress on a stress-strain curve obtained from a triaxial test. In the absence of measured stress-strain curves, typical values of ε_{50} are provided in Table 3.1.
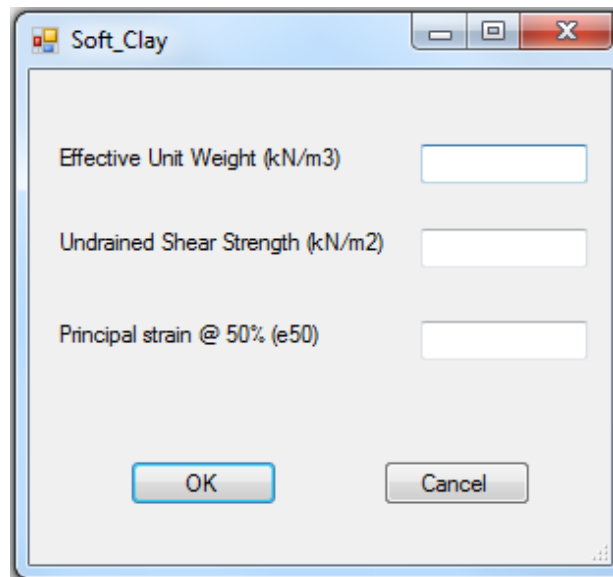
FIGURE 3.4
Required Input Properties for Soft Clay

TABLE 3.1
Representative Values of ε_{50} for Normally Consolidated Clays

Consistency of clay	Undrained shear strength* kN/m^2 (lb/in^2)	Principal strain @ 50% (ε_{50})
Soft	<48 (7)	0.02
Medium	48-96 (7-14)	0.01
Stiff	96-192 (14-28)	0.005

*(Peck et al. 1974)

(Source: Reese and Van Impe 2001)

3.15.2 Stiff Clay in the Presence of Free Water

Four properties including underlined effective unit weight, undrained shear strength, principal strain, and coefficient of subgrade reaction are required for generating *p-y* curves for stiff clay in the presence of free water, as shown in Figure 3.5. Representative values for ε_{50} are provided in Table 3.2 in the case that a stress-strain curve is available for the soil. The coefficient of subgrade reaction (k_{py}) can be determined from Table 3.3.
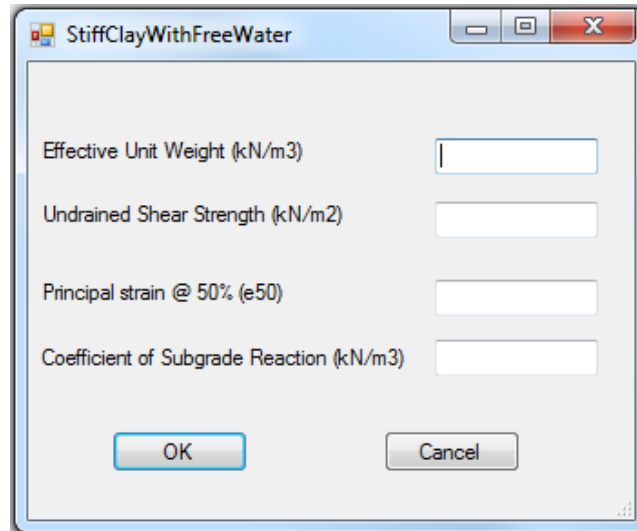
FIGURE 3.5
Required Input Properties for Stiff Clay in
Presence of Free Water

TABLE 3.2
Representative Values of ε_{50} for Overconsolidated Clays

Average undrained shear strength* kN/m^2 (lb/in^2)	Principal strain @ 50% (ε_{50})
50-100 (7-15)	0.007
100-200 (15-30)	0.005
300-400 (40-60)	0.004

*The average undrained shear strength should be computed from the shear strength of the soil to a depth of five pile diameters.

(Source: Reese and Van Impe 2001)

TABLE 3.3
Representative Values of k_{py} for Overconsolidated Clays

Average undrained shear strength kN/m^2 (lb/in^2)	Coefficient of subgrade reaction, k_{py} MN/m^3 (lb/in^3)	
	Static loading	Cyclic loading
50-100 (7-15)	135 (500)	55 (200)
100-200 (15-30)	270 (1000)	110 (400)
300-400 (40-60)	540 (2000)	540 (2000)

(Source: Reese and Van Impe 2001)

3.15.3 Stiff Clay without Free Water

The input parameters for stiff clay without free water include underlined effective unit weight, underlined undrained shear strength, and underlined principal strain at 50% of maximum stress, ε_{50}, as shown in Figure 3.6. In the absence of specific stress-strain curve data, typical values of ε_{50} can be obtained from Table 3.2.
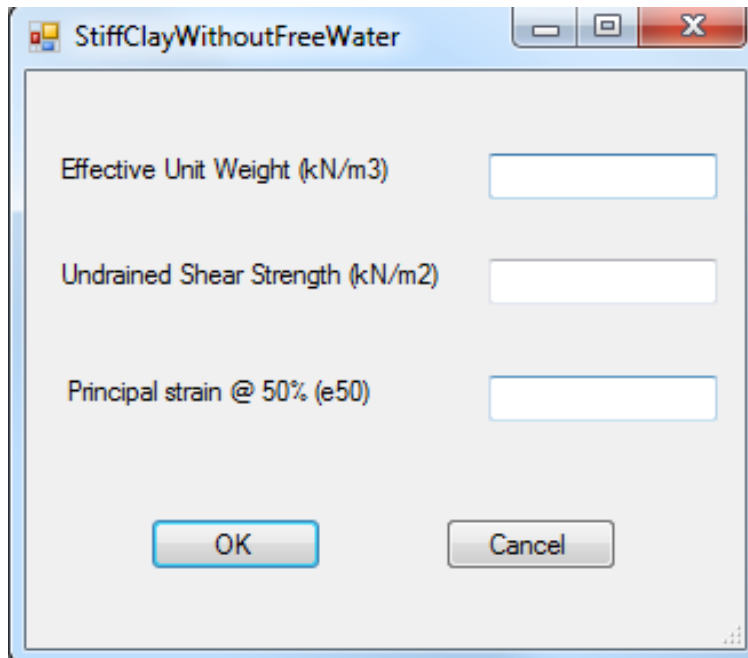
FIGURE 3.6
Required Input Properties for Stiff Clay without Free Water

3.15.4 Reese Sand

If the soil encountered by the pile foundation is cohesionless, then two *p-y* curves proposed by Reese et al. (1974) and API (1987) are available for use. The sand with the *p-y* curve proposed by Reese et al. (1974) is termed as Reese sand here. In Reese sand, <u>effective unit weight</u>, <u>effective friction angle</u>, and <u>coefficient of subgrade reaction are required</u>, as depicted in Figure 3.7.
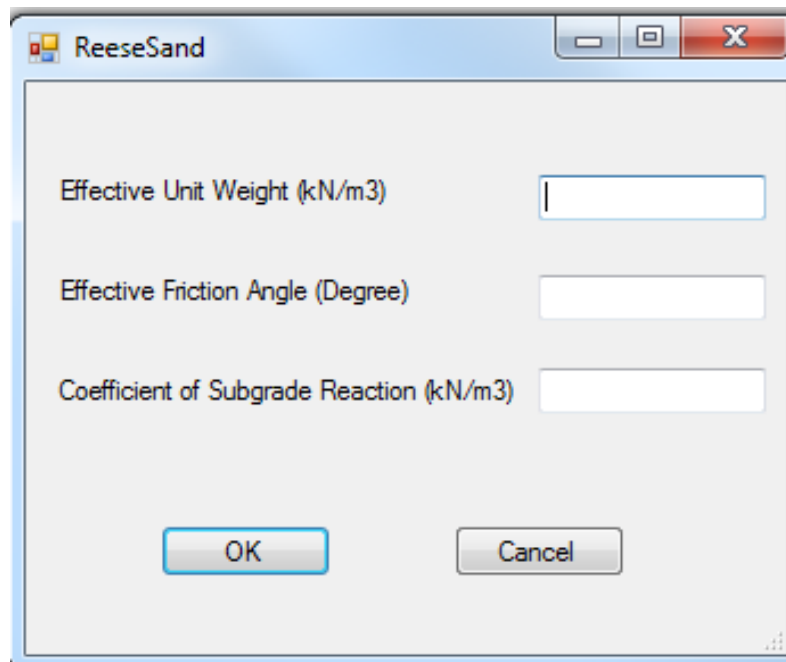
FIGURE 3.7
Required Input Properties for Reese Sand

Effective friction angle can be determined either from laboratory or field tests. Laboratory tests may include triaxial tests, plane strain tests, and direct shear tests in which effective friction angle can be directly derived. In field tests, the standard penetration test (SPT) and cone penetration test (CPT) are commonly used in practice. A series of correlations between effective friction angle and the SPT *N*-value or CPT tip resistance, q_c are given in the report by Kulhawy and Mayne (1990). Typical effective friction angles based on SPT *N* and CPT q_c are given in Tables 3.4 and 3.5.

Representative values of coefficient of subgrade reaction, k_{py} are given for sands below and above the water table in Tables 3.6 and 3.7.

TABLE 3.4
Typical Values of Effective Frictional Angle for Sand Correlated by SPT N

SPT N value (blow/ft or 305 mm)	Relative density	Approximate effective friction angle, ϕ' (degrees)	
		a	b
0 to 4	Very loose	<28	<30
4 to10	Loose	28 to 30	30 to35
10 to 30	Medium	30 to 36	35 to 40
30 to 50	Dense	36 to 41	40 to 45
>50	Very dense	>41	>45

a- Source: (Kulhawy and Mayne 1990)

b- Source: (Meyerhof 1956)

TABLE 3.5
Typical Values of Effective Frictional Angle for Sand Correlated by CPT q_c

Normalized cone tip resistance, q_c/p_a	Relative density	Approximate effective friction angle, ϕ' (degrees)
<20	Very loose	<30
20 to 40	Loose	30 to35
40 to 120	Medium	35 to 40
120 to 200	Dense	40 to 45
>200	Very dense	>45

Source: (Meyerhof 1956)

Note: p_a is atmospheric pressure

TABLE 3.6
Representative Values of k_{py} for Submerged Sand

	Relative density		
Recommended k_{py}	Loose	Medium	Dense
MN/m^3	5.4	16.3	34
(lb/in^3)	(20.0)	(60.0)	(125.0)

TABLE 3.7
Representative Values of k_{py} for Sand above
the Water Table

Recommended k_{py}	Relative density		
	Loose	**Medium**	**Dense**
MN/m^3	6.8	24.4	61.0
(lb/in^3)	(25.0)	(90.0)	(225.0)

3.15.5 API Sand

API Sand refers to sand for which the *p-y* curves were proposed by American Petroleum Institute (API) (1987). Similar to Reese Sand, API Sand also requires input of values for <u>effective unit weight</u>, <u>effective friction angle</u>, and <u>coefficient of subgrade reaction</u> to generate the *p-y* curves as seen in Figure 3.8. The value for Effective friction angle may be obtained as described for Reese Sand. The value for the coefficient of subgrade reaction, k_{py}, can be estimated on the basis of effective friction angles using the plot presented in Figure 3.9.
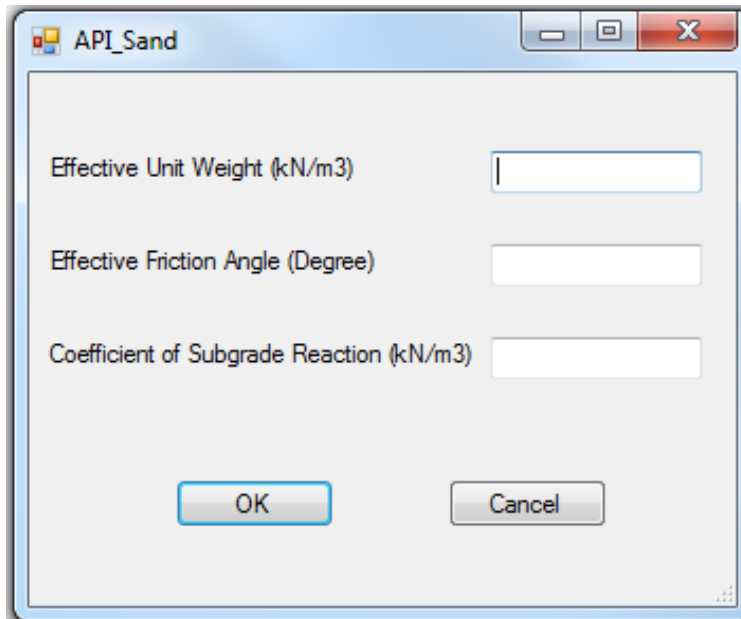
FIGURE 3.8
Required Input Properties for API Sand

Effective friction angle, ϕ'
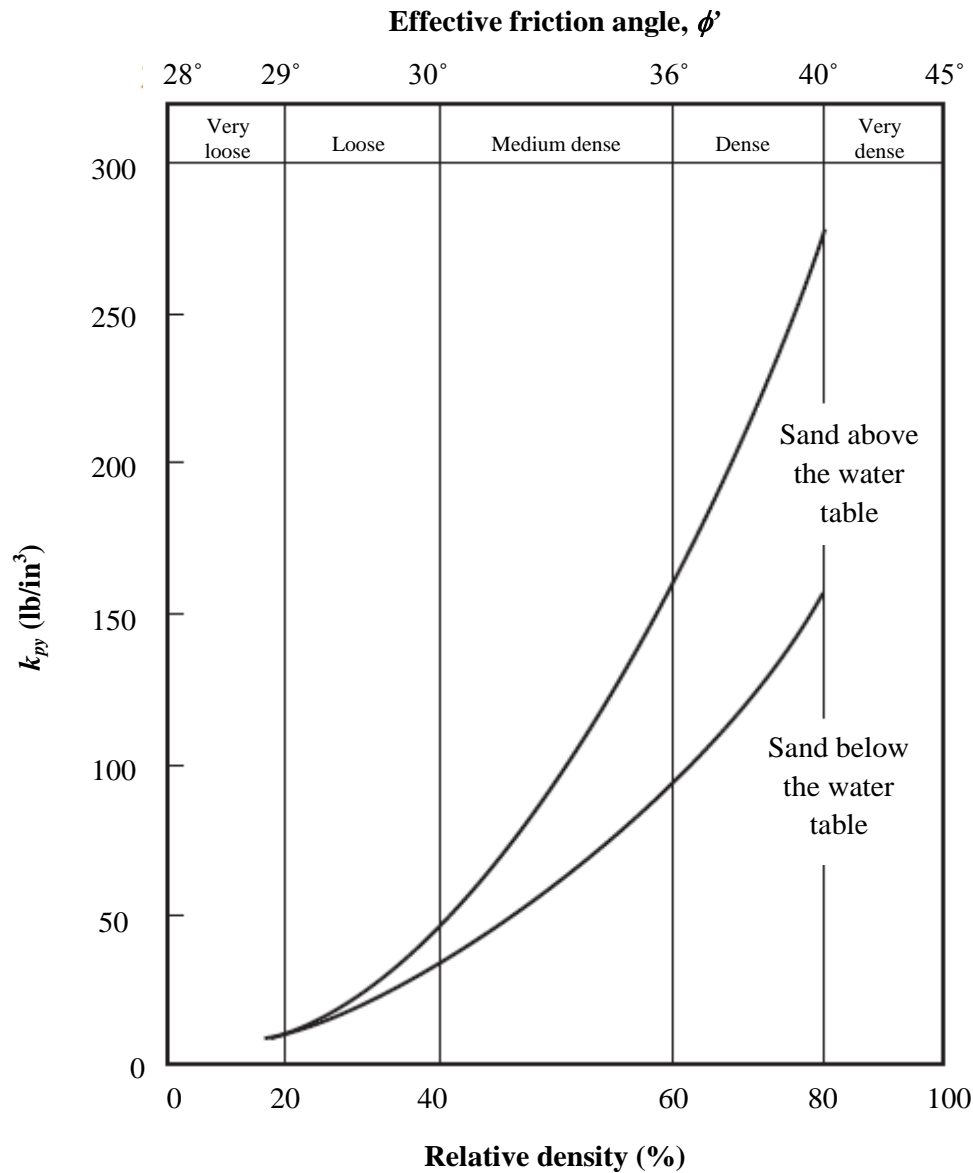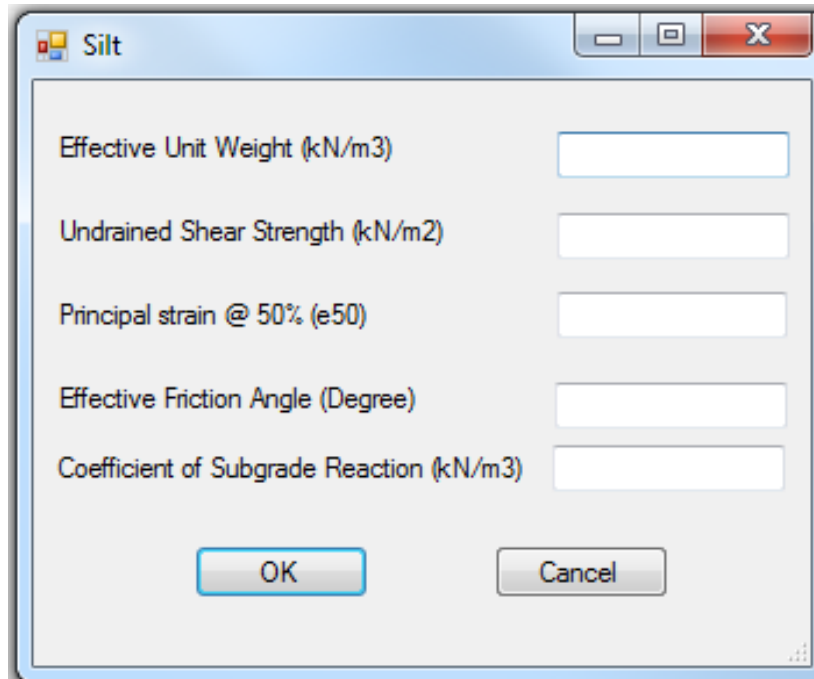
(Source: API 1987)

FIGURE 3.9
Coefficient of Subgrade Reaction, k_{py}, Used for API Sand Criteria

3.15.6 Silt, a c-ϕ Soil

The required parameters for silt are <u>effective unit weight</u>, <u>undrained shear strength</u>, <u>principal strain</u>, <u>effective friction angle</u>, and <u>coefficient of subgrade reaction</u> as shown in Figure 3.10. The principal strain at 50% of the maximum stress is given in Table 3.1. The value

for effective friction angle may be obtained as described for Reese Sand. The coefficient of subgrade reaction can be determined using Tables 3.6 and 3. 7.

FIGURE 3.10
Required Input Properties for Silt, a *c-φ* Soil

3.15.7 Strong Rock

Strong rock is defined as having compressive strength of intact specimens greater than 6.9 MPa (1,000 psi) (Reese and Van Impe 2001). The *p-y* curves for rocks are interim and need to be improved with more rigorous studies. As indicated in Figure 3.11, in addition to effective unit weight, Young's modulus and uniaxial compressive strength are required for generating strong rock's *p-y* curves. The correlation of Young's moduli may be estimated based on uniaxial compressive strengths as given in Figure 3.12, but the modulus values for the sample of the same type of rock may vary by several orders of magnitude (Resse and Van Impe 2001). Rock resistance to piles could depend on joint cracks and not on the strength of intact specimens. Therefore, these interim *p-y* curves developed based on the strength of intact specimens should be used with both judgment and caution.
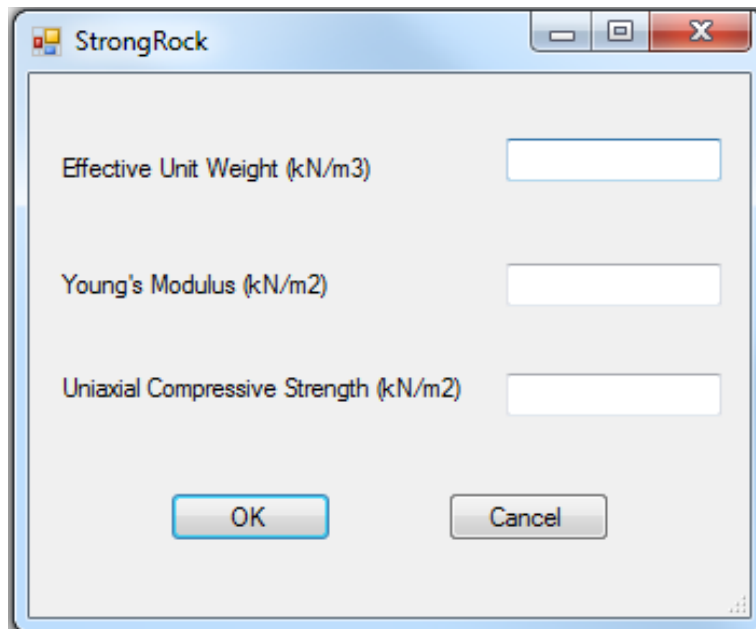
FIGURE 3.11
Required Input Properties for Strong Rock

3.15.8 Weak Rock

Compared with strong rock, *p-y* curves for weak rock have been well documented by Reese (1997) but still should be used with both judgment and caution. Figure 3.12 shows the required input parameters, among which the Rock Quality Designation (*RQD*) is used to estimate the degree of rock fracture and K_{rm} is a constant ranging from 0.0005 to 0.00005. Young's modulus can be approximately estimated using Figure 3.12, or the value can also be approximately determined using the relationship between E_{mass}/E_{core} and *RQD* as depicted in Figure 3.14. Young's modulus, which is assumed to be E_{mass}, may be estimated if a test of cored rock specimens is available.
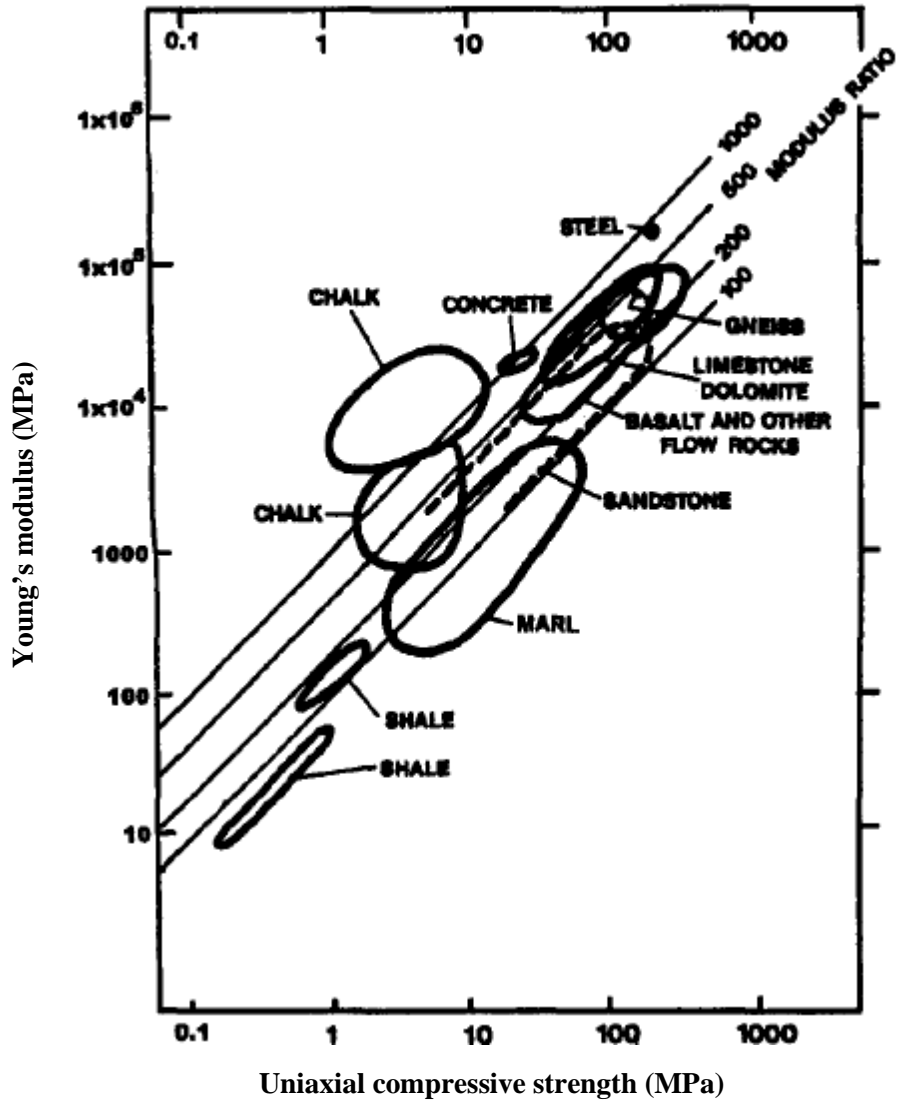
(Source: Deere 1968, Peck 1976, Horvath and Kenney 1979)

FIGURE 3.12
Engineering Classification of Intact Rock

FIGURE 3.13
Required Input Properties for Weak Rock
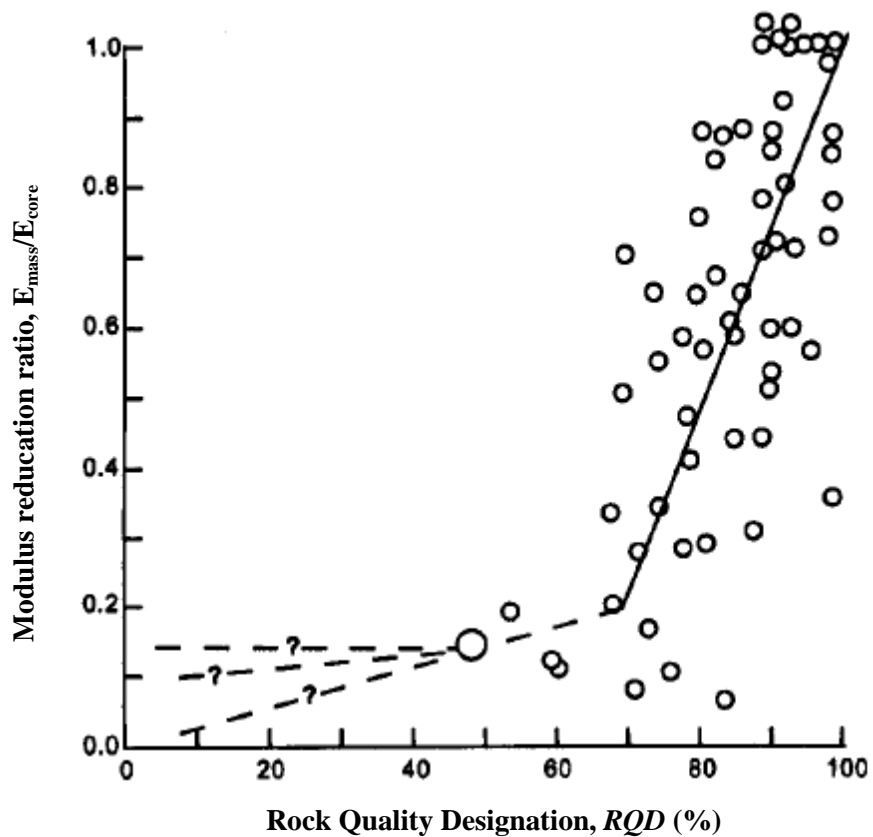
(Source: Bieniawski 1984)

FIGURE 3.14
Modulus Reduction Ratio versus RQD

3.15.9 User Input

The SSM also allows the user to input *p-y* curves directly when this information is available from field tests. As shown in Figure 3.15, the user needs to assign the effective unit weight, as well as a family of soil resistances per length, *p,* and lateral pile deflection at a depth, *y*.
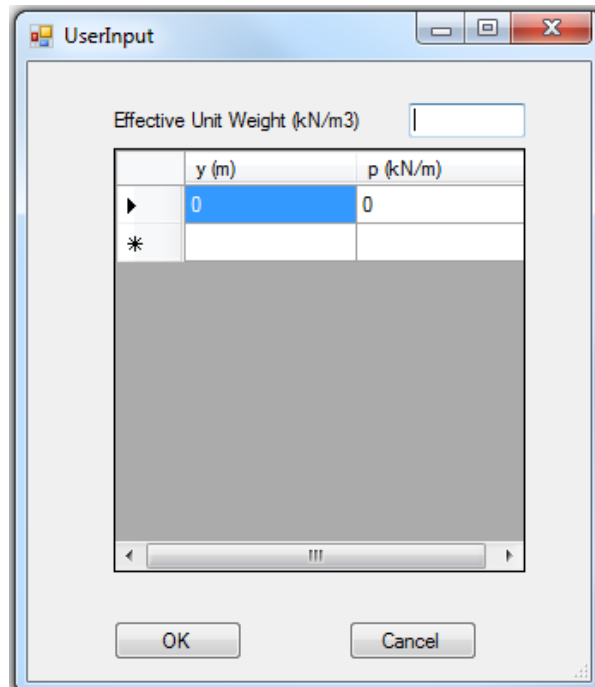
FIGURE 3.15
Required Input for User-Defined *p-y* Curves

3.16 Edit

The "**Edit**" button is used to enter soil parameters and also used to change the soil parameters. If soil parameters need to be changed, including the soil layer and elevation of the soil layer, the "**Edit**" button should be clicked to allow the SSM to recognize the change. The user can use the "**Profile**" button each time to visually check whether the change was successful.

3.17 Profile

Once input or modification of soil parameters is complete, the user can view the soil profile in relation to the pile head and ground surface by clicking the "**Profile**" button, as

illustrated in Figure 3.16. In addition, the profile view also presents the scour depth if a value is assigned for scour.
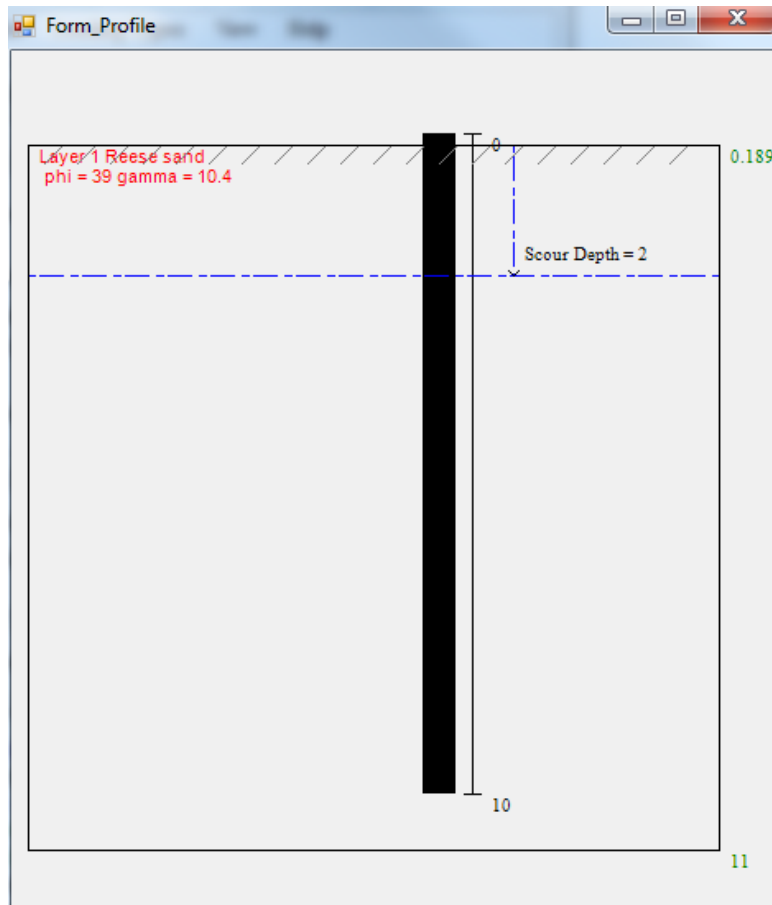
FIGURE 3.16
Profile of Soil and Pile in the SSM

3.18 Generation

The "**Generation**" button is used to generate the *p-y* curves based on the input parameters, and calculates the initial elastic spring stiffness and nonlinear spring stiffness for the soil springs in each soil layer. This function should be executed *after* inputting pile and soil parameters. If any existing parameters are modified, the user should click the "**Generation**" button to update the soil springs after every change.

25

3.19 Elastic Soil Springs

The "**Elastic Soil Springs**" button is automatically activated for use after the "**Generation**" command has been executed by the user. If a single pile is to be applied with soil springs, then click the "**Elastic Soil Springs**" button. The SSM will split the selected pile in STAAD.Pro according to the increment number and assign the elastic soil springs to the newly discretized pile elements. The user can continue to assign the elastic soil springs to another pile as long as the newly selected pile has the same dimensions as the previous one. Elastic soil springs can also be assigned to a pile group that consists of piles having the same dimensions. To do this, select the pile group in STAAD.Pro, and click "**Elastic Soil Springs**" in the SSM. The user can also select other pile group with the same configuration to be applied with soil springs. Figure 3.17 presents a pile group in a structure model after elastic soil springs have been assigned to it.
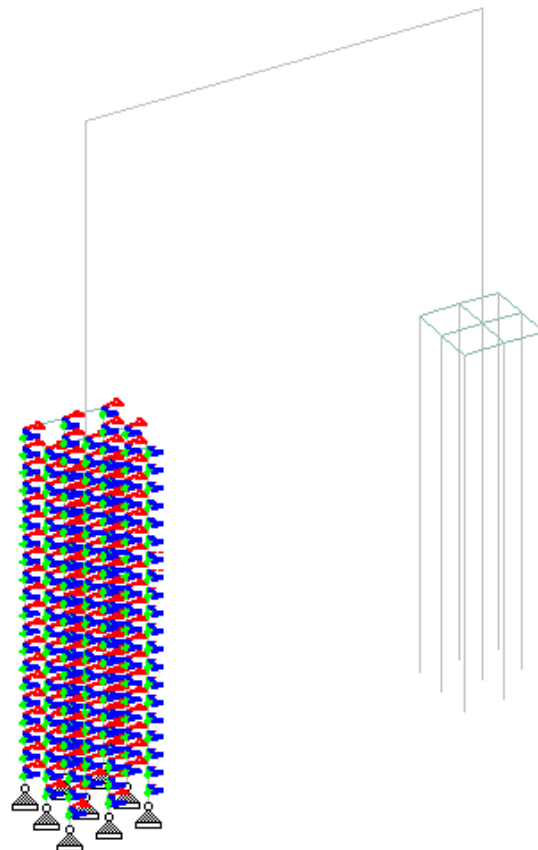
FIGURE 3.17
Structure Model in STAAD.Pro after
One of Its Pile Groups Has Been
Assigned Elastic Soil Springs

3.20 Multilinear Soil Springs

Multilinear soil springs are used to approximately represent the true behavior of nonlinear soil springs. All elastic soil springs should be applied to the piles *before* multilinear soil springs are assigned. Multilinear soil springs can be assigned to the piles which elastic soil springs have been applied to previously, with no need to select piles again because the SSM can store all the information for the selected piles during the assigning of elastic soil springs. After assigning multilinear soil springs, they will replace the previous elastic soil springs in the structure model. By clicking the "**Multilinear soil springs**" button, the structure model will be updated by going through a quick *close* and *open* process which may be interrupted by pop-up message box asking the user to save the current model as shown in Figure 3.19. If this occurs, the user must click "Yes" to continue the process.
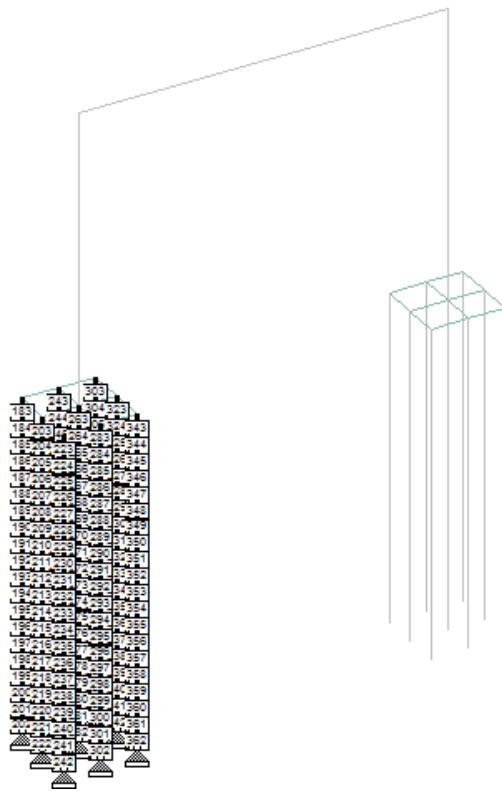
FIGURE 3.18
Structure Model in STAAD.Pro after One of Its Pile Groups Is Applied with Multilinear Soil Springs
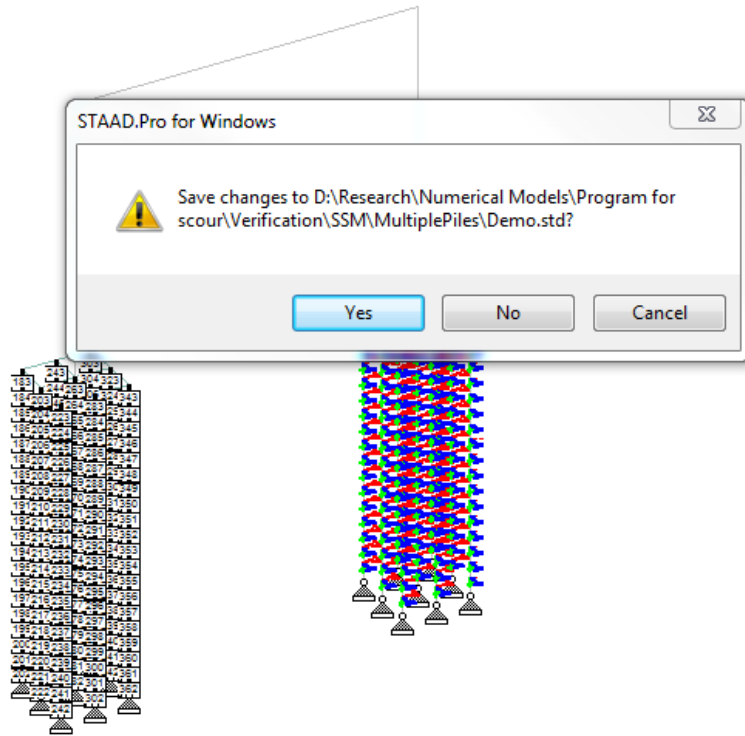
FIGURE 3.19
Structure Model Updated During the Assignment of
Multilinear Soil Springs

3.21 Scour

To run a scour analysis, the scour depth that is measured from the original ground line should be added to the textbox, as shown in Figure 3.20. Once a scour depth has been assigned, "**Profile**" will show the scour depth in the profile, also shown in Figure 3.20. Once scour depth has been inputted, two methods are available for the user to apply scour depth to the pile foundations. The SSM can assign the same scour depth to all the piles by clicking the "**Scour**" button. Alternatively, the SSM can also assign a specific scour depth to selected piles, but this approach requires selection of the pile nodes as indication of the desired scour depth. After selecting the piles, clicking the "**Scour**" button will assign scour depth to the selected piles. In general, the "**Scour**" function allows the user to simulate scour to not only part of the pile foundations as desired, but also to all the pile foundations.
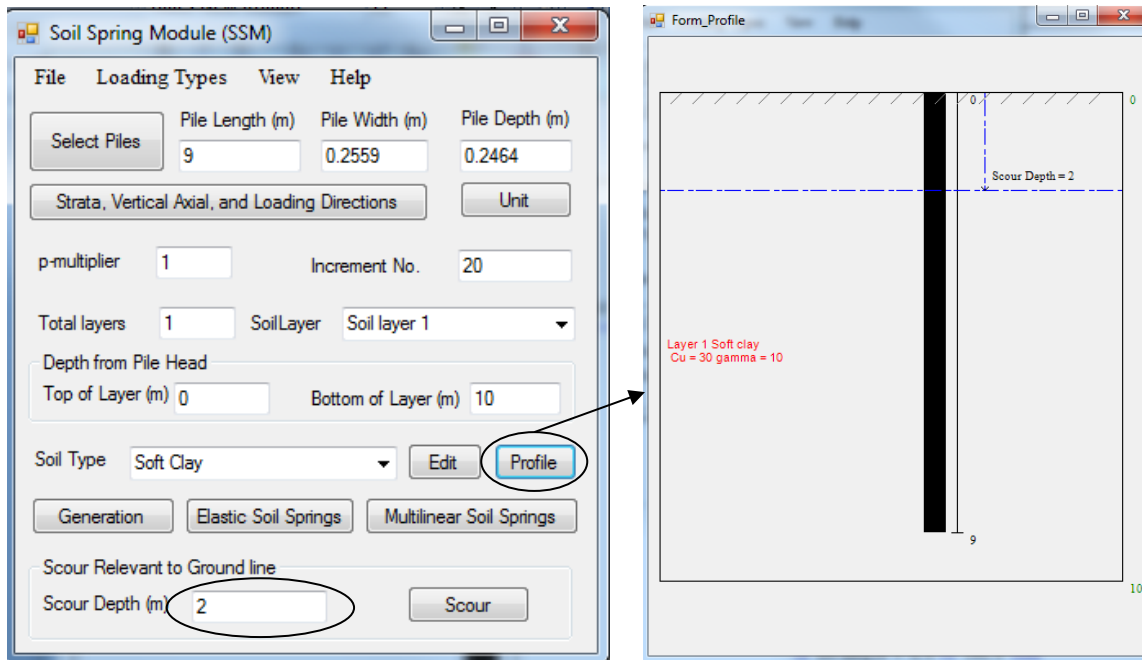
FIGURE 3.20
Illustration of Input of Scour Depth and Profile Graph

3.22 P-Delta Analysis

P-Delta effects should be analyzed through the SSM since STAAD.Pro is unable to consider second-order effects in models that contain multilinear spring conditions. First, the load case in STAAD.Pro which will produce the lateral displacement of bridge piers and piles needs to be added in the SSM. First-order analysis is executed after input of the load case. Finally, the P-Delta analysis should be performed after the execution of the first-order analysis. The user is cautioned that the P-Delta analysis option in the SSM is still approximate and the theory is documented in the technical description.

29

Chapter 4: Technical Description of Soil Spring Module

The SSM was developed to enable users of STAAD.Pro to analyze laterally loaded pile foundations in such a way that soil-structure interaction is accounted for. By incorporating the SSM, STAAD.Pro is able to evaluate an entire bridge including both structural elements and soils in an integrated system. In principle, the SSM serves to generate lateral soil resistance for the piles embedded in the soils. The soil resistance is represented by a series of soil springs which are derived from families of *p-y* curves as illustrated in Figure 4.1. These springs are Winkler springs and independent to each other. The *p-y* curves reflect the nonlinear relationship between soil resistance, *p,* and lateral displacement of the pile at each depth, *y;* these curves were developed based on full-scale tests. The *p-y* curves differ among different types of soil. Even within the same soil type, *p-y* curves can also vary with loading type, soil depth, and pile diameter. The *p-y* curves in the SSM are consistent with those embedded in LPILE 4.0. The theory of each *p-y* method in static loading conditions is described herein, and the user can also find details of the *p-y* theories in the book by Reese and Van Impe (2001) and the API (1987).
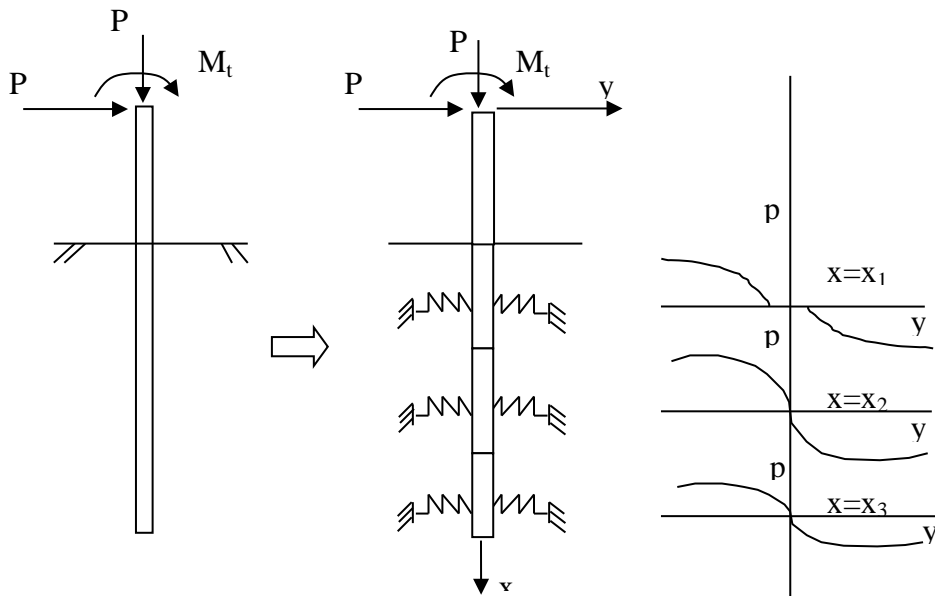
(Source: Reese and Van Impe 2001)

FIGURE 4.1
Illustration of *p-y* Curves Used in a Pile Analysis

4.1 The *p-y* Curves for Laterally Loaded Piles

4.1.1 Soft Clay

The following *p-y* curve used for soft clay in the SSM is applicable for short-term static loading (Matlock 1970), and is characterized by the relationship shown in Equation 4.1, which is illustrated in Figure 4.2.

$$p = \frac{p_{ult}}{2}\left(\frac{y}{y_{50}}\right)^{1/3}$$

Equation 4.1

where y_{50} is the lateral displacement at one-half the ultimate soil resistance as given in Equation 4.2; and p_{ult} is the ultimate soil resistance, using the smaller of the values given by Equations 4.3 and 4.4.

$$y_{50} = 2.5\varepsilon_{50}b$$

Equation 4.2

where ε_{50} is the strain when stress is equal to one-half the soil strength and *b* is the pile diameter.

$$p_{ult} = \left[3 + \frac{\gamma'}{c_u}z + \frac{J}{b}z\right]c_u b$$

Equation 4.3

where γ' is the average effective unit weight of the soil, *z* is the depth from ground line, C_u is the average undrained shear strength of the soil, and *J* is a constant, frequently taken as 0.5.

$$p_{ult} = 9c_u b$$

Equation 4.4

When lateral displacement, y, exceeds $15y_{50}$, the soil resistance, p, will remain constant at p_{ult}, as presented in Figure 4.2.
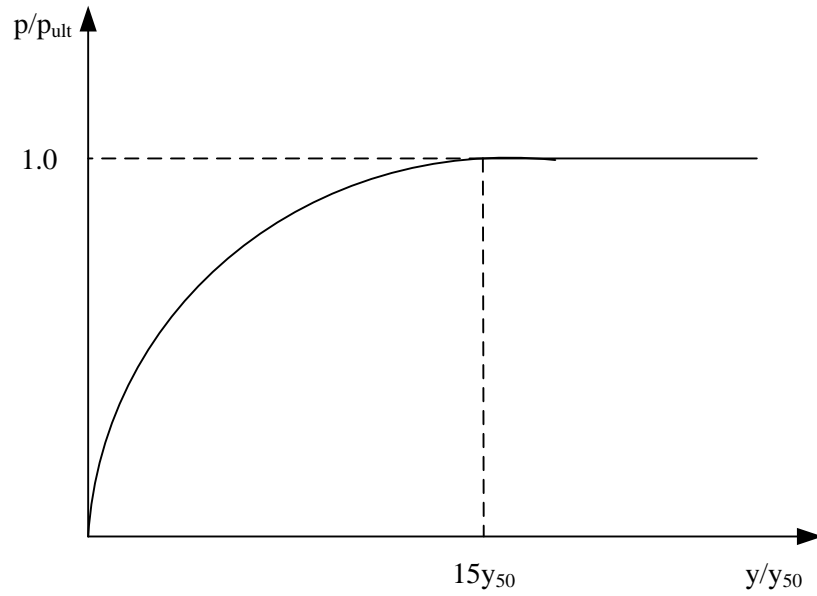
(Source: Reese and Van Impe 2001)

FIGURE 4.2
Illustration of the *p-y* Curves for Soft Clay

4.1.2 Stiff Clay in the Presence of Free Water

The *p-y* curves for stiff clay in the presence of free water described below are for short-term static loading. The *p-y* curves mainly consist of five parts, as seen in Figure 4.3.
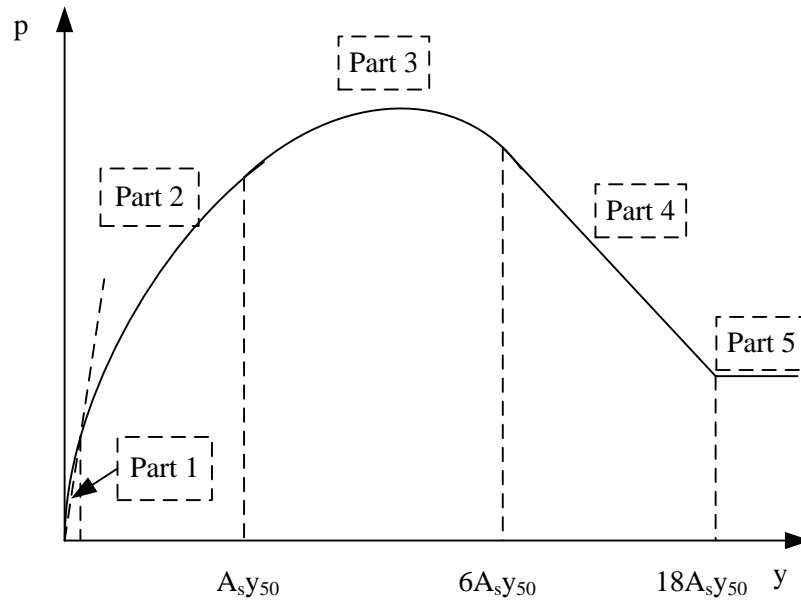
(Source: Reese and Van Impe 2001)

FIGURE 4.3
Illustration of the *p-y* Curves for Stiff Clay in the Presence of Free Water

Part 1: Initial Straight-Line Portion of the p-y Curve Is Established As Given by Equation 4.5

$$p = (k_s z) y$$

Equation 4.5

where k_s is the coefficient of subgrade reaction as tabulated in Table 3.3.

Part 2: the First Parabolic Portion of the *p-y* Curve Is Established As Given by Equation 4.6

33

$$p = \frac{p_{ult}}{2}\left(\frac{y}{y_{50}}\right)^{1/2}$$

where p_{ult} chooses the smaller of the values given by Equations 4.7 and 4.8; y_{50} is determined by Equation 4.9.

$$p_{ult} = \left[2 + \frac{\gamma'}{c_u}z + \frac{2.83}{b}z\right]c_u b$$

$$p_{ult} = 11c_u b$$

$$y_{50} = \varepsilon_{50}b$$

Part 3: the Second Parabolic Portion of the *p-y* Curve Is Established As Given by Equation 4.10

$$p = \frac{p_{ult}}{2}\left(\frac{y}{y_{50}}\right)^{0.5} - 0.055 p_{ult}\left(\frac{y - A_s y_{50}}{A_s y_{50}}\right)^{1.25}$$

where A_s is a constant for y_{50}, which can be determined in the figure below.

A_s or A_c

0   0.2   0.4   0.6   0.8   1

z/b

A_c A_s
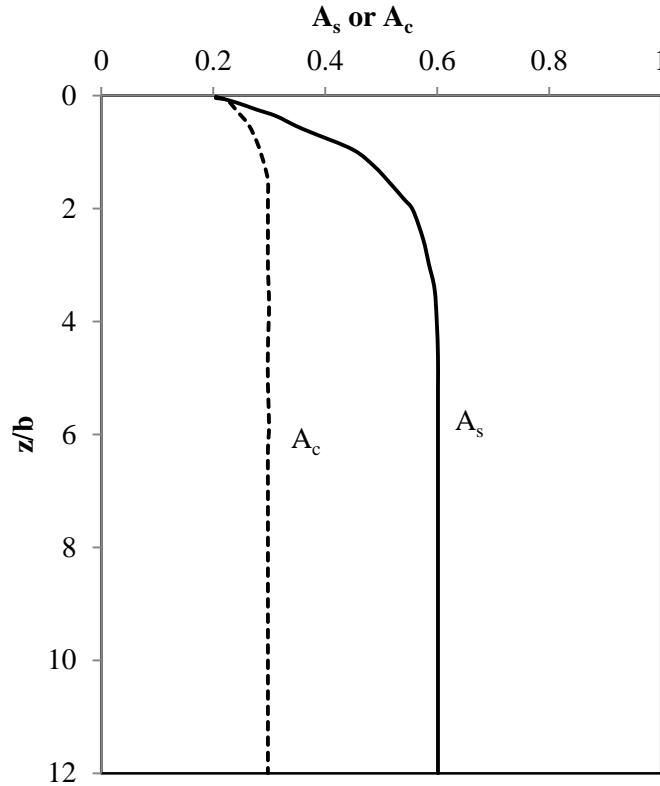
(Source: Reese and Van Impe 2001)

FIGURE 4.4
Values of Constants A_c and A_s

Part 4: the Next Straight-Line Portion of the *p-y* Curve Is Established As Given by Equation 4.11

$$p = \frac{p_{ult}}{2}\left(6A_s\right)^{0.5} - 0.411p_{ult} - \frac{0.0625}{y_{50}}p_{ult}(y - 6A_s y_{50})$$

Equation 4.11

Part 5: the Final Straight-Line Portion of the *p-y* Curve Is Established as Given by Equation 4.12

$$p = p_{ult}(1.225\sqrt{A_s} - 0.75A_s - 0.411)$$

Equation 4.12

35

4.1.3 Stiff Clay above Free Water

The *p-y* curves for stiff clay above free water are similar to those for soft clay. The minor difference is the *p-y* relationship, and the relationship for stiff clay above free water is given in 4.13:

$$p = \frac{p_{ult}}{2}\left(\frac{y}{y_{50}}\right)^{0.25}$$

Equation 4.13

4.1.4 Reese Sand

The *p-y* curves for Reese sand are established by four parts as presented in Figure 4.5 and are described below.

Part 1: Establish the First Linear Portion of the *p-y* Curve Given Below

$$p = (k_{py}z)y$$

Equation 4.14

Use the appropriate value of k_{py} from Tables 3.6 and 3.7.

Part 2: Establish the Parabolic Portion of the *p-y* Curve Given Below

$$p = Cy^{1/n}$$

Equation 4.15

where *C* and *n* can be determined by Equations 4.16, 4.17, and 4.18.

Part 3: Establish the Second Straight-Line Portion of the *p-y* Curve Given Below

$$m = \frac{p_u - p_m}{y_u - y_m}$$

Equation 4.16

36

$$n = \frac{p_m}{my_m}$$

<div align="right">**Equation 4.17**</div>

$$C = \frac{p_m}{y_m^{1/n}}$$

<div align="right">**Equation 4.18**</div>

where $y_u=3b/80$; $y_m=b/60$; $p_u =A_s p_s$; $p_m =B_s p_s$; p_s is the ultimate soil resistance which is determined by selecting the smaller value calculated in Equations 4.19 and 4.20; A_s and B_s can be determined using Figures 4.6 and 4.7.

$$p_{st} = \gamma ' z[\frac{K_o z \tan \varphi ' \sin \beta}{\tan(\beta - \varphi ')\cos \alpha} + \frac{\tan \beta}{\tan(\beta - \varphi ')}(b + z \tan \beta \tan \alpha)$$
$$+K_o z \tan \beta (\tan \varphi ' \sin \beta - \tan \alpha) - K_a b]$$

<div align="right">**Equation 4.19**</div>

$$p_{sd} = K_a b\gamma ' z(\tan^8 \beta - 1) + K_o b\gamma z \tan \phi ' \tan^4 \beta$$

<div align="right">**Equation 4.20**</div>

where

$$\alpha = \frac{\varphi '}{2}; \beta = 45 + \frac{\varphi '}{2}; K_o = 0.4; K_a = \tan^2(45° - \frac{\varphi '}{2})$$

Part 4: The Displacement at Which the Initial Linear Portion and the Parabolic Section Intersect Can Be Determined by Equation 4.21

$$y_k = \left(\frac{C}{k_{py}z} \right)^{\frac{n}{n-1}}$$

<div align="right">**Equation 4.21**</div>
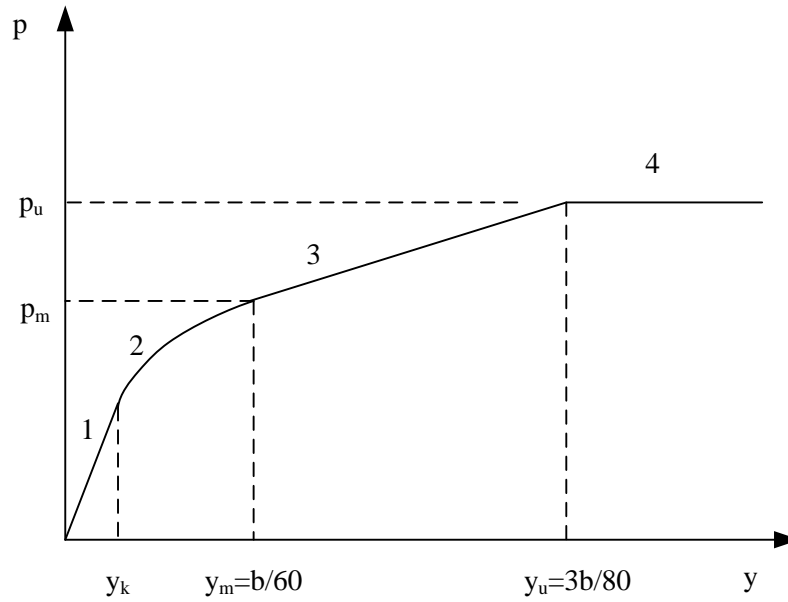
(Source: Reese and Van Impe 2001)

FIGURE 4.5
Illustration of the *p-y* Curves for Reese Sand
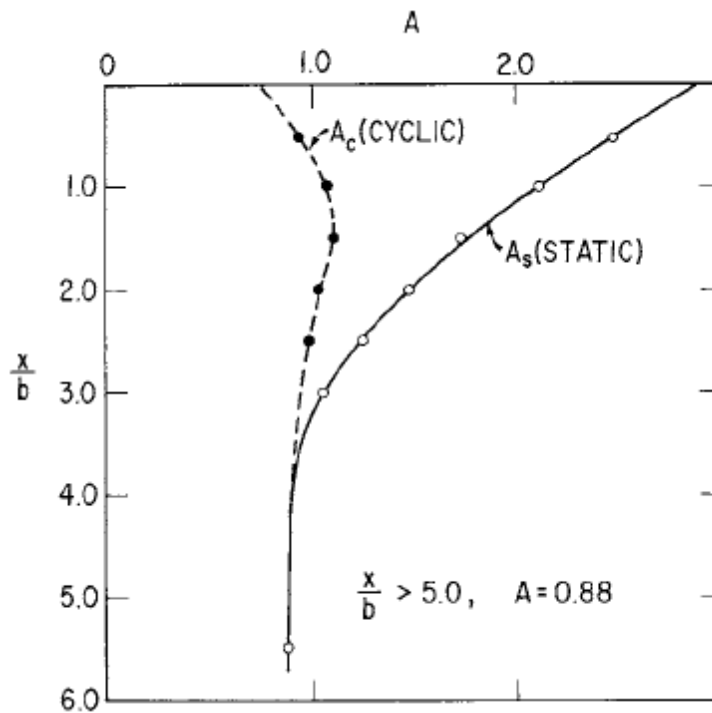
(Source: Reese and Van Impe 2001)

FIGURE 4.6
Values of Coefficients for A for Reese Sand
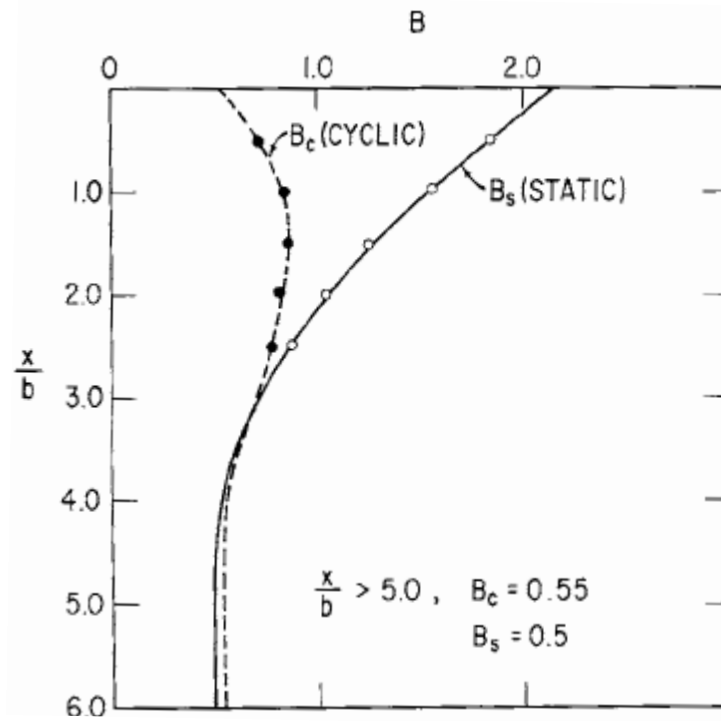
(Source: Reese and Van Impe 2001)

FIGURE 4.7
Values of Coefficients for B for Reese Sand

4.1.5 API Sand

The *p*-y relationship for API sand is characterized by a more convenient hyperbolic equation. The calculations for the ultimate soil resistance for API sand and Reese sand are the same.

$$p = Ap_u \tanh\left(\frac{kz}{Ap_u} y\right)$$ **Equation 4.22**

where $A = (3.0 - 0.8x/b) \geq 0.9$; p_u is the ultimate soil resistance, using the smaller value computed from Equations 4.19 and 4.20; k is the coefficient of subgrade reaction, and can be determined in Figure 3.9, z is the depth from ground line.

4.1.6 Silt, a Both Cohesion and Internal Friction Soil (c-φ Soil)

The procedure for establishing *p-y* curves for the *c-φ* soil (silt) is similar to that described for Reese sand; the only difference is that the ultimate soil resistance for *c-φ* soil is the combination of the ultimate soil resistance of sand and soft clay as presented in Equations 4.23 and 4.24.

$$p_m = 1.5 p_{u\phi} + p_{uc}$$

Equation 4.23

$$p_u = A_s p_{u\phi} + p_{uc}$$

Equation 4.24

where A_s can be determined in Figure 4.6; $p_{u\phi}$ is the ultimate soil resistance of sand, the smaller value computed from Equations 4.19 and 4.20; p_{uc} is the ultimate soil resistance of soft clay, the smaller value computed from Equations 4.3 and 4.4.

The general shape of *p-y* curve for the *c-φ* soil is shown in Figure 4.8.
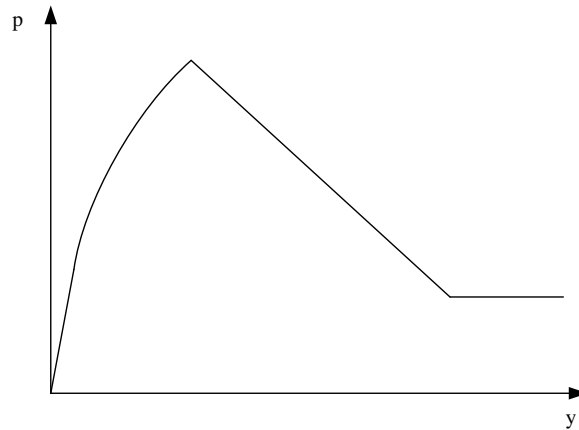
(Source: Reese and Van Impe 2001)

FIGURE 4.8
Illustration of the *p-y* Curves for *c-φ* Soil

4.1.7 Strong Rock

The procedure for generating *p-y* curves for strong rock can be easily established using the relationships presented in Figure 4.9. Strong rock refers to the material having a compressive strength for the intact specimen, q_{ur}, greater than 6.9 MPa (1000 psi). In Figure 4.9, S_u represents the compressive shear strength which is one-half the value for q_{ur}. The *p-y* curve shown in Figure 4.9 is recommended for interim use. As it was establish based on limited experiments and a great variability of properties exist for rock, the *p-y* curve should be used with judgment and caution.
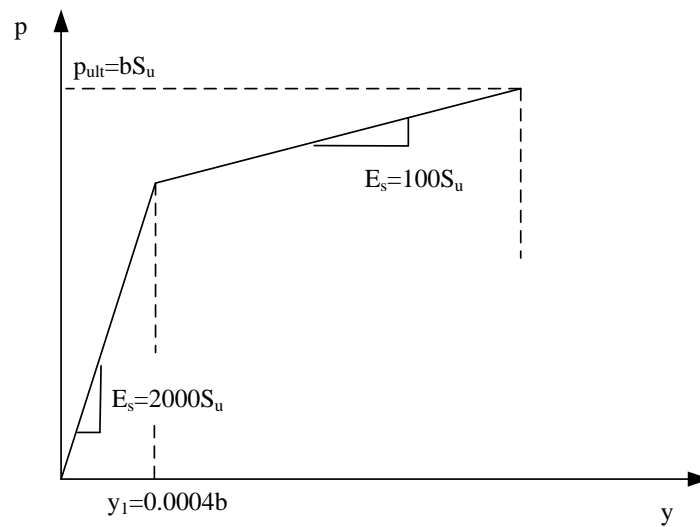
(Source: Reese and Van Impe 2001)

FIGURE 4.9
Illustration of the *p-y* Curves for Strong Rock

4.1.8 Weak Rock

In contrast to strong rock, weak rock has a small compressive strength, normally less than 6.9 MPa (1000 psi). Similar to those for strong rock, the *p-y* curves for weak rock included in the SSM should be used with caution. The general procedure used to develop the *p-y* curves for weak rock are stated in Equations 4.25, 4.26, 4.27, and 4.28. A typical *p-y* curve for weak rock based on this procedure is illustrated in Figure 4.10.

$$p = K_{ir}\, y \qquad\qquad \text{for } y \leq y_A \qquad\qquad \textbf{Equation 4.25}$$

$$p = \frac{p_{ur}}{2}\left(\frac{y}{y_{rm}}\right)^{0.25} \qquad\qquad \text{for } y > y_A \, , \, P < P_{ur} \qquad \textbf{Equation 4.26}$$

$$p = p_{ur} \qquad\qquad \text{for } y > 16\, y_{rm} \qquad\qquad \textbf{Equation 4.27}$$

$$y_{rm} = k_{rm}\, b \qquad\qquad\qquad\qquad \textbf{Equation 4.28}$$

where K_{ir} can be determined from Equation 4.29; p_{ur} can be estimated from Equations 4.30 and 4.31 by using a smaller value; y_A can be calculated from Equation 4.32; k_{rm} is a constant with the values ranging from 0.0005 to 0.00005; and *b* is the pile diameter.

$$K_{ir} \cong k_{ir}\, E_{ir} \qquad\qquad\qquad \textbf{Equation 4.29}$$

where E_{ir} is the initial modulus of rock and can be approximately estimated Figure 3.12 or Figure 3.14, and

$$k_{ir} = \left(100 + \frac{400 x_r}{3b}\right) \text{ for } 0 \leq x_r \leq 3b, \text{ and } 500 \text{ for } x_r > 3b, \text{ and } x_r \text{ is depth from ground}$$

$$p_{ur} = \alpha_r q_{ur} b \left(1 + 1.4 \frac{x_r}{b} \right)$$

$$p_{ur} = 5.2 \alpha_r q_{ur} b$$

where q_{ur} is compressive strength of the rock; α_r is strength reduction factor, 1/3 for RQD of 100 and linearly increases to 1 at RQD of zero.

$$y_A = \left(\frac{p_{ur}}{2(y_{rm})^{0.25} K_{ir}} \right)^{1.333}$$
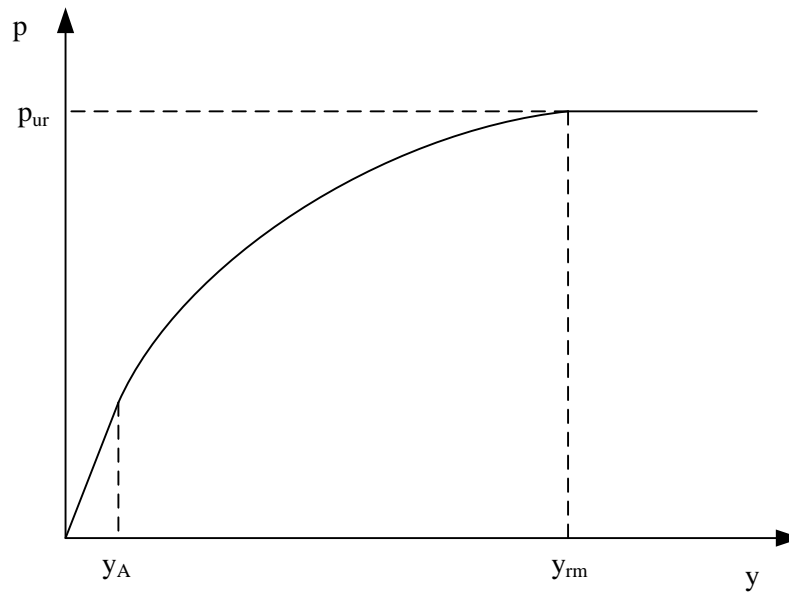
(Source: Reese and Van Impe 2001)

FIGURE 4.10
Illustration of the *p-y* Curves for Weak Rock

4.2 The *p-y* Curves for the Layered Soil

As the characteristics of *p-y* curves are primarily dependent on the ultimate soil resistance, the SSM adopted the approach used by Georgiadis (1983) for the analysis of layered soil problems. In this approach, an upper and lower layer of soil are considered such that the layered soil can be treated as a single layer (the lower layer). To accomplish this, the process involves seeking an equivalent soil thickness (L_{eq}) so that the calculated lateral ultimate resistance force using the soil parameters of the lower layer (soil 2) and L_{eq} is equal to that of the upper layer (soil 1). An equivalent depth used by the second layer is thus calculated based on the equal ultimate resistance forces, as calculated in Equations 4.33 and 4.34. By equating Equation 4.33 to 4.34, the equivalent depth, L_{eq} can be calculated. Then, the first layer soil with the depth from the ground to L_1 can be substituted by the soil of the second layer with the depth from ground to L_{eq}, and the real locations of the second layer are also modified by adjusting its top elevation, L_2, to L_{eq}.

$$F_{ult} = \int_0^{L_1} p_{ult1} dz$$

Equation 4.33

$$F_{ult} = \int_0^{L_{eq}} p_{ult2} dz$$

Equation 4.34

where F_{ult} is the ultimate lateral resistance force, F (e.g. kN); p_{ult1} and p_{ult2} are the ultimate soil resistance, F/L (e.g. kN/m), as described in the previous section; z is the depth from ground line, L; L_1 is the depth of the top layer, L; L_{eq} is the equivalent depth used by the underlying layer, L.

4.3 Generation of Elastic Soil Springs

Elastic soil springs, K_e, are calculated in accordance with the relationship presented in Equation 4.35.

$$K_{ei} = k_{oi} \times L_i$$

In Equation 4.35, k_{oi} is the initial slope of the p-y curve at a given depth, z_i, and L_i is the corresponding element length at z_i, as shown in Figure 4.11. The units of K_{ei}, and k_{oi}, respectively, are force per unit length (F/L) and force per unit length squared (F/L^2).
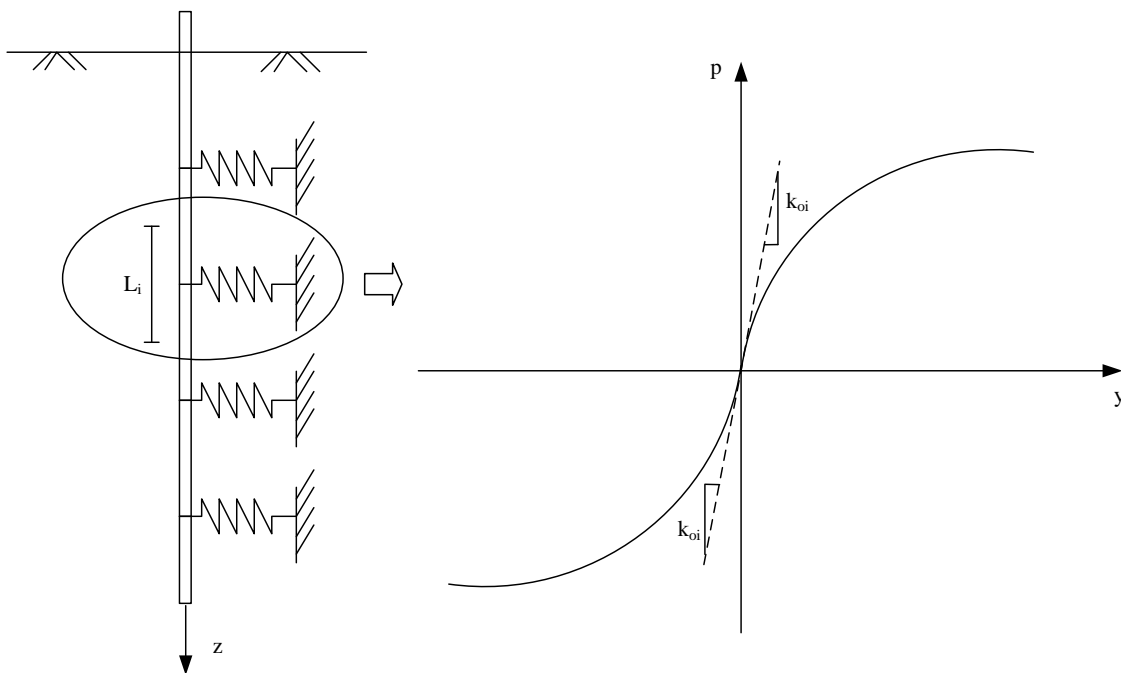
FIGURE 4.11
Illustration of Generation of Elastic Soil Springs

4.4 Generation of Multilinear Soil Springs

Generating multilinear soil springs should be performed after the elastic soil springs have been generated. The multilinear soil springs are generated using piecewise sloped lines to approximate the nonlinear p-y curve, as depicted in Figure 4.12, and then multiplying the slope of that p-y curve segment by the element length, L_i. The multilinear soil springs are thus not only dependent on soil depth but also on lateral displacement, given by Equation 4.36:

$$K_{ij} = k_{ij} \times L_i$$

Equation 4.36

In Equation 4.36, K_{ij} respresents the multilinear soil spring stiffness at given soil depth, z_i, and lateral displacement, y_j; k_{ij} is the slope of the p-y curve at y_j and z_i; and L_i is the corresponding element length at x_i, as shown in Figure 4.12. The units of K_{ij}, and k_{ij} are F/L and F/L^2, respectively.
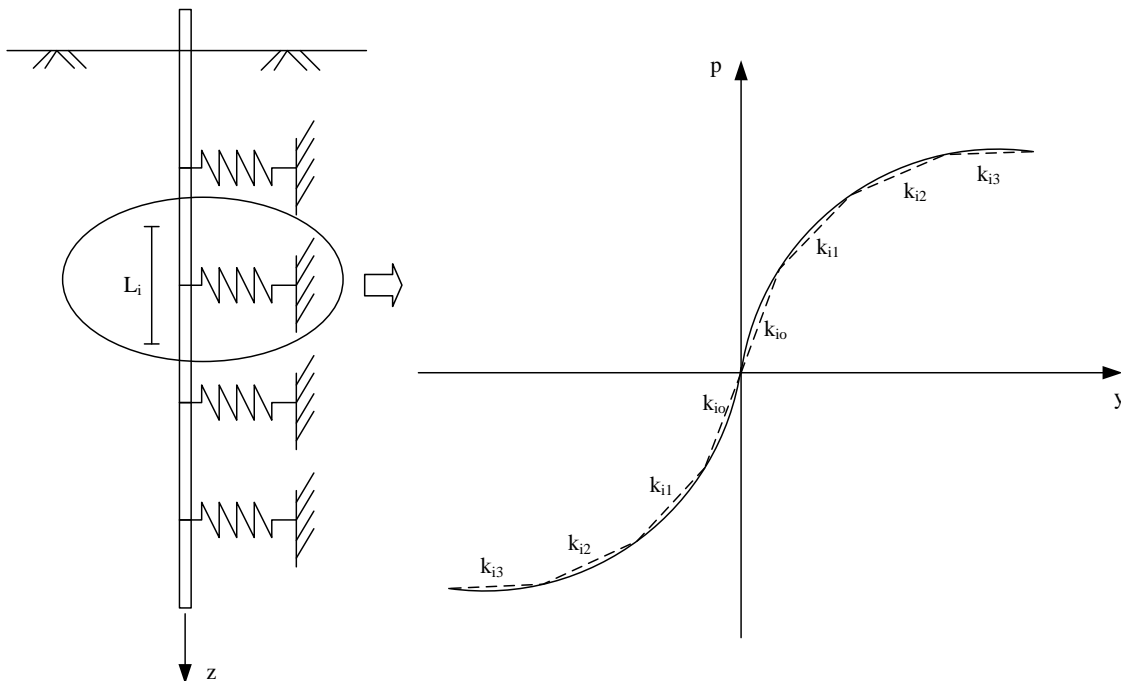
FIGURE 4.12
Approximation of Multilinear Lines to Nonlinear *p-y* Curves

4.5 Scour Analysis

A scour analysis can be performed after a specific scour depth has been inputted (with reference to the original ground line). The SSM achieves the scour analysis by recalculating the soil spring stiffnesses (either elastic or multilinear) for the structure model in STAAD.Pro, rather than simply removing the existing soil springs from the structure. This is because the ground surface after scour changes from original location to a new location at the scour depth, which indicates that the same point in the soil has smaller relative soil depth to the ground surface after scour than before scour, as illustrated in Figure 4.13. Since soil spring stiffness increases with soil depth, if the original ground surface were used as the reference the calculated soil springs would be stiffer than they would if the new ground surface was used. Therefore, the existing soil springs cannot be simply removed, as the remaining soil springs were calculated by referring the soil depth to the original ground surface. Instead, the soil springs in the remaining soil are recalculated in reference to the new ground surface. In fact, the real soil stress lies in between conditions (a) and (b) in the figure where condition (a) leads to aggressive analysis and condition (b) results in conservative analysis. In the SSM, the conservative analysis approach (b) for scour analysis is considered.
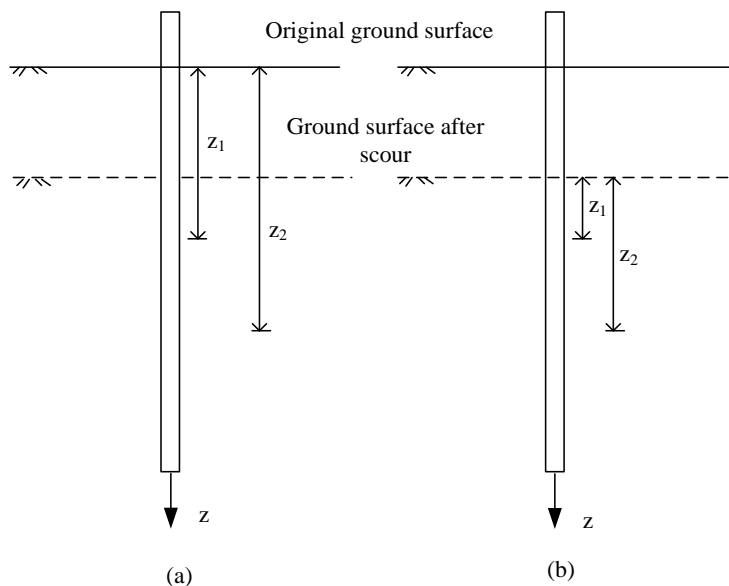
FIGURE 4.13
Changes of Soil Depth with the Change of Ground
Surface after Scour: (a) Removal of the Existing
Soil Springs; (b) Re-Calculation of the Soil Springs
Using the New Soil Depth

4.6 P-Delta Analysis

In STAAD.Pro, a P-Delta analysis can only be performed if frame elements are used in the structure model. P-Delta effects cannot be calculated in models that use solid-type elements. Another limitation to performing a second-order analysis in STAAD.Pro is that a P-Delta analysis cannot be performed when a model includes multilinear springs. Since the models discussed so far inherently rely on the use of multilinear springs, and it is readily acknowledged that consideration of second-order stability effects should not be neglected in this application, it was deemed important to capture P-Delta effects in an approximate sense in the developed model framework. Therefore, an approximate approach to capturing second-order effects has been used in the SSM, as illustrated in Figure 4.14. This approximate solution uses linear secant springs calculated under lateral loading in the P-Delta load case, substituted in the model for the original multilinear spring. The P-Delta analysis is thus achieved using the secant spring supports. Two analyses are required to achieve the approximate second-order solution. The first analysis is performed to calculate the lateral displacements for each node of the pile under the lateral loading case, which employs the "first order analysis" in STAAD.Pro, and requires the input of the load case to be used for the P-Delta analysis. Once the lateral displacements are obtained, elastic secant stiffnesses are calculated from the *p-y* curves for the various springs at different depths, as shown in Figure 4.14 (b). Next, the computed linear secant springs are used to replace all the multilinear springs in the original model. With the elastic secant spring supports, the P-Delta analysis is performed, as presented in Figure 4.14 (c).
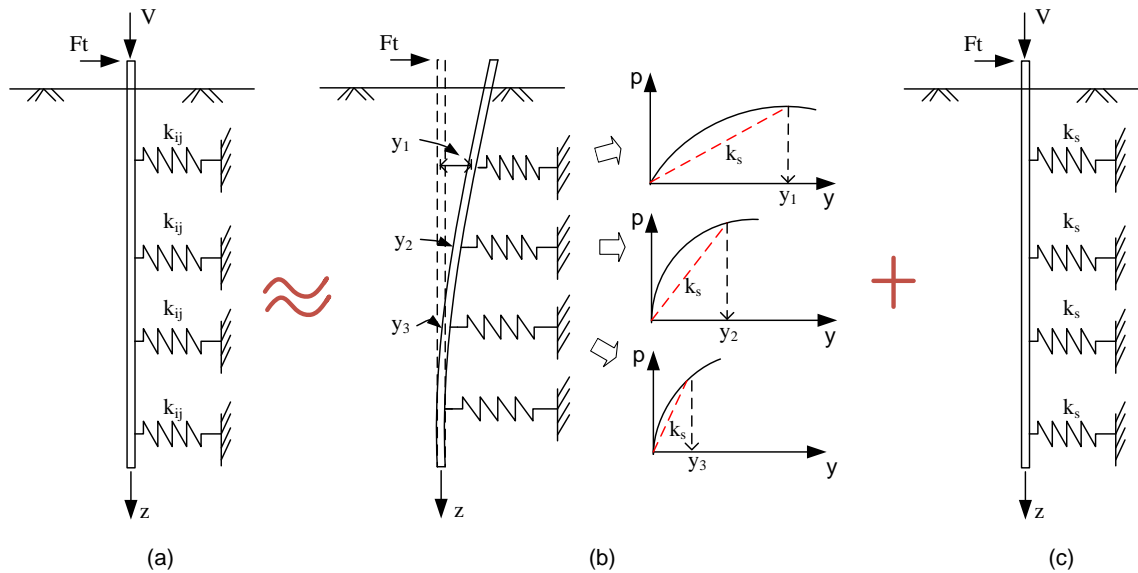
FIGURE 4.14
Approximate Solution for P-Delta Effect: (a) P-Delta Analysis under Multilinear Soil Springs; (b) Calculation of Displacements under Lateral Loading and Corresponding Elastic Secant Springs; (c) P-Delta Analysis Using Elastic Secant Spring Supports

4.7 Development of the SSM

The program structure of the SSM is illustrated in Figure 4.15. The component names in the program structure correspond to the command functions described in the previous chapters. The program structure mainly includes a subroutine of inputted pile and soil parameters, a subroutine for the generation of p-y curves and soil springs, a subroutine for the assignment of soil springs, and a subroutine for scour analysis and P-Delta analysis. The pile parameters that the SSM retrieves from STAAD.Pro are achieved using OpenSTAAD functionality. OpenSTAAD also enables the assignment of the elastic and multilinear soil springs from the SSM to the structure model in STAAD.Pro.
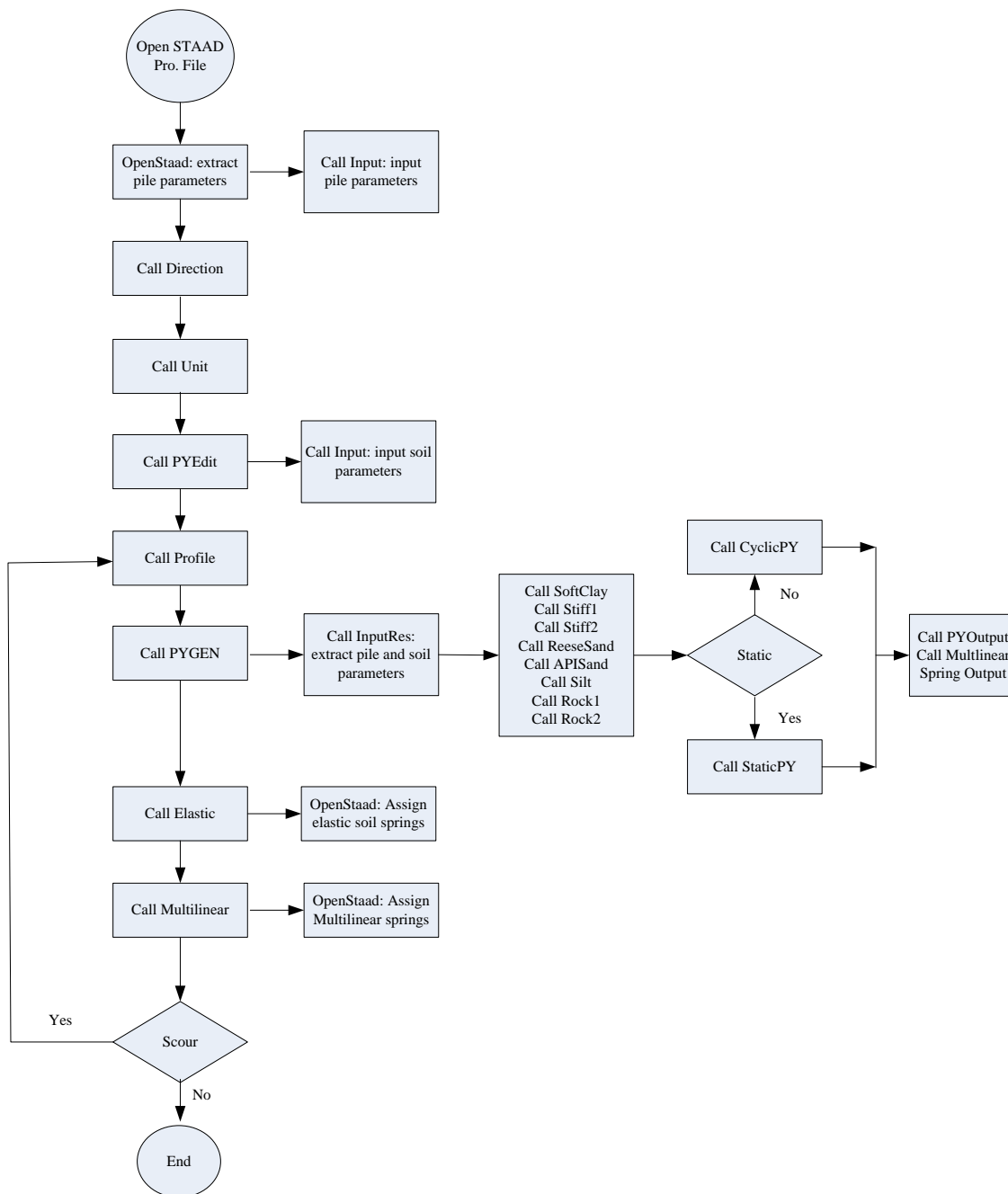
FIGURE 4.15
Flow Chart of the SSM

Chapter 5: Buckling Capacity of the Bridge and Bridge Piles under Scour Conditions

Stability issues for the bridge and bridge components are of concern in the evaluation of bridge susceptibility to scour events. The following discussion describes one method for determining the buckling susceptibility of a system (bridge superstructure and bridge piles), and for determining the buckling susceptibility of just the piles, using the buckling analysis function in STAAD.Pro 2007. The buckling analysis available in STAAD.Pro (2007) computes the elastic buckling loads for frame structures by estimating the buckling factors under primary load cases. The buckling loads are simply the product of the applied loads and the computed buckling factors. For each primary load case, four buckling factors corresponding to four buckling failure modes are provided. The principle for computation of buckling capacity is detailed in the technical manual of STAAD. Pro 2007 (Bentley System Inc. 2007). In the following sections, procedures are proposed for determining the buckling susceptibility of the bridge and bridge piles under different scour depths. Additionally, application of each of these techniques is discussed further in the last example presented in Chapter 6, in Section 6.4.

5.1 Buckling Capacity of the Bridge

To analyze the buckling capacity of a bridge system, select the "**Perform Buckling Analysis**" engine in STAAD.Pro. The buckling factor and corresponding elastic buckling failure modes are then directly calculated by STAAD.Pro. It should be noted that even though structures under lateral loading can be analyzed using the buckling function in STAAD.Pro, the results are erroneous. Additionally, if lateral loads and vertical loads are defined as different primary load cases, the primary load case for vertical load should be placed in front of that for lateral load. Otherwise, for unknown reasons, the presence of the lateral load case in front of the vertical load case can lead to abnormal and incorrect buckling factors. As a result, it is recommended to combine different loads under one primary load case when utilizing the buckling analysis function in STAAD. Pro 2007.

5.2 Buckling Capacity of the Bridge Piles

The buckling capacity of individual bridge piles cannot be accurately calculated when the entire bridge is analyzed using the IAP. However, from the holistic analysis of the bridge, the superstructure stiffnesses can be examined at the locations where the piles are connected to the superstructure. By applying the superstructure stiffnesses to the pile head (in a separate STAAD.Pro model), the buckling capacity of the pile can be determined in the individual single pile model. In practice, without having the benefit of knowledge regarding superstructure stiffnesses, pile head boundaries are often assumed to be either free or fixed during computation of pile buckling capacities; these assumptions may result in either conservative or unconservative buckling capacities, respectively. As a result, with the IAP approach, buckling analysis of single pile will become more rational since pile boundary conditions are indeed known.

To obtain the buckling capacity of the pile in the single pile model, the superstructure stiffnesses for the pile head must first be determined. Prior to determining the superstructure stiffnesses for the pile head, it should be understood that stiffnesses at a pile head are comprised of contributing stiffnesses from superstructure (i.e. pile cap) and soils as given by Equation 5.1:

$$[K]_{\text{tot}} = [K]_{\text{sup}} + [K]_{\text{soil}}$$

Equation 5.1

where $[K]_{\text{tot}}$, $[K]_{\text{sup}}$, and $[K]_{\text{soil}}$ are 6x6 matrix of stiffnesses for pile head, stiffnesses from superstructure, and stiffnesses from soils respectively.

According to Equation 5.1, the superstructure stiffnesses for pile head, $[K]_{\text{sup}}$, can be obtained by subtracting stiffnesses from soils, $[K]_{\text{soil}}$ from total stiffness for pile head, $[K]_{\text{tot}}$. As such, to determine $[K]_{\text{sup}}$, $[K]_{\text{tot}}$ and $[K]_{\text{soil}}$ should be first determined.

Stiffnesses at pile head, $[K]_{\text{tot}}$ may be approximated by $\{K\}_{\text{tot}}$ which is a 1x6 matrix of spring stiffnesses that can be calculated by dividing the loads at pile head by displacement or rotations in the corresponding loading directions as follows:

$$\{F\}_{6\times1} = [K]_{tot,\,6\times6}\{u\}_{6\times1} = \{K\}_{tot,\,1\times6}\{u\}_{6\times1}$$

Equation 5.2

where $\{F\}_{6\times1}$ and $\{u\}_{6\times1}$ are loads and displacements (including three rotations) with their directions in reference to standard coordinate system in STAAD.Pro (i.e. **x**, **y**, and **z** axes). Equation 5.2 is expanded below:

$$\begin{Bmatrix} F_x \\ F_y \\ F_z \\ F_{r_x} \\ F_{r_y} \\ F_{r_z} \end{Bmatrix} = \{K_x, K_y, K_z, K_{rx}, K_{ry}, K_{rz}\} \begin{Bmatrix} x \\ y \\ z \\ r_x \\ r_y \\ r_z \end{Bmatrix}$$

Equation 5.3

where x, y, and z are displacements along **x**, **y**, **z** axes and r_x, r_y, and r_y are the rotations about **x**, **y**, **z** axes. F_x, F_y, F_z, F_{rx}, F_{ry}, and F_{rz} are corresponding forces and bending moments in the displacement directions.

Based on Equation 5.3, the approximate stiffnesses at pile head, $\{K\}_{tot}$, can be determined. The load vector, $\{F\}_{6x1}$ and displacement vector, $\{u\}_{6x1}$ in Equation 5.3 can be determined from the entire bridge analysis using IAP.

Next, $[K]_{soil}$ is also approximated using $\{K\}_{soil}$ with a similar approach to $\{K\}_{tot}$. To determine $\{K\}_{soil}$ from soils, the model for single pile in soils should be established in IAP, separating from the entire bridge model; then the same displacements at pile-head, $\{u\}_{6x1}$ that are calculated from entire bridge model are applied as loads to pile head in the single pile model. After analysis of the single pile using displacement loading, the reaction loads at pile head can be calculated. $\{K\}_{soil}$ is then determined by dividing the reaction loads by the applied displacements.

Once approximate stiffnesses at pile head, $\{K\}_{tot}$, and stiffnesses from soils, $\{K\}_{soil}$, are obtained, the approximated stiffnesses from superstructure, $\{K\}_{sup}$ is given by Equation 5.4:

$$\{K\}_{sup} = \{K\}_{tot} - \{K\}_{soil}$$

<div align="right">**Equation 5.4**</div>

By applying $\{K\}_{sup}$ to the pile head in the model of the individual pile, the buckling capacity of the single pile can be computed in the IAP. A demonstration regarding the calculation of buckling capacity of bridge piles has been detailed in the Example presented in Section 6.4.

Chapter 6: Examples

Chapter 6 of this report presents four examples. The first three examples describe the analysis of a laterally loaded single pile (Section 6.1), a laterally loaded pile group (Section 6.2), and an entire bridge under scour conditions (Section 6.3). The fourth example presents the calculation of the buckling capacity of a bridge and bridge piles (Section 6.4). The examples were originally performed using metric units, but equivalent US units have been provided wherever practical. US units are shown in blue in the tables.

6.1 Response of a Laterally Loaded Single Pile in Soft Clay

This example presents use of the IAP for a single laterally loaded pile. The purpose of this example is to illustrate the basic functionality of the IAP and the SSM in a step-by-step manner.

A laterally loaded single pipe pile in soft clay, representative of a test performed in Lake Austin, TX (Matlock 1970) was analyzed in the IAP. Parameters of the pipe pile and soft clay are tabulated in Tables 6.1 and 6.2. The lateral load was applied to the pile head at a distance 0.0635 m (2.5 in) above the ground line, and the water table was kept above the ground line.

TABLE 6.1
Parameters for the Pipe Pile

Outside diameter, D m (ft)	Inside diameter, d m (ft)	Pile length, L m (ft)	Moment of inertia, I m^4 (ft^4)	Elastic modulus, E kN/m^2 (ksi)	Yielding moment, M_{y1} (kN-m) (k-ft)	Moment at full hinge, M_{y2} (kN-m) (k-ft)
0.319 (1.05)	0.294 (0.96)	12.8 (42)	1.44×10^{-4} (1.7×10^{-2})	2.18×10^{8} (31,618)	231 (170)	304 (224)

(Source: Matlock 1970)

TABLE 6.2
Parameters for the Soft Clay in Lake Austin

Effective unit weight, γ' kN/m^3 (lb/ft^3)	Undrained shear strength, C_u kN/m^2 (lb/in^2)	Strain at 50% of the maximum stress, ε_{50}
10 (63.7)	32.3 (4.67)	0.012

(Source: Matlock 1970)

The following discussion is intended to guide a user to accomplish the analysis step-by-step using IAP.

Step 1: Open STAAD.Pro, create a model of the structure, and assign properties to the model, as shown in Figure 6.1. Once the properties are assigned, select the pile.

Step 2: Open the SSM. By clicking "**Select Piles**"; the pile dimensions are shown in the textboxes. Then, by clicking "**Strata, Vertical Axis, and Loading Directions**", select the directions associated with the deposit of the strata, global vertical axis in STAAD.Pro, and lateral loading in global coordinate system in STAAD.Pro. The default directions are the directions along Y- axis, Y- axis, and +X- axis, respectively. In this case, we'll set the strata deposited along Y- axis. The global vertical axis is the Y- axis as seen in Figure 6.1. The lateral load will be applied to the pile head in the positive X- direction. Once the lateral loading direction has been selected in the SSM, the user should apply the lateral load with the same direction later in STAAD.Pro. For the laterally loaded single pile, the *p*-multiplier is equal to 1.0 because there is no group effect. The increment number for the pile should be set to 20 (considered by the authors to be a reasonable level of discretization for this pile length). Next, assign the soil profile. For the first soil layer, select "**Soil layer 1**" in the "**Soillayer**" drop box. The depth for the soil layer is from 0.06 m to 13 m, measured from the pile head. In the drop "**soil type**", select "**soft clay**" and then use the "**Edit**" button to input the properties of the soft clay, as illustrated in Figure 6.2 The soil and pile profile can also be viewed by clicking the "**Profile**" button as shown in Figure 6.2

Once the soil parameters have been completely inputted, use the "**Generation**" function to generate the soil springs, after which the "**Elastic Soil Springs**" button is automatically activated. Note that the "**Generation**" command is only used to generate *p-y* curves and soil springs that are stored in the file of SSM_Output.txt and MultiLinearSprings.txt. These two files can be viewed by opening the corresponding file under the menu "**View**". Next, click the "**Elastic Soil Springs**" button to assign the elastic soil springs to the structure model (the single pile) in STAAD.Pro. Figure 6.3 (a) shows the structure model in STAAD.Pro after elastic soil springs have been assigned. If the user only needs to perform the analysis of the pile in an elastic soil mass, then skip "**Multilinear Soil Springs**" and move directly to step 3. If nonlinear soil behavior is to be simulated, then click "**Multilinear Soil Springs**" to assign the nonlinear soil springs to the pile; it should also be noted that the "**Multilinear Soil Springs**" button is activated only after the execution of the "**Elastic Soil Springs**" command. Figure 6.3 (b) shows the model after it has been assigned the nonlinear soil springs.
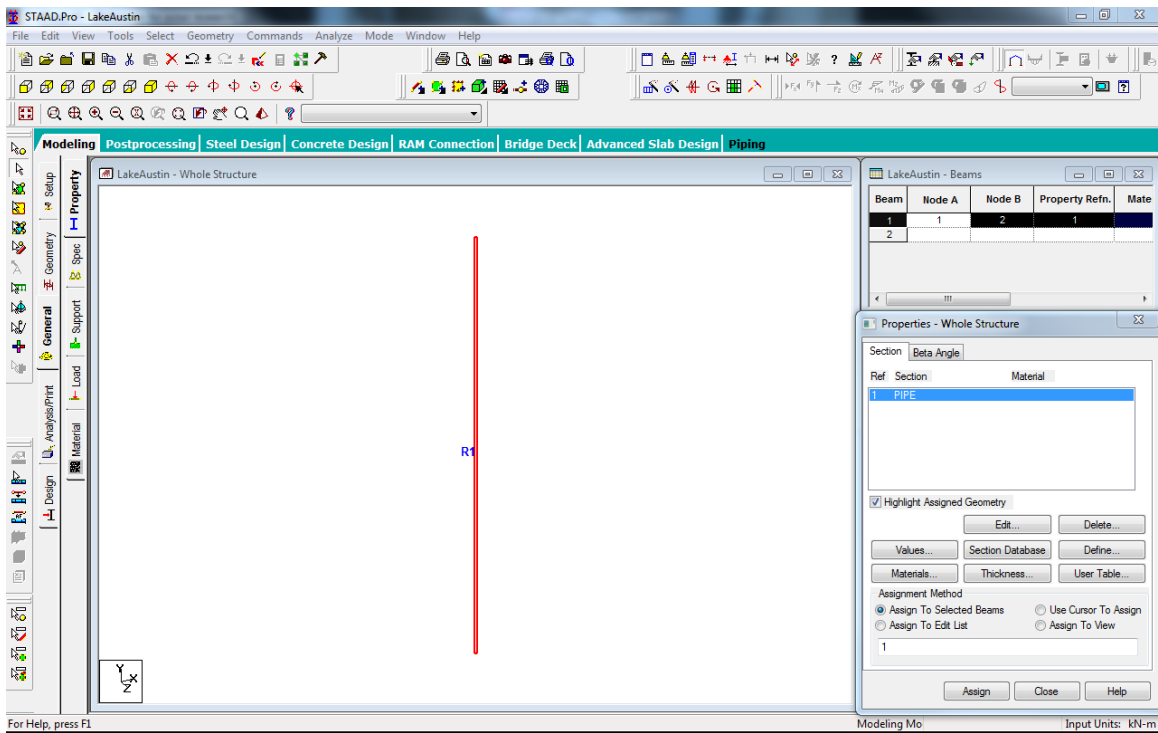

FIGURE 6.1
Establishment of a Pipe Pile Model and Assignment of the Properties in STAAD.Pro
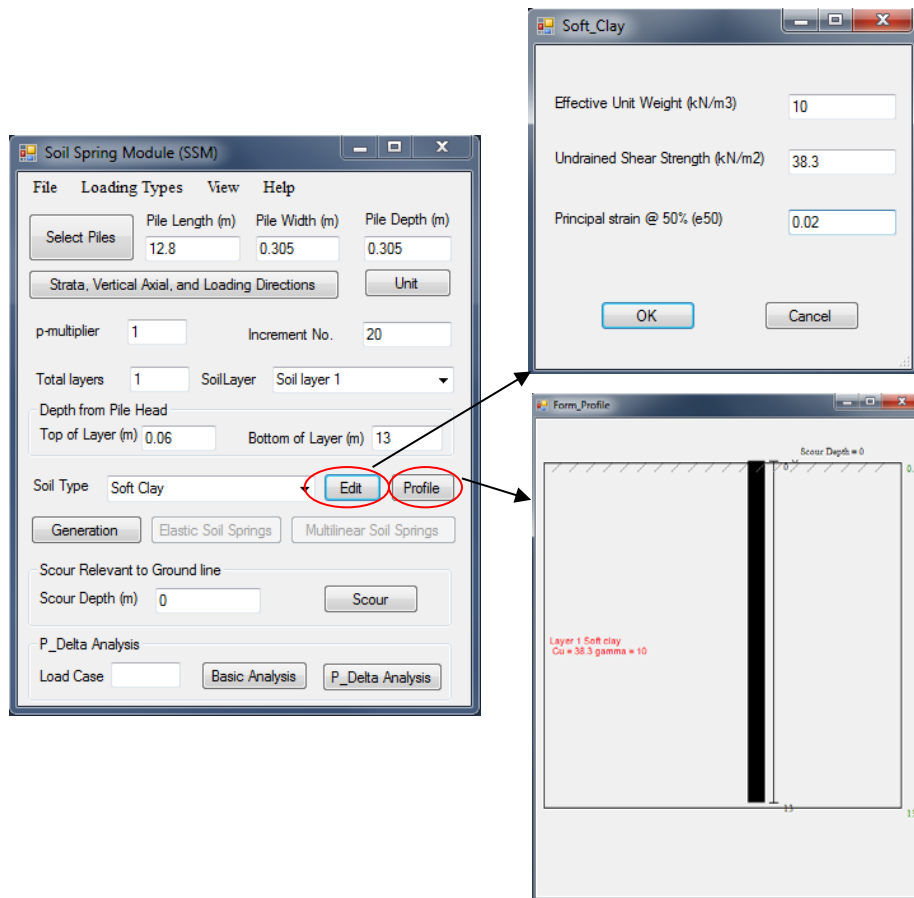
FIGURE 6.2
Input of Soil Parameters in the SSM

(a)   (b)
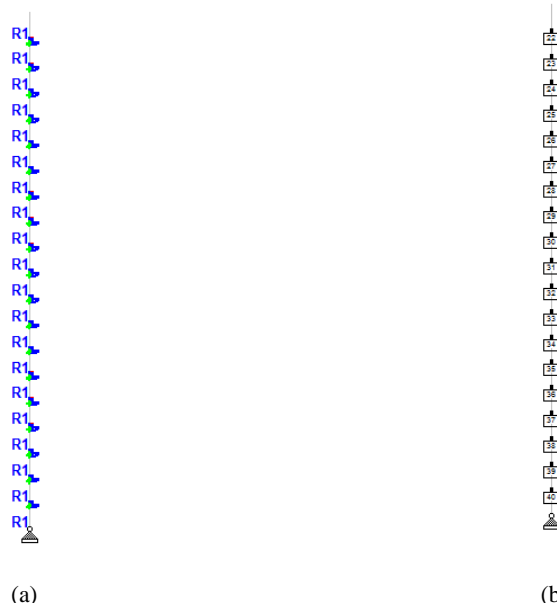
FIGURE 6.3
The Structure Model after Assignment of Soil Springs: (a) Elastic Soil Springs; (b) Multilinear Soil Springs

58

Step 3: Return to the structure model in STAAD.Pro. The user can go to the "**Support**" command under the "**General**" tab to check that the soil springs were properly applied. After applying loads and material properties to the structure model, a first-order analysis can now be executed. It should be pointed out that the lateral load direction should be kept consistent with the direction selected in Step 2, and P-Delta effects cannot be directly calculated for the model with multilinear soil spring supports, as discussed in Section 4.6.

Based on the analysis described in Steps 1 - 3, the analysis results of interest, including lateral displacement of pile head and maximum bending moment, are plotted in Figures 6.4 and 6.5. From the figures, it can be seen that the analysis results from the IAP compared well with those measured from the field test and computed from LPILE. If a factor of safety of 2.0 (Reese and Van Impe 2001) is used for calculating the allowable bending moment at the first yield, which is equal to one-half 231 kN-m (170 k-ft), then the maximum lateral load would be 81 kN (18.2 kips), as seen in Figure 6.5. Some researchers also use 20% of the pile diameter as a maximum lateral displacement of the pile at ground line to evaluate the maximum lateral load, because, as described by Broms (1964), the maximum resistance of pile is usually reached at this displacement. In this case, if 20% of the pile diameter is set as a limit, the allowable displacement is 63.8 mm (2.5 in) and the corresponding maximum lateral load should be over 100 kN (22.5 kips), as shown in Figure 6.5.
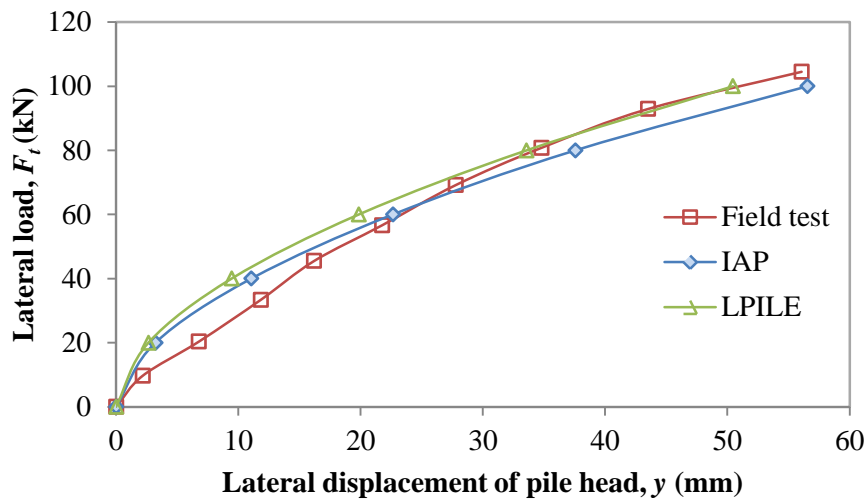
FIGURE 6.4
Comparison of Lateral Displacement of Pile Head from Field Test, IAP, and LPILE
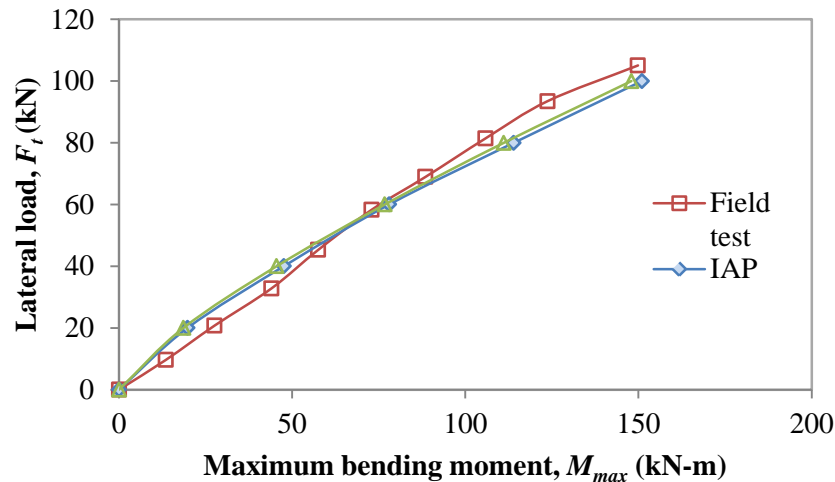
FIGURE 6.5
Comparison of Maximum Bending Moment from Field Test, IAP and LPILE

Step 4: The scour analysis may now be conducted after the above first-order analysis has been completed. The scour depth is always measured from the original ground line (before scour), as shown in the profile in Figure 6.6. The scour analysis is performed by inputting the scour depth and clicking the "**scour**" button in the SSM, and then running the analysis in STAAD.Pro. Figure 6.7 shows the distributions of lateral displacement and bending moment of the pile after scour analysis. Figure 6.8 and Figure 6.9 present the comparison of lateral displacement of pile head and maximum bending moment of the pile before and after scour under a lateral load, F_t=100 kN (22.5 kips). The significant increase of lateral displacement and maximum bending moment with the increase of scour depth can be observed in the figures.
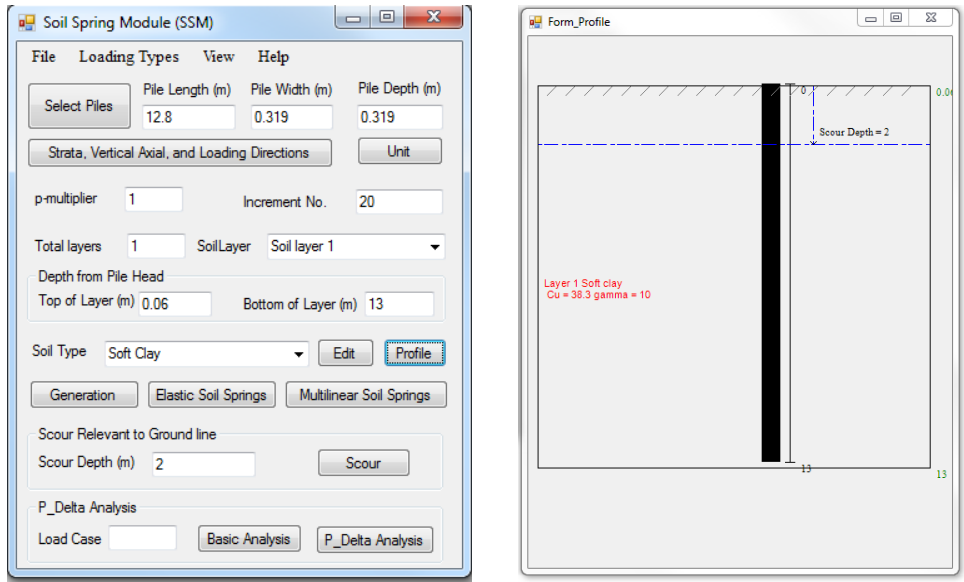
FIGURE 6.6
Illustration of Scour Analysis in the SSM
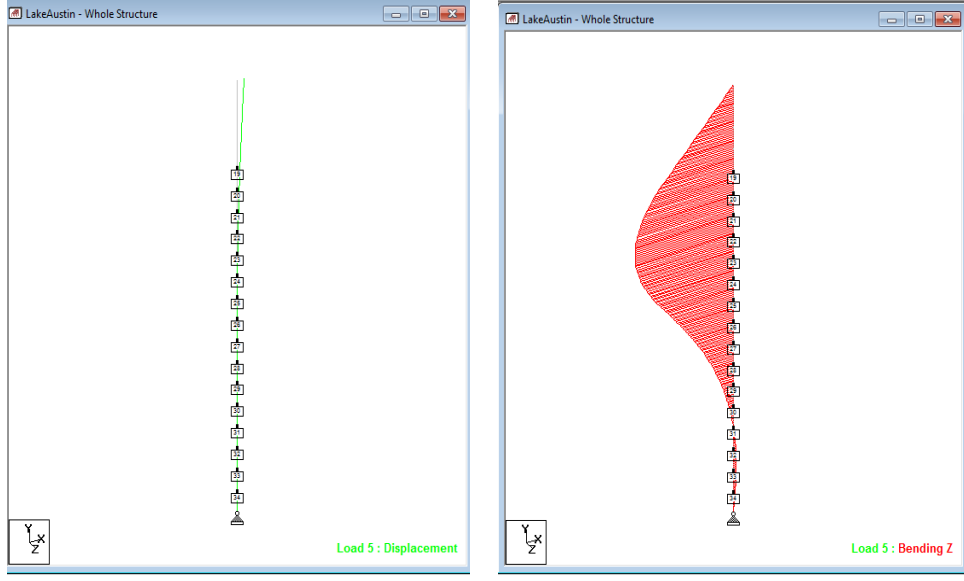
FIGURE 6.7
Distributions of Lateral Displacement and Bending Moment along the Pile at Lateral Load, F_t=100 kN (22.5 kips)
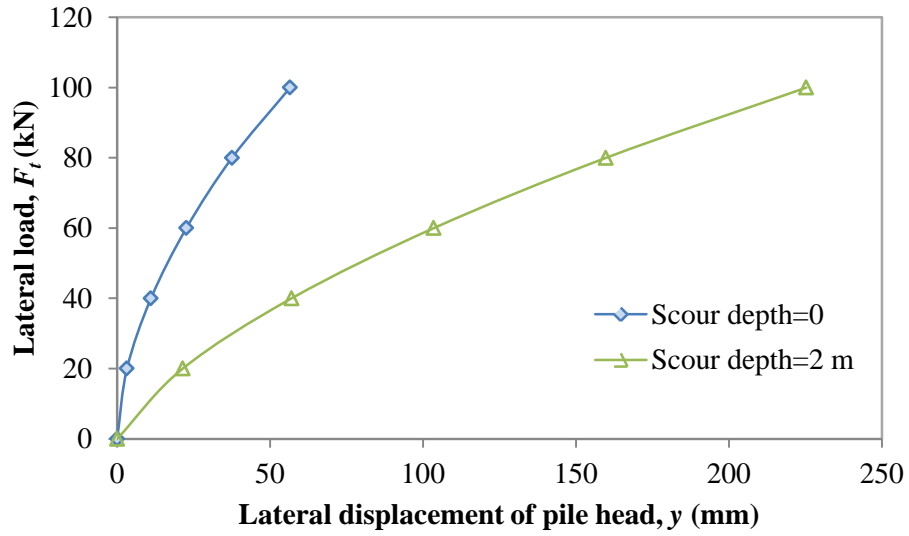
FIGURE 6.8
Comparison of Lateral Displacement of Pile Head before and after Scour
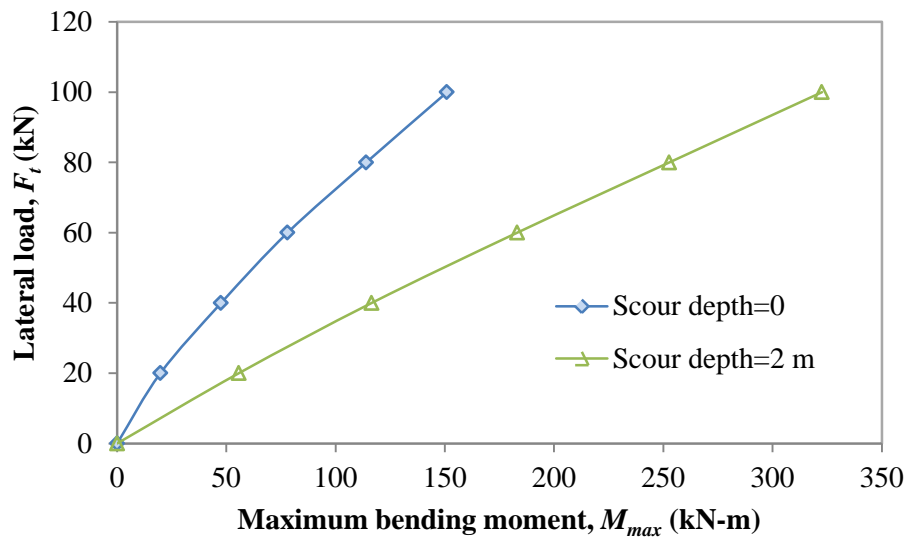
FIGURE 6.9
Comparison of Maximum Bending Moment of Pile Head before and after Scour

6.2 Response of a Laterally Loaded Pile Group in Sand

This example presents use of the IAP for a laterally loaded pile group composed of nine piles connected by a rigid pile cap. Data regarding the pile dimensions and soil properties were sourced from a field test performed on a pile group in the 1970s. The IAP process is presented in a step-wise manner, and concludes by showing a comparison of pile head displacements and bending moments in the piles before and after scour.

In this example, a 3x3 pipe pile group installed in sand is analyzed under lateral loading. This example uses the same properties for the piles and the soil as those encountered in the lateral loading test performed in Mustang Island (Cox et al. 1974). However, the configuration of the pile group and the pile cap have been assumed for this calculation. The parameters for the piles are tabulated in Table 6.3, and the center-to-center spacing of the piles has been taken as three times the outside diameter of the pile ($3D$). The pile cap only serves to rigidly connect the piles together, and was assigned an elastic modulus of 2.17×10^7 kN/m^2 (2,147 ksi) and dimensions of 1 m $\times$ 1.83 m $\times$ 1.83 m (3.28 ft x 6 ft x 6 ft) (thickness $\times$ length $\times$ width). The piles were embedded 0.5 m (1.64 ft) into thickness of the pile cap. The ground line was taken at the same elevation as the pile cap base. The soil properties are summarized in Table 6.4.

TABLE 6.3
Parameters for the Pipe Pile

Outside diameter, D m (ft)	Inside diameter, d m (ft)	Pile length, L m (ft)	Moment of inertia, I m^4 (ft^4)	Elastic modulus, E kN/m^2 (ksi)	Yielding moment, M_{y1} kN-m (k-ft)	Moment at full hinge, M_{y2} kN-m (k-ft)
0.61 (2.00)	0.59 (1.94)	21 (68.9)	8.08×10^{-4} (9.36×10^{-2})	2.02×10^8 (29,297)	640 (472)	828 (611)

TABLE 6.4
Parameters for the Sand

Effective unit weight, γ' kN/m^3 (lb/ft^3)	Friction angle, ϕ ($^{\mathrm{o}}$)	Coefficient of subgrade reaction, k MN/m^3 (lb/in^3)
10.4 (66.21)	39	34 (125.9)

First, the structure model of the pile group and pile cap should be assembled in STAAD.Pro, based on the parameters described above. Figure 6.10 provides the three-dimensional view of the structure model in STAAD.Pro. Next, select the pile group in STAAD.Pro, and click "**Select Piles**" in the SSM. Use the default directions for strata, vertical axis, and lateral loading. For a pile group, *p*-multipliers are calculated internally in the SSM, and thus no user input is needed here. Use the default increment number, i.e. 20. Since only one soil type is encountered, "**Total Layers**" should be taken equal to one. Select "**Soil layer 1**" in the "**SoilLayer**" drop box. The top of the layer should be set to 0.5 m (1.64 ft), and the bottom of layer set to 22 m (72.2 ft). The top of the layer is 0.5 m (1.64 ft) because it is measured from pile head, and the pile head is embedded 0.5 m (1.64 ft) into the pile cap. Therefore, the ground line (i.e. the top layer elevation) is 0.5 m (1.64 ft) from the pile head. The bottom of the layer should be set below the pile tip, which is 21 m (68.9 ft) from pile head. Figure 6.11 shows all the input parameters and the profile view in the SSM. If more than one soil layer is encountered in the analysis, the user should go back to "**SoilLayer**" to select the next layer and assign the corresponding locations and soil properties. Once all the input parameters are added, click "**Generation**" and the SSM will automatically calculate the soil springs. Next, click "**Elastic Soil Springs**" and after the structure model is applied with the elastic soil springs as shown in Figure 6.12 (a), click "**Multilinear Soil Springs**" to assign the nonlinear soil springs, as can be viewed in Figure 6.12 (b).
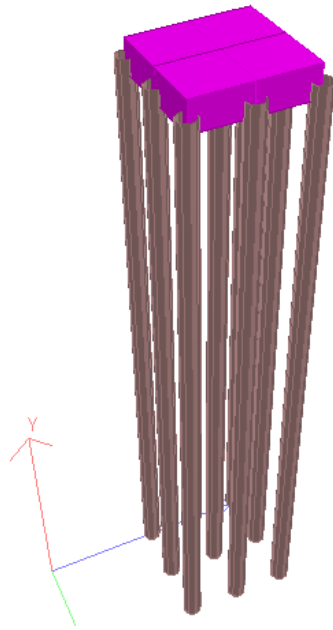
FIGURE 6.10
Pile Group Model in STAAD.Pro
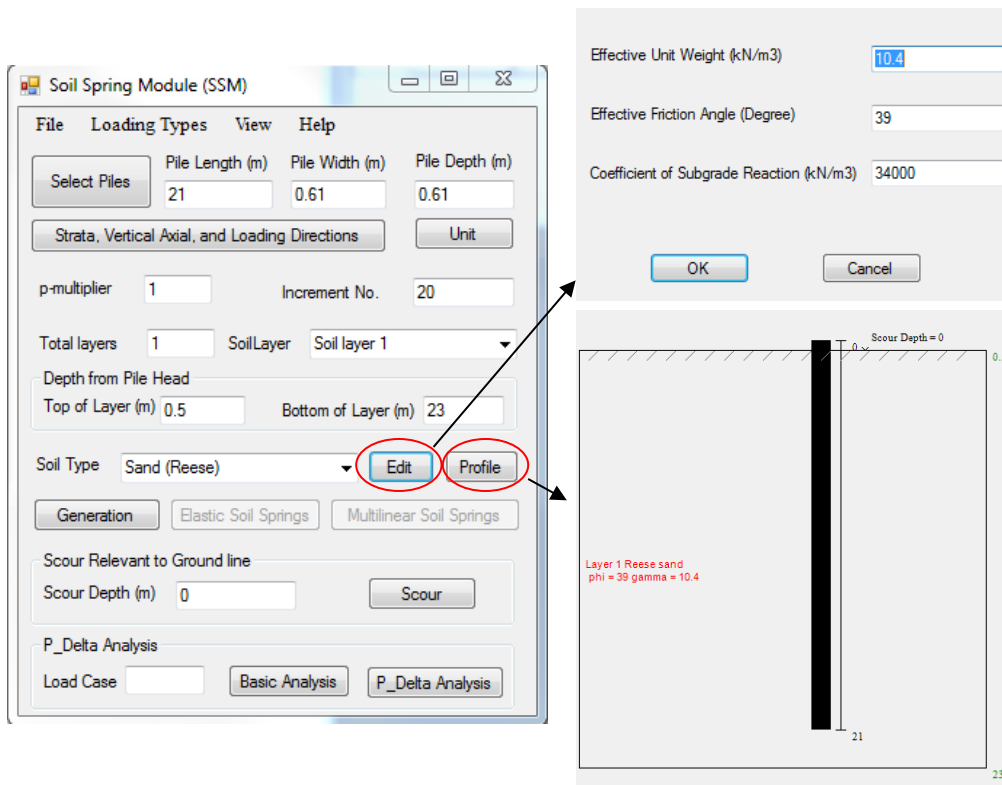
FIGURE 6.11
Input Parameters and Profile View of the Soil and Pile in the SSM

The calculated results from the IAP were compared with those computed using the software package FB-Multipier for the condition before scour, as presented in Figure 6.13. As shown in Figure 6.13, if the same *p*-multiplier is employed in FB-Multipier, f_m, as was used within the SSM (i.e. 0.82, 0.68, and 0.58 for the leading to trailing piles), then the calculated lateral displacement of the pile cap is found to be very similar for the FB-Multipier and the SSM results. If using the default f_m value in FB-Multipier, which is 1.0, 0.3, and 0.3, respectively, for leading to trailing piles, the calculated displacement as indicated by FB-Multipier_2 in Figure 6.13 is about 10–30% greater than the result obtained from the IAP.

A scour analysis was also performed on this system, considering scour to a depth equal to 3 m (9.8 ft) from the original ground line. The calculated results have been presented and compared in Figure 6.14, showing the calculated lateral displacement of the pile cap. Figures 6.15 and 6.16 show the distribution of lateral displacement and bending moment at a lateral load of 1500 kN (337). It can be clearly seen that scour significantly increased both the lateral displacement and bending moments in the piles.

(a)   (b)
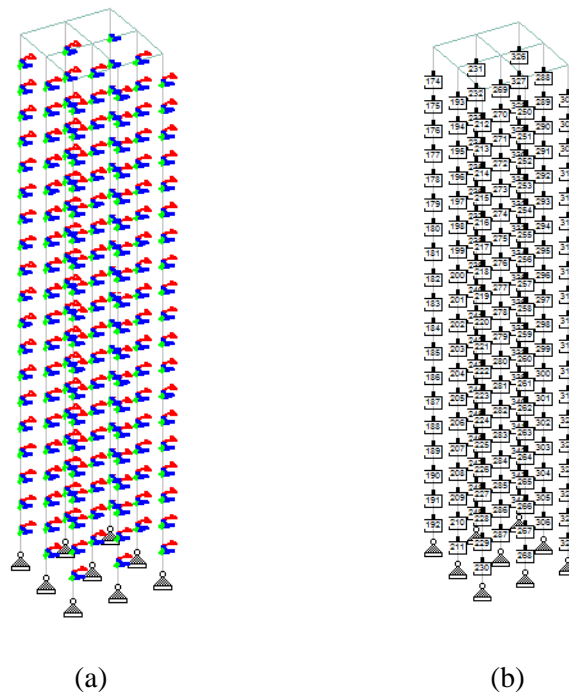
FIGURE 6.12
The Structure Model after Being
Assigned with (a) Elastic Soil springs
and (b) Multilinear Soil Springs
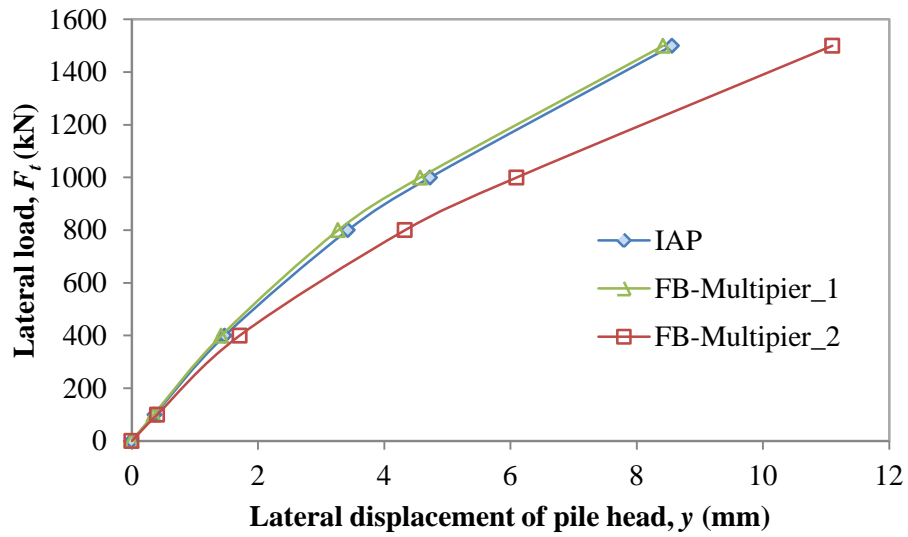
FIGURE 6.13
Comparison of Lateral Displacement before Scour Calculated from IAP and FB-Multipier
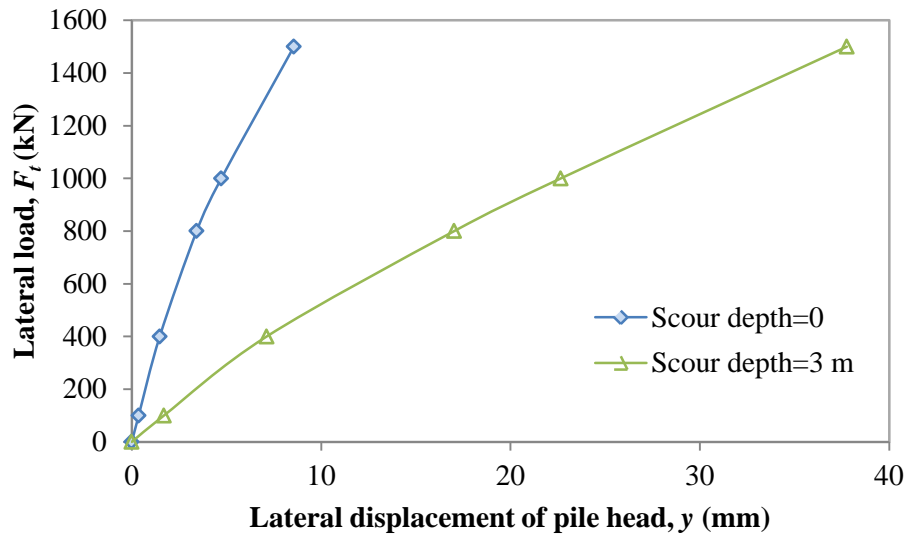
FIGURE 6.14
Comparison of Lateral Displacement of the Pile Cap before and after Scour
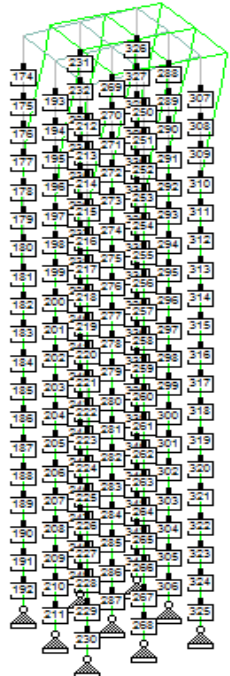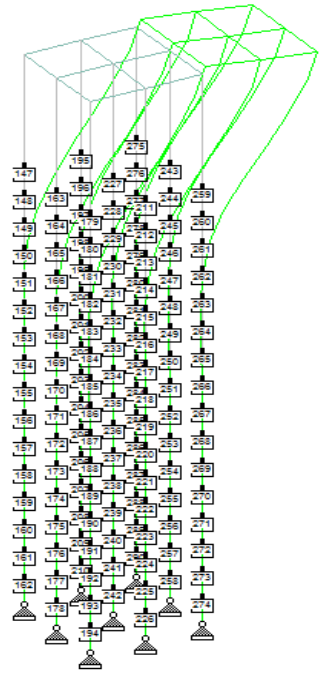
(a)   (b)

FIGURE 6.15
Comparison of Lateral Displacement of the Pile
Group (a) before Scour and (b) after Scour; at F_t
=1500 kN (337 kips) (the Displacements Are
Amplified 100 Times)

(a)   (b)
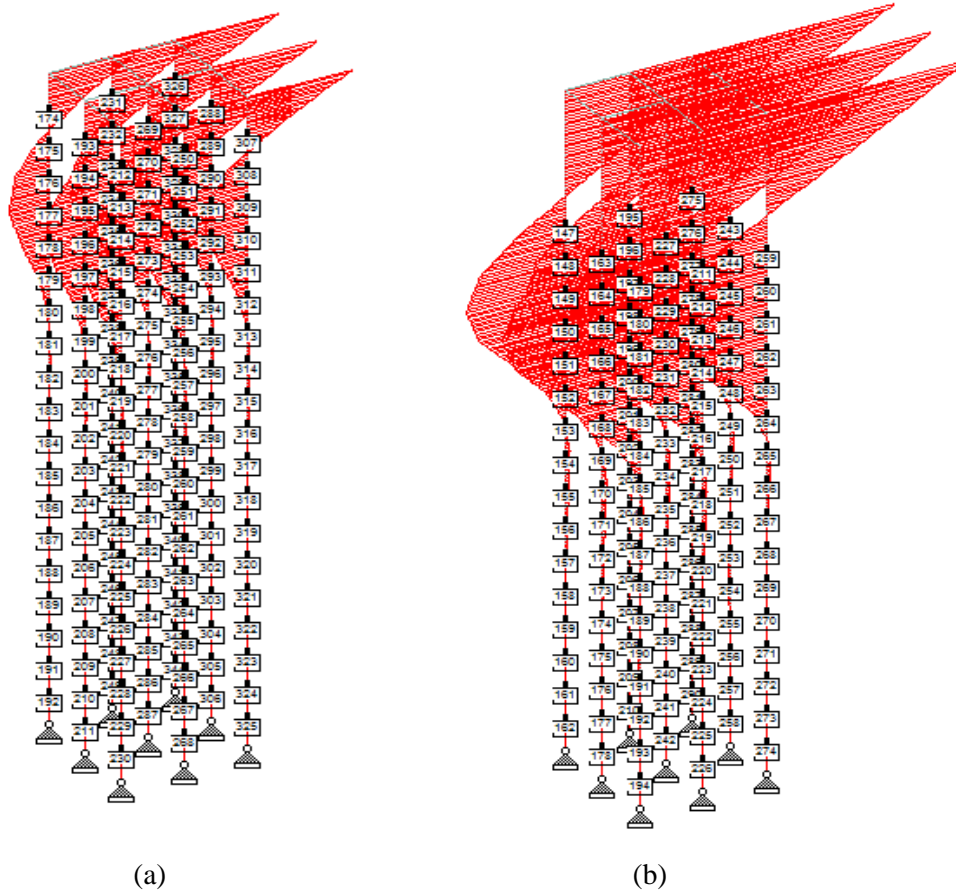
FIGURE 6.16
Comparison of Bending Moment of the Pile Group (a) before Scour and (b) after Scour; at F_t=1500 kN (337 Kips)

6.3 Lateral Responses of an Entire Bridge under Lateral Loading

This example presents use of the IAP for a whole bridge system, using the five-span Kansas Bridge No. 45 in Jewell Co., KS, as the basis for the example. This example presents a scenario that is likely similar to how many end users will choose to utilize the IAP and the SSM.

6.3.1 Bridge Description

Bridge 45 is situated in Jewell County, Kansas, and carries State Highway K14 over a local creek. The five-span bridge was constructed in 1956 and has a total length of 112 m (367 ft). Four W33x141 steel girders with a spacing of 2.3 m (7.55 ft) support the bridge deck, as shown in Figure 6.17. Bridge 45 has eight piers (four bents), and each pier is supported by a group of eight HP10x42 piles with average length of 10 m (32.8 ft) as shown in Figure 6.18. In Figure 6.18, γ' = effective unit weight of soil; C_u = undrained shear strength; ϕ = effective friction angle of soil; ε_{50} = strain value of soil at 50% of the maximum stress; K = coefficient of subgrade reaction.
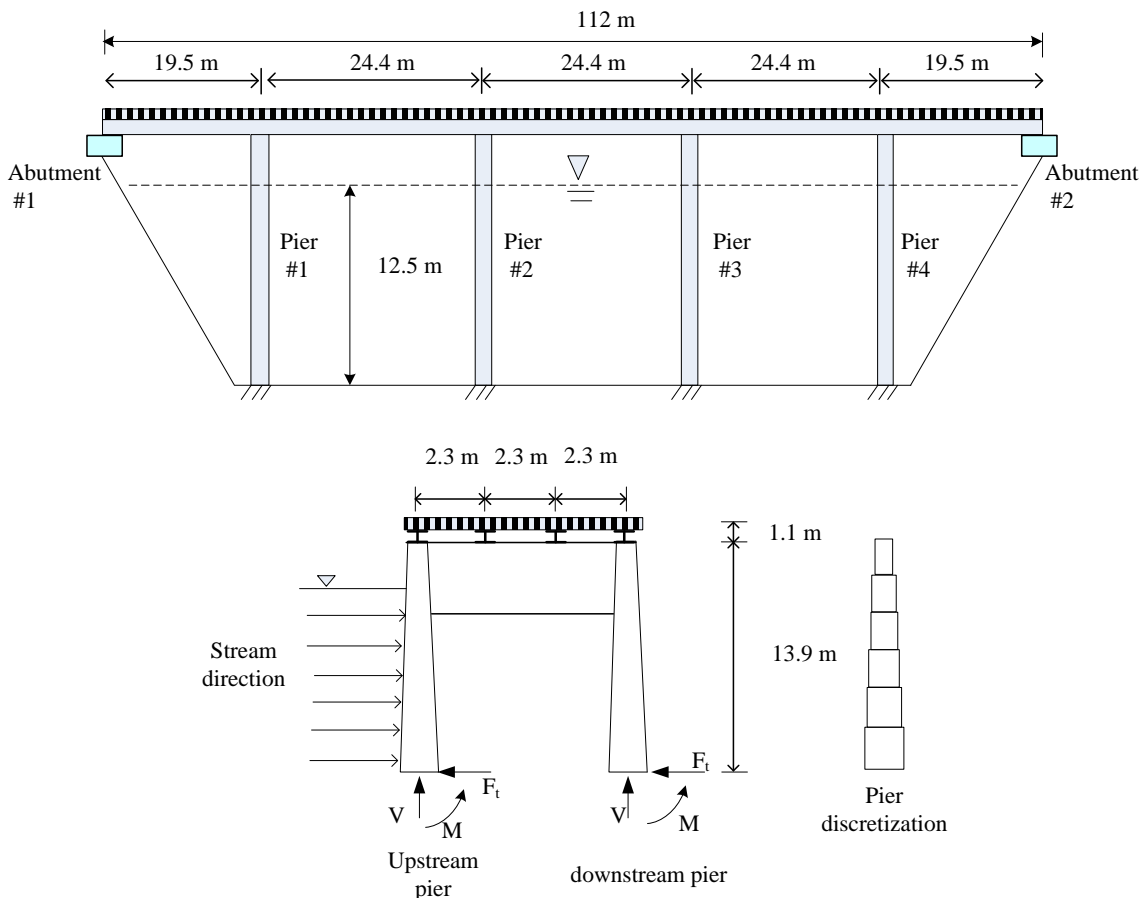
FIGURE 6.17
Bridge K45 Superstructure
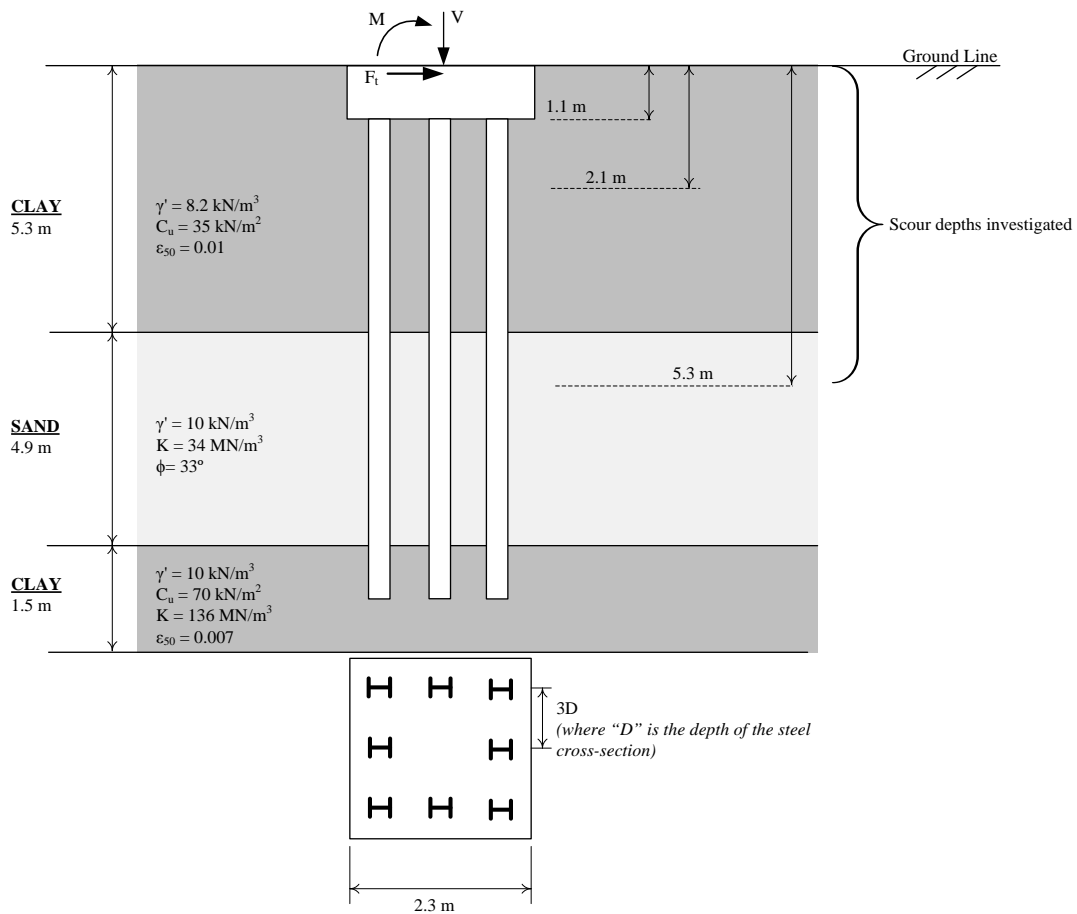
FIGURE 6.18
Cross Section of the Pile Foundation at Piers and Scour Depths Investigated

6.3.2 Load Treatment

Loads considered in the analysis included flood loads (including debris loads) and wind loads, while vertical loads included self-weight of the bridge. The applied loads were combined using load factors of 1.0 to reflect the actual behavior of the existing bridge system. The loads used in this case study represent one combination of lateral and gravity loads that a bridge would be likely to experience during a scour event. It is expected that end users of the IAP will likely be interested in exploring multiple load combinations.

Hydraulic loads were calculated using Equation 6.1 based on equation C3.7.3.1-1 from the 4th Edition AASHTO-LRFD Bridge Design Specifications (AASHTO 2007), provided here in metric units.

$$p = C_D \gamma V^2 \times 10^{-6} / 2$$

Equation 6.1

where V = water velocity (m/sec); C_D = drag coefficient; γ = density of water (kg/m^3); p = water pressure (MPa).

The design 100-year flood for the bridge was taken at the design elevation of 12.5 m (41.0 ft) above the base of piers. The design flood velocity used in the calculation was 3.66 m/sec (12 ft/sec). In addition to water loads, debris forces were calculated by multiplying the water pressure (Equation 6.1) by the area of debris accumulation at a pier based on Section C3.7.3.1 of the AASHTO-LRFD Bridge Design Specifications (AASHTO 2007). The dimension of debris-accumulation was simplified as an inverted triangle in which the width was taken as half the sum of adjacent span lengths, but not greater than 13.5 m (44.3 ft), and the depth was taken as half the water depth, not greater than 3.0 m (9.8 ft). Debris forces were applied only to the upstream piers of the bridge due to the relatively short distance between the upstream and downstream piers (6.90 m [22.6 ft]) as compared with the width of debris at a pier (13.7 m [44.9 ft]). Debris loads were applied to piers as concentrated loads, while hydraulic loads were applied as pressure to the piers below the maximum depth of debris-accumulation.

Wind loads were calculated using Equations 6.2 and 6.3, based on Equations 3.8.1.2.1-1 and 3.8.1.1-1 from the 4th Edition AASHTO-LRFD Bridge Design Specifications (AASHTO 2007), provided here in metric units.

$$P_D = P_B \left(V_{DZ} / V_B \right)^2$$

Equation 6.2

where

$$V_{DZ} = 2.5 V_o \left(V_{10} / V_B \right) \ln \left(Z / Z_o \right)$$

Equation 6.3

In Equations 6.2 and 6.3, P_D = wind pressure (MPa); P_B = base wind pressure (MPa); V_{DZ} = design wind velocity at design elevation (km/hr); V_B = base wind velocity, typically taken as 160 km/hr; Z = height of structure at which wind loads are calculated (mm); V_o = friction velocity (km/hr); V_{10} = wind velocity at 10,000 mm above low ground (km/hr); and Z_o = friction length of upstream fetch (mm).

Wind loads were calculated above the flood level and applied as concentrated loads to the bridge girders at the location of piers. The concentrated wind loads were determined by multiplying the tributary area of the bridge deck and fascia girder normal to wind loads by the wind pressure calculated using Equation 6.2.

6.3.2 Analysis in IAP

An entire bridge model was first assembled in STAAD.Pro, as shown in Figure 6.19. This structure model included the superstructure elements, piers, pile caps, and piles. The abutments were supported using pin supports, which were applied to the model before assigning any soil springs. (Note: It is recommended that structural supports other than the SSM-generated soil spring supports be applied to the model in advance to avoid any errors.) A similar analysis procedure as described in Section 6.2 was followed here. The only difference was that the current case requires the user to select pile groups and assign elastic soil springs to them group by group. As there are eight pile groups and each group contains eight piles, it takes several minutes to complete the process. It is recommended that the user apply elastic soil springs to all of the pile groups in advance and then multilinear soil springs. Otherwise, if the elastic soil springs are not completely assigned before the multilinear soil springs, it will produce an erroneous code reading in STAAD.Pro during the analysis. Figure 6.20 shows the model after complete assignment of elastic soil springs (a) and multilinear soil springs (b).
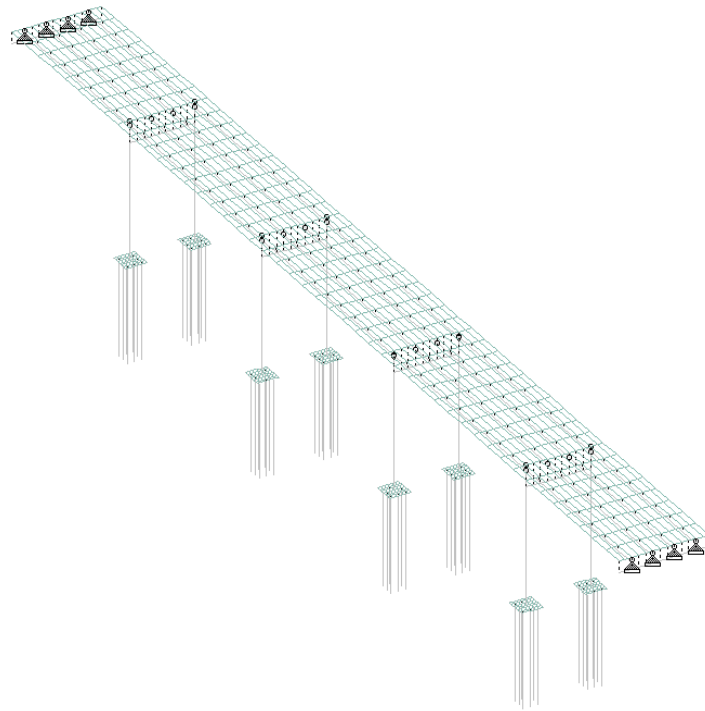
FIGURE 6.19
Bridge Model in STAAD.Pro before Being
Assigned Soil Springs

(a) (b)
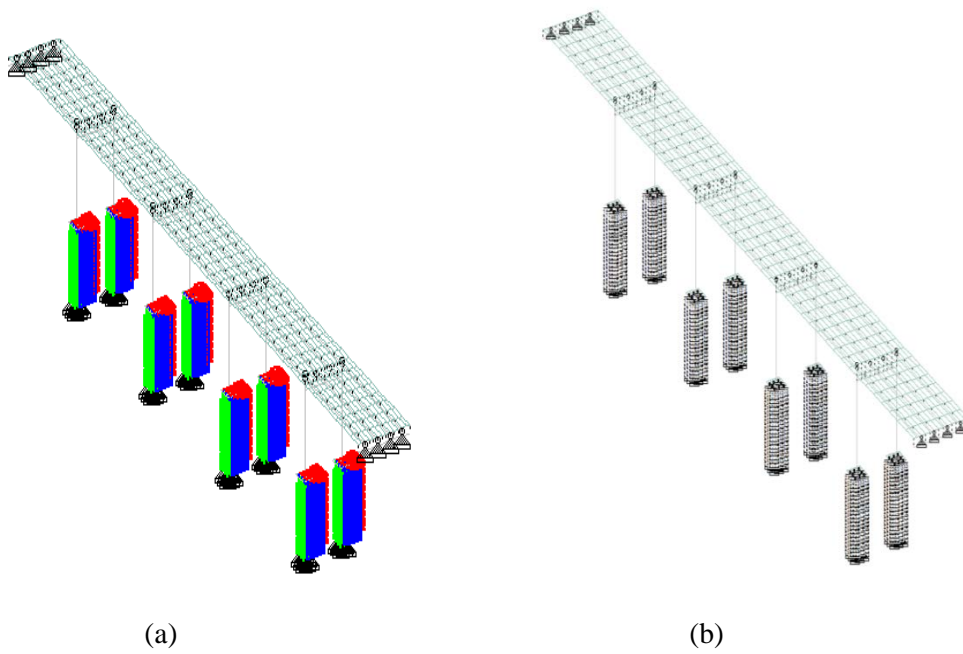
FIGURE 6.20
Bridge Model in STAAD.Pro after (a) Being Assigned with Elastic
Soil Springs and (b) Multilinear Soil Springs

Figures 6.21 and 6.22 compare the deformation and bending moment distribution of the bridge both before and after scour with a scour depth equal to 5.3 m (17.4 ft) under the lateral loading case.

(a)

(b)
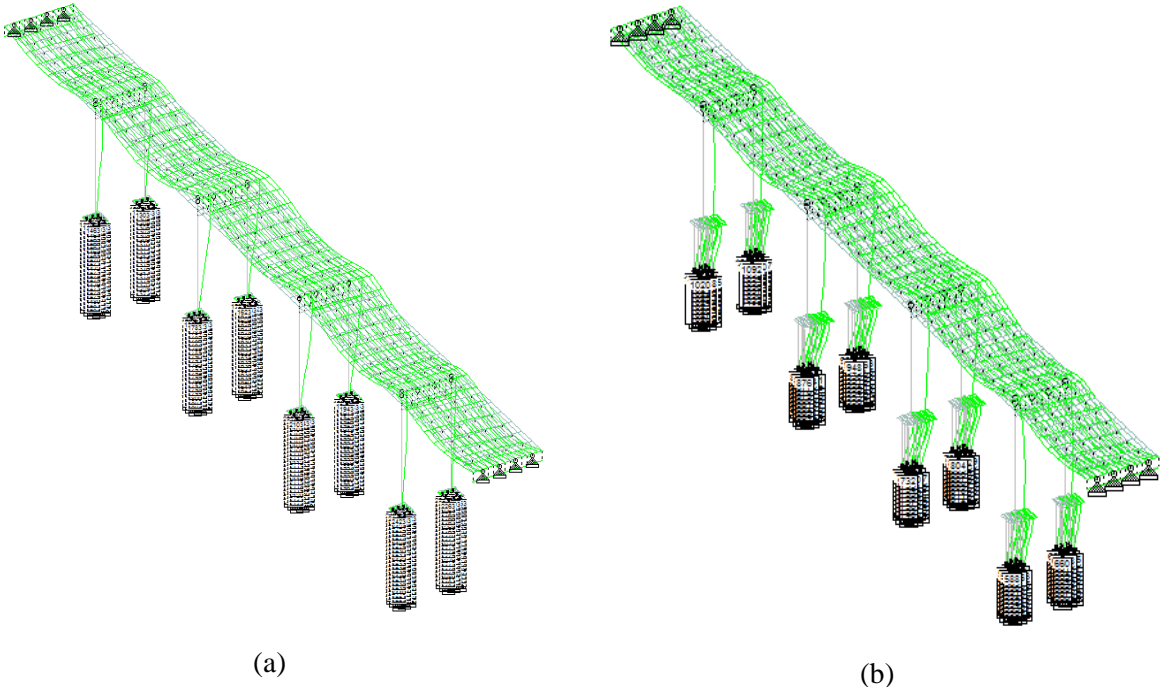
FIGURE 6.21
Deformation of the Bridge (a) before Scour and (b) after Scour with Scour Depth,
S_d=5.3m (17.4 ft)

(a)

(b)
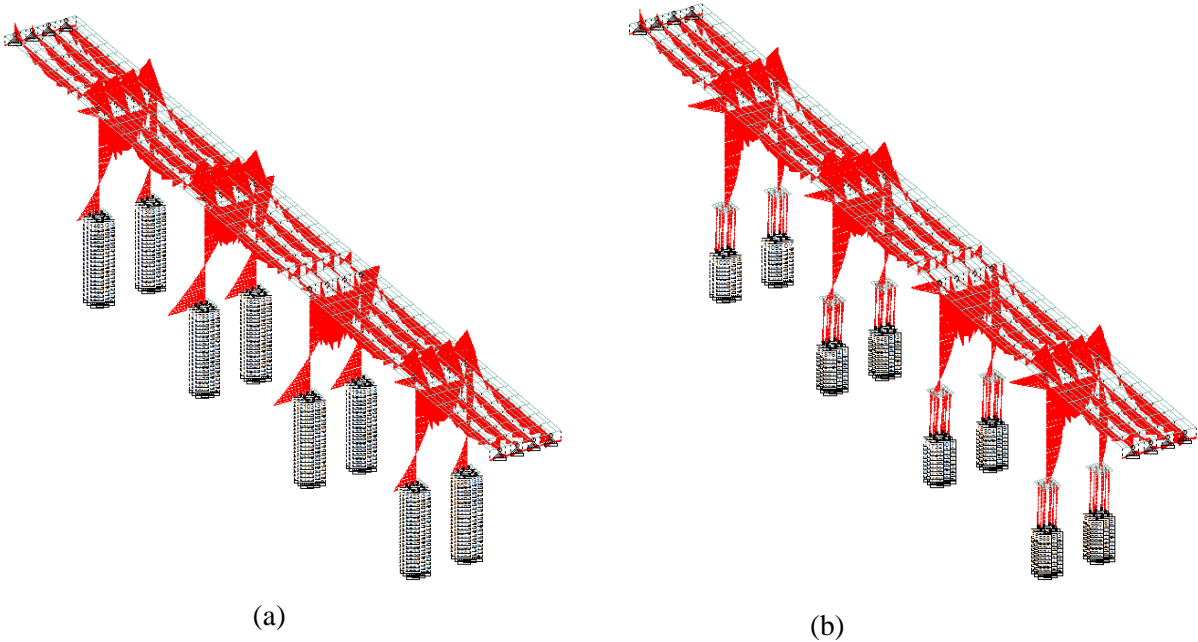
FIGURE 6.22
Bending Moment of the Bridge (a) before Scour and (b) after Scour with Scour Depth,
S_d=5.3 m (17.4 ft)

Figures 6.23 and 6.24 present the maximum lateral displacement that occurred in pile cap and bridge deck.
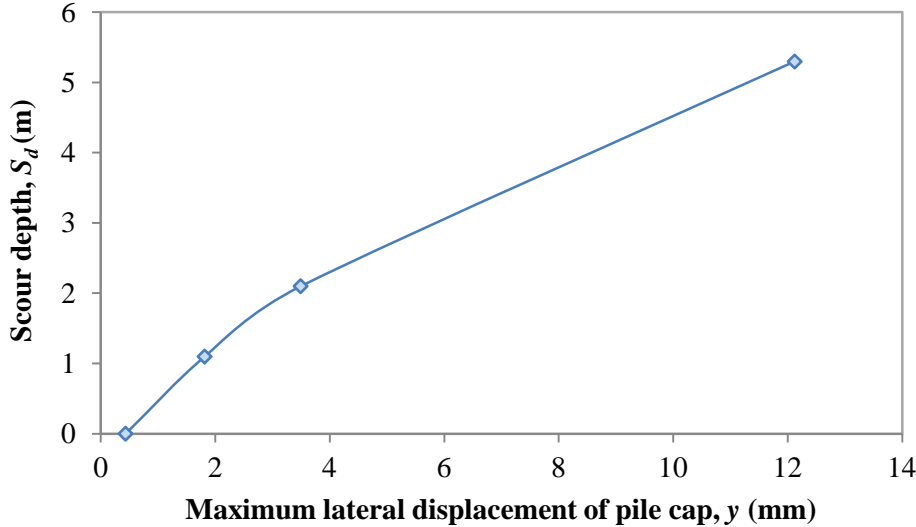
FIGURE 6.23
The Maximum Lateral Displacement of Pile Cap under Scour
Depths
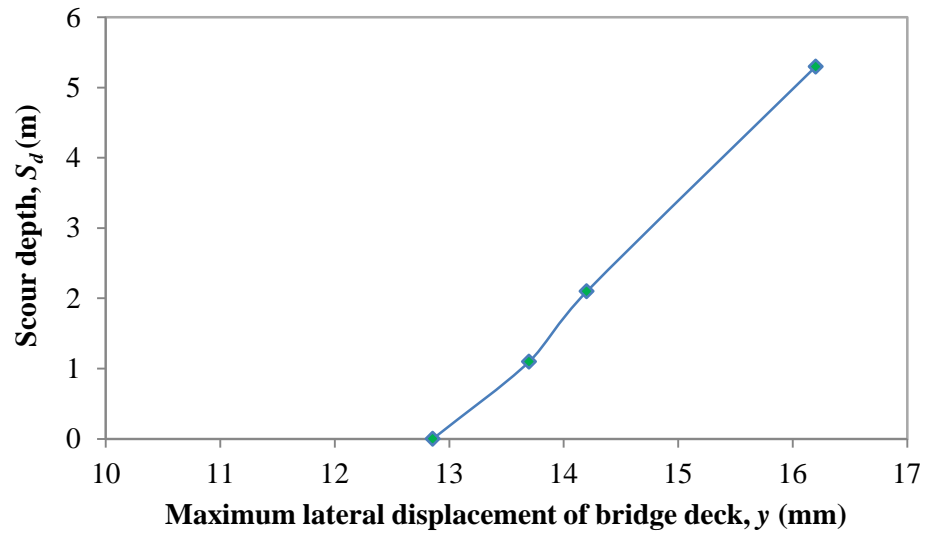
FIGURE 6.24
The Maximum Lateral Displacement of the Bridge Deck under Scour Depths

6.4 Buckling Capacity of Bridge and Bridge Piles

This example presents an elastic buckling analysis performed for the bridge system analyzed in Section 6.3, as well as a buckling analysis for a single pile chosen from the system analysis. The purpose of this example is to show methods for determining buckling susceptibility under scour.

In this section, a buckling analysis was performed for the bridge and associated bridge piles. The bridge configuration and soil conditions were the same as presented in Section 6.3, with exception of load cases. As stated in Section 5, to perform a buckling analysis in STAAD.Pro 2007, it is better to combine different loads under the same primary load case. The following description is intended to illustrate the procedure for calculating the buckling capacity of the entire bridge and then the bridge piles.

6.4.1 Buckling Capacity of Bridge

Follow the procedure described for performing the lateral load analysis for the bridge in Section 6.3. Change the loading conditions in STAAD.Pro 2007 by combining two primary load cases into one primary load case, and deleting the combined load cases as shown from left to right in Figure 6.25. Then, instead of selecting "**Perform Analysis,**" select "**Perform Buckling Analysis**" under "**Analysis/Print**." Input 15 iterations and select "**All**" under "**print option**" as can be seen in Figure 6.26. Next, run the buckling analysis. Buckling factors and corresponding failure modes can be viewed by selecting "**Buckling**" under "**Postprocessing**," as shown in Figure 6.27.
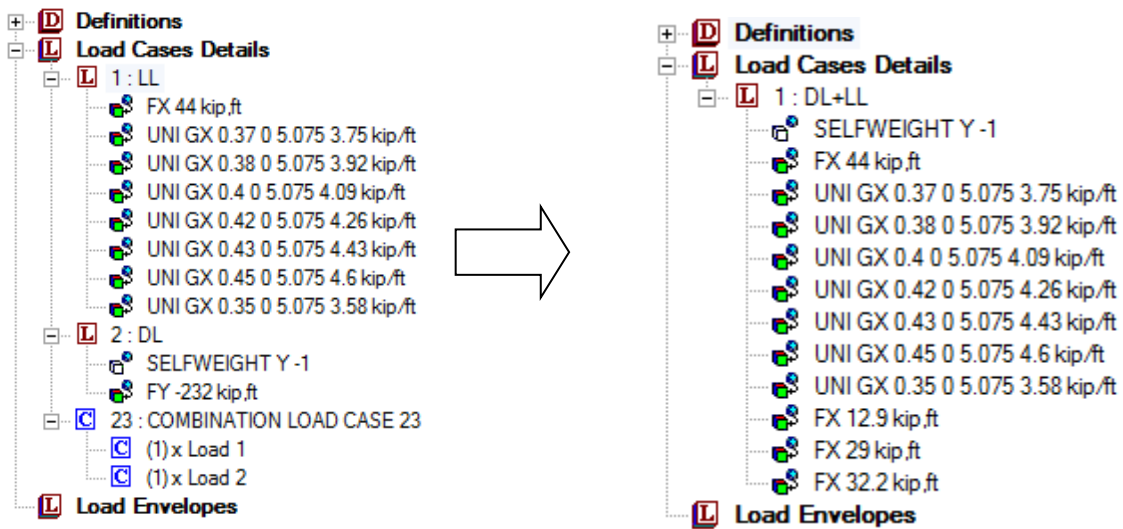
FIGURE 6.25
Change of Load Case Setting for Buckling Analysis
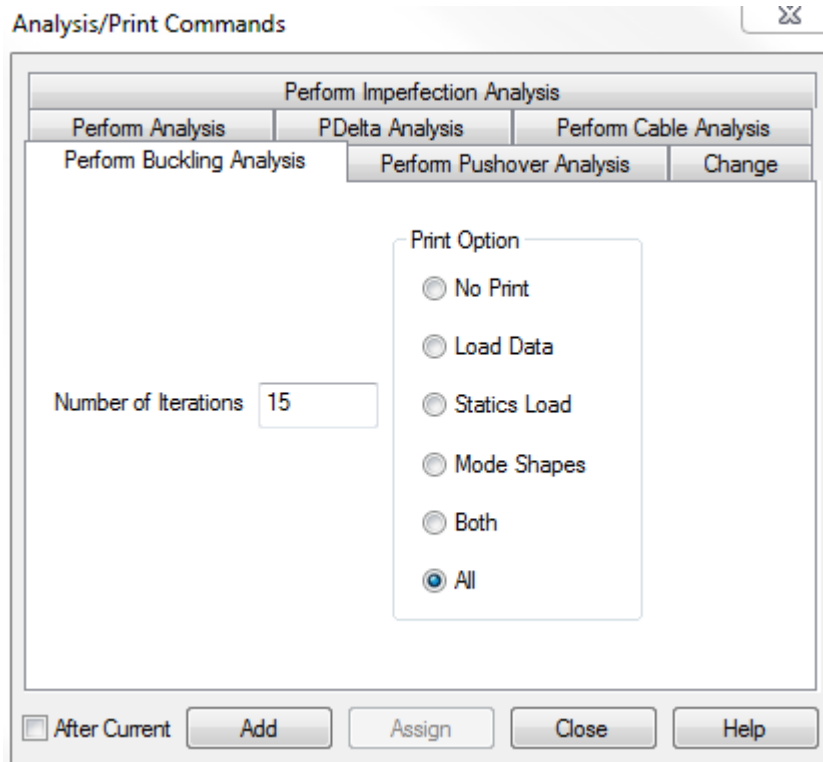
FIGURE 6.26
Buckling Analysis Function in STAAD.Pro 2007
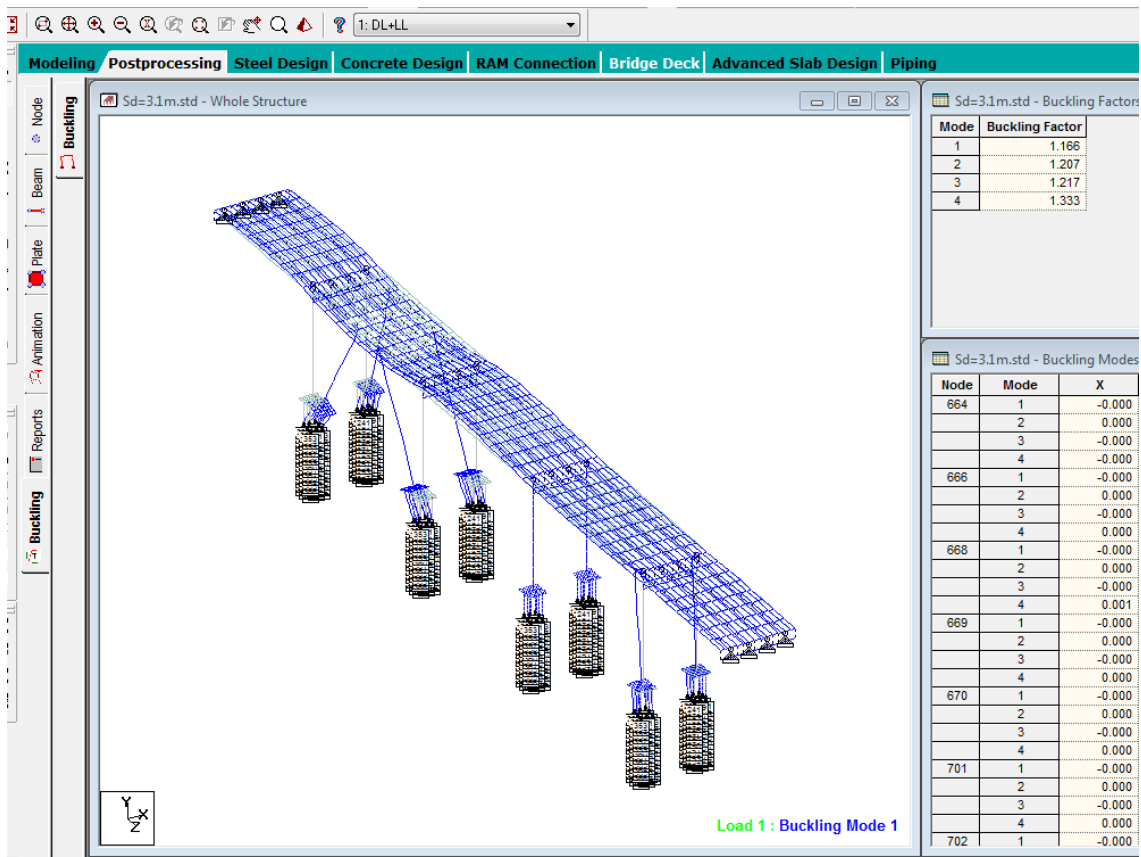
FIGURE 6.27
Buckling Factors and Buckling Failure Modes

Using this procedure, buckling analyses were performed for five different scour depths (i.e. S_d = 0, 1.1, 2.1, 3.1, and 5.3 m [0.0, 3.6, 6.9, 10.2, 17.4 ft]). The minimum of four buckling factors calculated at each scour depth was plotted in Figure 6.28. Figure 6.28 indicates that the bridge system fails by buckling when scour depth reaches 3.8 m (12.5 ft). Buckling failure is indicated wherever the buckling factor is less than 1, as a buckling factor of 1 implies a load equal to that specified in the load combination will produce buckling in the bridge system.
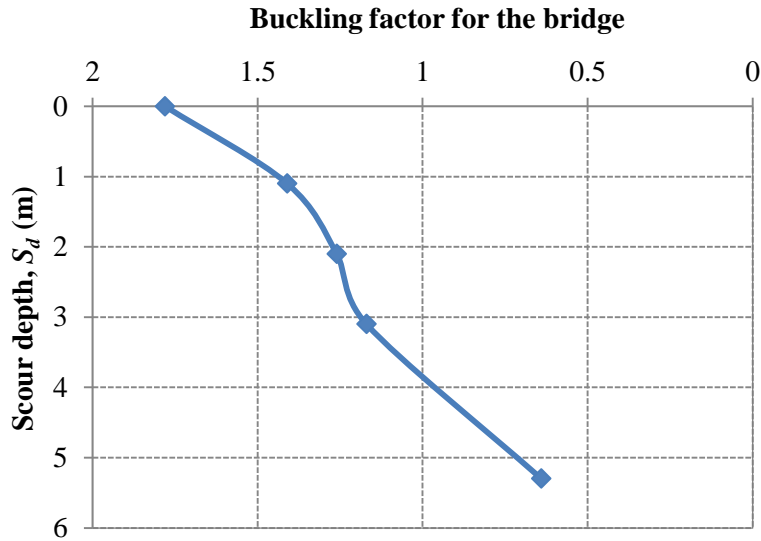
FIGURE 6.28
Buckling Factors versus Scour Depth

It should be noted that while this treatment of buckling is a rather "blunt" tool, it is a meaningful way to evaluate whether the bridge system is susceptible to buckling under various load combinations. Additionally, performing this buckling analysis is a fairly straight-forward task. However, a drawback to this approach is as follows: since the buckling mode generated in this manner is usually a *system* buckling mode, the user cannot determine an effective length factor for an individual pile without taking additional steps. This may be something that is considered useful to the user, who may wish to calculate an effective length factor (*k*) for a pile in order to calculate the design resistance of the pile using provisions set forth by, for example, the AISC Manual for Steel Construction or ACI 318.

One very approximate manner in which a user could attempt to determine a "*k*" value for a pile would be to do so geometrically, examining the deformed shape of the bridge system after the buckling analysis (Figure 6.27). An effective length (*k*-factor) simply describes the ratio between the effective length and the actual unbraced length of the member. The effective length of a column is simply the length of an equivalent pin-pin column having the same load-carrying capacity as the member under consideration. Another way to state this is that the effective length of a column / pile is just the distance between successive inflection points or points of zero moment. This latter definition is more useful for columns / piles that do not

"sway" under load. Since the deformations of piles in bridge systems will often be controlled by "sidesway" modes of failure, the deformed shape of the pile would need to be extrapolated in an approximate manner to determine the effective length, and thus, an effective length factor. *This approach will be very approximate, and the accuracy of k will depend on the level of geometric detail utilized.*

As a rule, k will always be less than one for a non-sway case ($0<k<1$), and will always be greater than 1 for a sway case, with no upper bound ($1<k<\infty$). Approaching the analysis with too small of a k-value is un-conservative, and will lead to a solution that over-predicts buckling capacity. Therefore, the user is advised to exercise caution when determining k-values for sway-cases, especially. A value of k=1 for a sway case will <u>always</u> be un-conservative. For non-sway cases, using a k=1 is recommended, as it will always be conservative for a non-sway case.

If the user wishes to determine a "k" value for a particular pile, they make choose to take increasingly sophisticated approaches to the problem, beyond the very approximate approach just described. One such approach specific to the bridge piles is detailed in the following section.

6.4.1 Buckling Capacity of Bridge Piles

After performing the bridge buckling analysis, the responses of any bridge piles, including loads and displacements, can be monitored. The case for scour depth=5.3 m is employed herein for demonstrating the procedure for analyzing pile buckling capacity.

First, under the view of "**Postprocessing**," select the pile of interest for the buckling analysis (Figure 6.29) and obtain loads at the selected pile head and the corresponding displacements. The loads at pile head, $\{F\}$ can be obtained by checking member "**Forces**" under "**Beam**," while pile head displacements, $\{u\}$ can be obtained by using "**Displacement**" under "**Node**". The approximate stiffnesses at the pile head, $\{K\}_{tot}$, can be calculated by dividing the loads, $\{F\}$ by the corresponding displacements, $\{u\}$. The results for $\{K\}_{tot}$ for the selected pile head are illustrated in Table 6.5.

Next, separate the selected pile and associated soils from the entire bridge such that only the single pile model exists, as shown on the left side of Figure 6.30 (we suggest making a copy of the original model before performing this step). Then apply the displacement, $\{u\}$, in Table 6.5 to the pile head. To apply the displacement as a load, select "**Support Displacement**" for "**Nodal Load**" under "**Load**," and then input displacements as shown in Figure 6.31. Meanwhile, the pile head should be restrained using "**Reforced**" support in order for displacement load to be effective. After assigning the "**Reforced**" support to pile head, the model state can be seen in Figure 6.30. After conducting first order analysis of the single pile model using the "**Perform analysis**" command, the pile-head reaction forces can be calculated. Then, soil stiffness, $\{K\}_{\text{soil}}$, can be determined by dividing reaction forces by the displacements. Results are presented in Table 6.6.
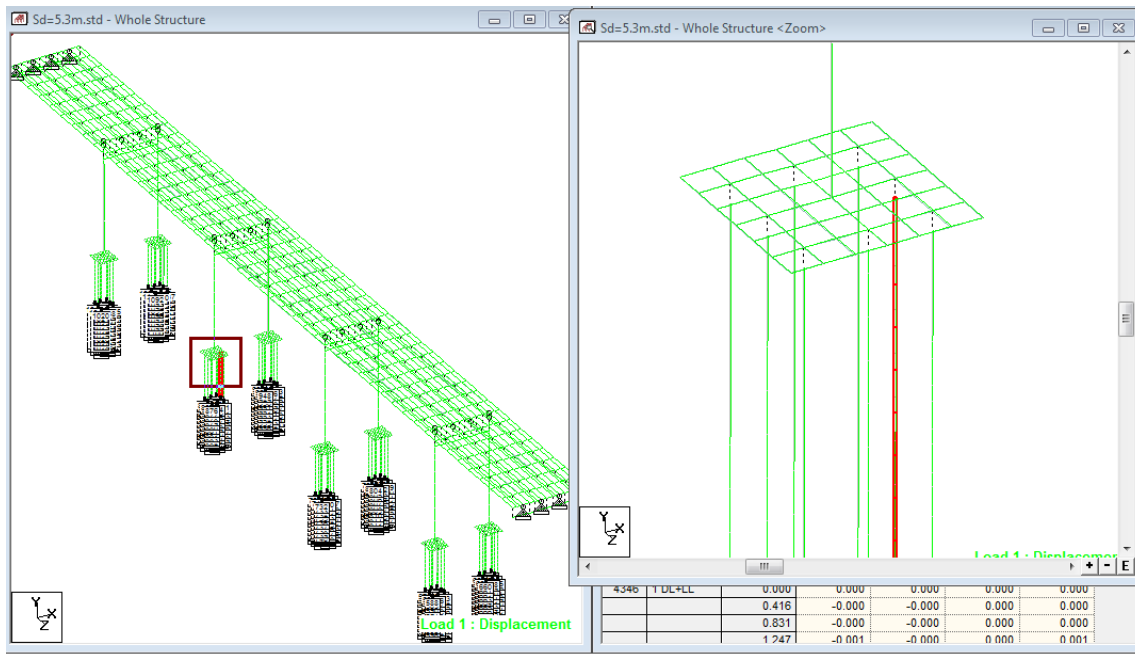
FIGURE 6.29
Buckling Factors and Buckling Failure Modes

TABLE 6.5
Calculation of Approximate Stiffnesses at Pile Head

		Load, $\{F\}$			
F_x	F_y	F_z	F_{rx}	F_{ry}	F_{rz}
kN	kN	kN	kN-m	kN-m	kN-m
(kips)	(kips)	(kips)	(kips)	(kips)	(kips)
8.6	-257.4	0.0	0.0	0.0	24.5
(1.93)	(57.9)	(0.0)	(0.0)	(0.0)	(5.51)

		Displacement, $\{u\}$			
x	y	z	r_x	r_y	r_z
mm	mm	mm			
(in)	(in)	(in)	deg	deg	deg
11.31	-1.65	-0.06			
(0.445)	(-0.065)	(-0.0024)	0.00	0.05	-0.03

		Approximate stiffnesses at pile head, $\{K\}_{tot}$			
K_x	K_y	K_z	K_{rx}	K_{ry}	K_{rz}
kN/m	kN/m	kN/m	kN-m/deg	kN-m/deg	kN-m/deg
(lb/in)	(lb/in)	(lb/in)	(k-ft/deg)	(k-ft/deg)	(k-ft/deg)
758.4	155980.6	0.0	20.0	0.1	741.7
(4331)	(890,673)	(0.0)	(14.75)	(0.0738)	(547.1)
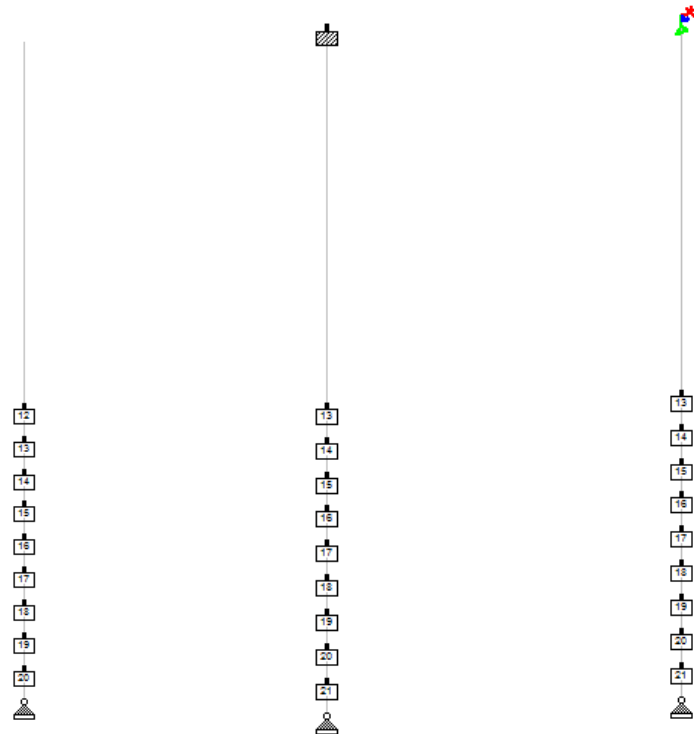
FIGURE 6.30
Model of Single Pile with Soils
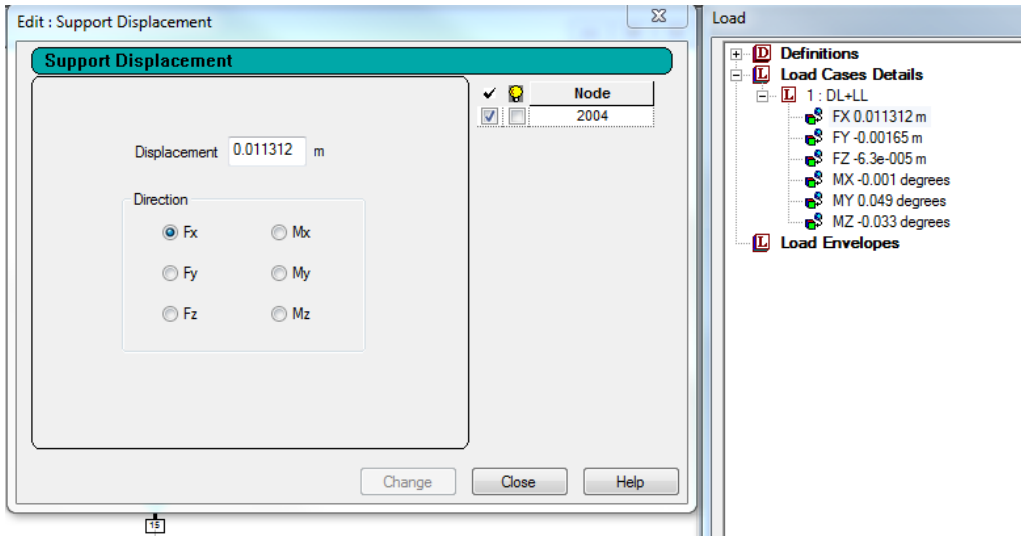
FIGURE 6.31
Apply Displacement As a Load to Pile Head

TABLE 6.6
Calculation of Approximate Stiffnesses from Soils

		Load, $\{F\}$			
F_x kN (kips)	F_y kN (kips)	F_z kN (kips)	F_{rx} kN-m (k-ft)	F_{ry} kN-m (k-ft)	F_{rz} kN-m (k-ft)
7.1	-254.7	-0.002	-0.009	0.004	21.4
(1.60)	(-57.3)	(0.00)	(0.00)	(0.00)	(4.81)

		Displacement, $\{u\}$			
x mm (in)	y mm (in)	z mm (in)	r_x deg	r_y deg	r_z deg
11.31	-1.65	-0.06			
(0.445)	(-0.065)	(-0.0024)	0.00	0.05	-0.03

		Approximate stiffnesses from soils, $\{K\}_{soil}$			
K_x kN/m (lb/in)	K_y kN/m (lb/in)	K_z kN/m (lb/in)	K_{rx} kN-m/deg (k-ft/deg)	K_{ry} kN-m/deg (k-ft/deg)	K_{rz} kN-m/deg (k-ft/deg)
626.5	154352.1	31.7	9.0	0.1	648.8
(3577)	(881374)	(181)	(6.6)	(0.074)	(478.5)

The superstructure stiffnesses for the pile head, $\{K\}_{\text{sup}}$, can then be determined by subtracting the soil stiffnesses, $\{K\}_{\text{soil}}$, from the stiffnesses at the pile head, $\{K\}_{\text{tot}}$; the results from this operation are shown in Table 6.7. These superstructure stiffnesses will be used as spring supports to the pile head to reflect the restraints from the superstructure (i.e. pile cap), as shown in the right side of Figure 6.30. Then buckling analysis of the single pile can be performed using the "**Perform bucking analysis**" command, with the results illustrated in Figure 6.32. It can be seen clearly that the minimum buckling factor for this case (i.e. S_d =5.3 m [17.4 ft]) is 2.235, which leads to the buckling load of P_{cr} = -575 kN (129 kips). However, the previous buckling analysis for the entire bridge has indicated that bridge already failed as buckling failure with buckling factor of 0.64 for a scour depth of 5.3 m (17.4 ft). This comparison indicates that bridge as a system may fail as buckling failure earlier than individual piles. Nonetheless, the developers have presented this approach in case individual pile performance is of interest to the end user.

TABLE 6.7
Calculation of Approximate Stiffnesses from Superstructure

Approximate stiffnesses from superstructure, $\{K\}_{\text{sup}}$					
K_x	K_y	K_z	K_{rx}	K_{ry}	K_{rz}
kN/m	kN/m	kN/m	kN-m/deg	kN-m/deg	kN-m/deg
(lb/in)	(lb/in)	(lb/in)	(k-ft/deg)	(k-ft/deg)	(k-ft/deg)
131.9	1628.5	0.0	11.0	0.0	92.9
(753.2)	(9299)	(0.0)	(8.1)	(0.0)	(68.5)
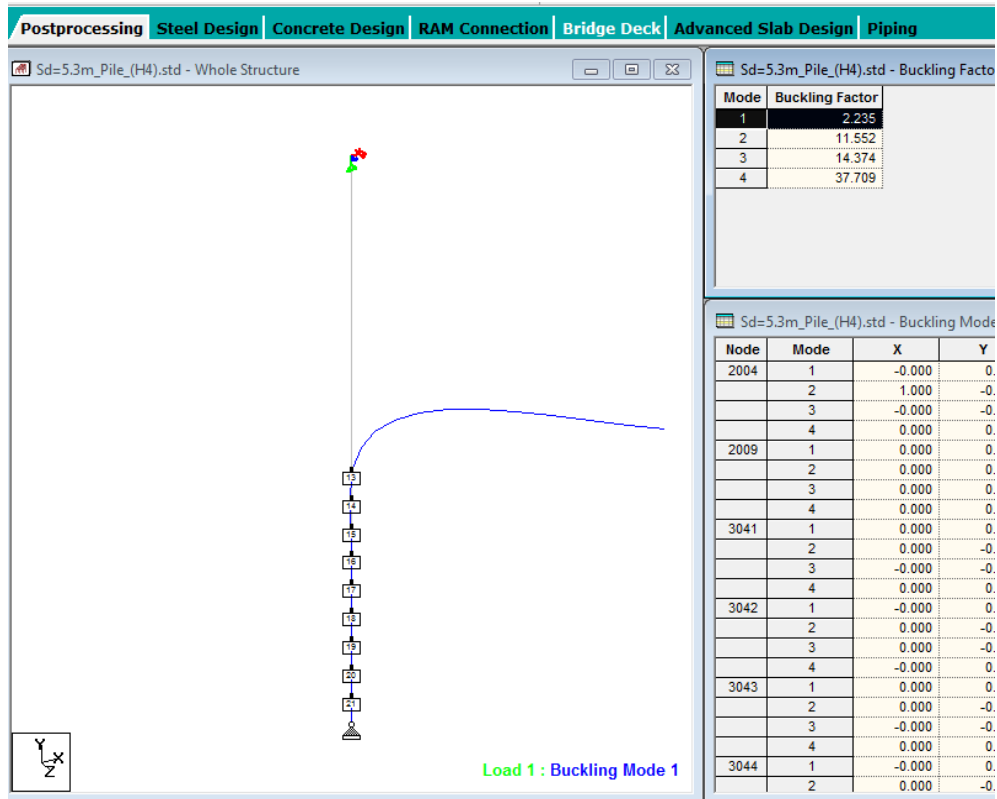
FIGURE 6.32
Buckling Factor and Failure Mode of Single Pile

From the Euler buckling equation, the effective length factor, K_e for pile slenderness can be back-calculated using Equation 6.1. K_e is calculated to be 1.73 for this scenario, which falls between the condition of fixed pile tip and rotation fixed pile head (K_e =1.2) and the condition of fixed pile tip and free pile-head (K_e =2.0).

$$K_e = \sqrt{\left(\frac{\pi^2 EI}{P_{cr}} \frac{r}{L} \right)}$$

Equation 6.1

where r is radius of gyration, L is pile length, P_{cr} is buckling load, EI is flexural stiffnesses of the pile sections.

Chapter 7: Conclusions

This report has presented the development and use of the Integrated Analysis Program (IAP), which was created at the University of Kansas under a K-TRAN research project funded by the Kansas Department of Transportation.

Chapters 2 and 3 describe the functionality of the IAP. The IAP works by linking the well-known structural analysis software package, STAAD.Pro 2007 with the Soil Spring Module (SSM) created at the University of Kansas. The IAP allows the user to generate structure models using STAAD.Pro; the structure models should include the superstructure and substructure elements, but do not initially include the supporting soils. The SSM is then used to generate the soil supports, through a GUI interface in which the user inputs values characterizing various soil layers surrounding the pile foundation. Once the soil springs are generated, they appear in the STAAD.Pro model, and the user can manipulate the STAAD.Pro model as desired.

Chapter 4 of this report describes the technical background behind the development of the SSM, and Chapter 5 describes the technical background for buckling analyses used in conjunction with the IAP.

A series of four examples have been presented in Chapter 6. These examples are intended to help the user implement the IAP in a step-by-step manner, and also illustrate how some of the results may be viewed.

Appendix A: Unit Conversions

Some useful conversion factors between the Metric and US units used in this report are provided here.

Metric	Multiply by	To get US equivalent
Distance		
m	3.28	ft
m	39.37	in
Force		
kN	0.2248	kips
Moment		
kN-m	0.73756	k-ft
Force/length		
kN/m	5.71015	lb/in
kN/m	68.521	lb/ft
Pressure (Stress)		
kN/m^2	0.14504	lb/in^2
kN/m^2	20.8854	lb/ft^2
kN/m2	0.00014504	kips/in^2
kN/m2	0.0208854	kips/ft^2
MPa	0.14504	kips/in^2
Second Moment of Area (Moment of Inertia)		
m^4	115.86	ft^4
m^4	2402509.61	in^4
Density (Unit Weight)		
kN/m3	0.00368	lb/in^3
kN/m3	6.3659	lb/ft^3
MN/m3	3.68	lb/in^3

References

American Association of State Highway and Transportation Officials (AASHTO). 2007. *AASHTO LRFD Bridge Design Specifications*, SI Units, 4th Edition, Washington, D.C.

American Petroleum Institute (ACI). 1987. "Recommended Practice for Planning, Designing and Constructing Fixed Offshore Platforms." *API Recommended Practice 2A (RP-2A),* 17th Edition, Washington, D.C.

Bentley System Inc. 2007. *Manual for STAAD*. Pro 2007 Bentley System Inc., Exton, PA.

Bieniawski, Z. T. 1984. *Rock Mechanics Design in Mining and Tunneling*. A. A. Balkema, Rotterdam, The Netherlands.

Cox, W. R., Reese, L. C., and Grubbs, B. R. 1974. "Field Testing of Laterally Loaded Piles in Sand." *Proceedings of the Offshore Technology Conference,* Houston, Texas, Paper No. 2079.

Deere, D. V. 1968. "Chapter 1: Geological Considerations." *Rock Mechanics in Engineering Practice*, K. G. Stagg and O. C. Zienkiewicz, eds., John Wiley & Sons, Inc., New York, N.Y., 1–20.

Georgiadis, M. 1983. "Development of *p-y* Curves for Layered Soils." *Proceedings of the Conference on Geotechnical Practice in Offshore Engineering*, ASCE, 536–545.

Horvath, R. G., and Kenney, T. C. 1979. "Shaft Resistance of Rock-Socketed Drilled Piers." *Proceedings of Symposium on Deep Foundation*, ASCE, New York, N.Y., 182–184.

Kulhawy, F. H., and Mayne, P. W. 1990. "Manual on Estimating Soil Properties for Foundation Design." *Report EL-6800*, Electric Power Research Institute, Palo Alto, California.

Matlock, H. 1970. "Correlations for Design of Laterally Loaded Piles in Soft Clay." *Proceeding of the II Annual Offshore Technology Conference*, Houston, Texas, 577–594.

Meyerhof, G. G. 1956. "Penetration Tests and Bearing Capacity of Cohesionless Soils." *Journal of the Soil Mechanics and Foundations Division*, ASCE, 82(SM1), 1–19.

Mokwa, R. L., Duncan, J. M., and Charles, E. V. 2000. "Investigation of the Resistance of Pile Caps and Integral Abutments to Lateral Loading." *FHWA/VTRC 00-CR4*, Virginia Transportation Research Council, Charlottesville, Virginia.

Peck, R. B., Hanson, W. E., and Thornburn, T. H. 1974. *Foundation Engineering*, Wiley, New York.

Peck, R. B. 1976. "Rock Foundations for Structures." *Proceedings of Specialty Conference on Rock Engineering for Foundations and Slopes*, ASCE, New York, N.Y.

Reese, L. C., Cox, W. R., and Koop, F. D. 1974. "Analysis of Laterally Loaded Piles in Sand." *Proceeding of the VI Annual Offshore Technology Conference*, Houston, Texas, 473–485.

Reese, L. C. 1997. "Analysis of Laterally Loaded Piles in Weak Rock." *Journal of Geotechnical and Geoenvironmental Engineering* 123 (11): 1010–1017.

Reese, L. C., and Van Impe, W. F. 2001. *Single Piles and Pile Groups under Lateral Loading*, A.A. Balkema Publishers, Leiden, the Netherlands.

K-TRAN

KANSAS TRANSPORTATION RESEARCH
AND
NEW-DEVELOPMENT PROGRAM

AD ASTRA PER ASPERA

Kansas
Department of Transportation